

TIMING AND MODERN CHARACTER OF THE WESTERN PUERTO RICO FAULT SYSTEM USING CARBONATE STRATIGRAPHY AND FLUVIAL TERRACE CHRONOLOGY FOR THE RÍO CULEBRINAS FAULT VALLEY

By:

Michael Moul Bogunovic

A thesis submitted in partial fulfillment of the requirements for the degree of

MASTER OF SCIENCE
in
GEOLOGY

**UNIVERSITY OF PUERTO RICO
MAYAGÜEZ CAMPUS**

2019

Approved by:

K. Stephen Hughes, Ph.D.
President, Graduate Committee

Date

James Joyce, Ph.D.
Member, Graduate Committee

Date

Wilson R. Ramírez, Ph.D.
Member, Graduate Committee

Date

Sylvia Rodríguez Abudo, Ph.D.
Representative of Graduate Studies

Date

Lizzette Rodríguez, Ph.D.
Department Director

Date

Abstract

The Western Puerto Rico Fault System has been the subject of previous geomorphological, geophysical, structural, and paleoseismic studies. However, its modern kinematic style and origin are not well understood. To better understand the modern kinematic style of the initially normal-style fault system samples from fluvial terraces along the Río Culebrinas fault valley were dated using Optically Stimulated Luminescence (OSL). Incision rates derived from the ages of these samples were compared to regional uplift rates to discern if any downward vertical motion is occurring within Río Culebrinas fault valley. The resulting incision rates indicate that downward vertical motion on the fault system, if any, is not detectable within the effects of Pleistocene to Holocene climate cycling. To better understand the origin of the system, fossil *Kuphus incrassatus* specimens from limestones interpreted to be coeval with initial fault activity were dated via $^{87}\text{Sr}/^{86}\text{Sr}$. The resulting ages suggest initiation of the system began during the Mid Miocene around 15 Ma. This data also highlights a local hiatus in carbonate deposition between 23 and 16 Ma which has also been described by Ortega-Ariza et al. (2015) in Puerto Rico and Hispaniola. This depositional hiatus does not appear in the traditional stratigraphic interpretations of the island emphasizing the need to revise the chronostratigraphy of Oligocene - Miocene limestones in the region.

This study dates the onset of regional-scale fault activity in Western Puerto Rico to the Mid Miocene and demonstrates that this period was not a time of tectonic quiescence in the region, as has been traditionally modeled. The presence of seismic activity along the system and the perseverance of the topographic signature of this system in tropical terrain suggest that vertical fault motion was not limited to the Mid Miocene, but that it may have continued to the near present. OSL analyses reveal that at least in the past 65,000 years, there is no detectable fluvial geomorphic signature of dominant dip-slip movement. This suggests that the faults may currently be accommodating dominantly strike-slip motion, similar to the large plate boundary to the north of the island. As potential strike-slip vectors, they pose more of a shaking risk to citizens than if they remained active as normal faults. The timing of the cessation of dip-slip movement is unknown but speculatively may be related to a shift from subsidence to uplift that occurred around 5 Ma. This relatively recent kinematic conversion could account for the lingering half-graben topography.

Resumen

El *Sistema de Fallas del Oeste de Puerto Rico* ha sido el enfoque de varios estudios geomórficos, geofísicos, estructurales, y paleosísmicos a través de los años. Sin embargo, hasta ahora no se conoce mucho sobre su origen, ni estilo cinemático moderno. Para determinar el estilo cinemático moderno del sistema comparamos razones de incisión fluvial a lo largo del Río Culebrinas con la razón de levantamiento tectónico. Esto se hizo con el fin de determinar si todavía está ocurriendo desplazamiento vertical-normal asociado con la falla Estas razones se calcularon con edades geológicas de terrazas fluviales pertenecientes al Río. Estas edades fueron calculadas utilizando técnicas de datación por Luminiscencia Óptica Estimulada (OSL por sus siglas en el inglés). Las tasas de incisión derivadas de estas muestras indican que el movimiento vertical en el sistema de fallas, si lo hubiera, no es detectable dentro de los efectos de las variaciones climáticas del Holoceno-Pleistoceno. Con el fin de comprender mejor el origen del sistema, especímenes fósiles de *Kuphus incrassatus* de depósitos interpretados como coetáneos con la actividad de fallamiento inicial fueron datados a través de métodos de datación isotópica de $^{87}\text{Sr} / ^{86}\text{Sr}$. Las edades resultantes sugieren que el inicio del sistema se produjo durante el Mioceno Medio alrededor de 15 Ma. Además, estos datos señalan un hiato local en deposición de carbonato entre 23 y 16 Ma descrito por Ortega-Ariza et al. (2015) en Puerto Rico y la República Dominicana. Este hiato en deposición de carbonato no está descrito en la estratigrafía aceptada de la isla, lo cual sugiere que está en orden una revisión de la cronoestratigrafía de las rocas calizas del Oligoceno - Mioceno de la región.

Los resultados de este estudio datan el inicio de fallamiento a escala regional en el oeste de Puerto Rico y demuestran que este período no fue uno de inactividad tectónica en la región, como se ha modelado tradicionalmente. La presencia de actividad micro sísmica a lo largo del sistema junto a la perseverancia de la delineación topográfica de este sistema en el clima tropical de Puerto Rico sugiere que el movimiento de falla vertical no se limitó al Mioceno Medio, sino que pudo haber continuado hasta casi el presente. Los análisis de OSL revelan que, al menos en los últimos 65,000 años no hay señales fluviales geomórficas que indiquen fallamiento normal (mociones verticales). Esto implica que las fallas pueden estar acomodando un movimiento de deslizamiento horizontal con un menor componente vertical, similar al límite de placa grande al norte de la isla. Como posibles vectores de deslizamiento horizontal, estos representan un riesgo mayor para los ciudadanos que si permanecieran activos como fallas normales (movimiento vertical). El momento de la cesación del fallamiento normal es desconocido, pero puede estar relacionado especulativamente con un cambio de subsidencia tectónica a levantamiento que ocurrió alrededor de 4 millones años atrás. Esta inversión cinemática es relativamente reciente, el cual podría explicar la persistente delineación topografía del sistema original.

Acknowledgements

I would like to thank all of those who have helped me through life. Most importantly my parents, for raising me the right way and always supporting me in my life and academic decisions (for better or worse). To all my grade school science teachers and college professors- without your encouragement and love for the natural sciences I would not be here. To the wonderful faculty, staff, and people at the UPRM's Geology Department - I would not have made it through Colegio without your help, humor, understanding, and comradeship through all the stressful periods in a graduate student's life. I would like to personally thank Dr. K. Stephen Hughes for accepting me on this project, Dr. James Joyce for letting me hangout with his field class while I was a toddler and sowing the seed of geology, Dr. Wilson R. Ramírez for some of the most entertaining and hands on classes I have taken to date and telling me that "being a professor is the best job in the world"- motivating me even further to pursue higher degrees, and Dr. John Dickey, without your acquaintance and suggestion that I study Geology I would be halfway through a unfulfilling career path.

I would also like to give a special thanks to those people who made this project possible logistically. To the Puerto Rico Science, Technology, and Research Trust (PRSTRT) for the generous funding provided for analysis, travel abroad, and conference/presentation. To Yelitsa I. González for showing me the ins and outs of the GASSI Lab. I would like to give a special thanks to Shannon Mahan, Director at the USGS Luminescence lab in Denver, CO for your expert knowledge and hands on experience. Your hospitality and humor go unrivaled. To Dr. Drew Coleman, Dr. Ryan Mills, and the rest of the gang at the Geochronology and Geochemistry Isotope Lab, UNC Chapel Hill for the use of your facilities, expert knowledge, and beer. To Catherine, for your amazing secretarial skills, and Claudia, my amazing cubicle mate and contemporary.

Last but far from the least, my four-legged friends who stood staring at me intently but lovingly through it all ...

Table of Contents

Purpose	1-2
Chapter 1	
Background	
1.1 Neo-Tectonic Setting & Geologic History	3-5
1.2 North and South Coast Carbonate Sequences	5-8
1.3 Seismicity and Faulting in Western Puerto Rico.....	8-10
1.4 Rivers and Geomorphic Change.....	10-11
1.5 Fluvial Terraces as Geochronological Markers.....	11-13
1.6 Study Area.....	13-14
Chapter 2	
Methodology	
2.1 Optically Stimulated Luminescence (OSL)	15-17
2.2 Sampling Procedure	17
2.3 Sample Preparation	18
2.4 Sites Sampled.....	18-23
2.5 Strontium Isotope Geochronology	23-25
2.6 Sample Preparation and Thin Sectioning.....	26
2.7 Strontium Isolation and Loading for ID-TIMS.....	26-27
Chapter 3	
Results and Discussion	
3.1 Río Culebrinas Terrace Ages	28-30
3.2 Incision Rates.....	30
3.3 Implications: Tectonics.....	30-32
3.4 Implications: Paleoclimate.....	32-33
3.5 $\delta^{13}\text{C}$ $\delta^{18}\text{O}$ Stable Isotope Analysis of <i>Kuphus incrassatus</i> and <i>Ostrea sp.</i>	34
3.6 $^{87}\text{Sr}/^{86}\text{Sr}$ Isotope Analysis of <i>Kuphus incrassatus</i> and <i>Ostrea sp.</i>	35-37
Chapter 4	
Conclusions.....	38-40
References.....	40-50
Figures.....	51-84
Tables	85-88
Appendix.....	89-97

List of Figures:

1	Regional Tectonic Setting.....	52
2	Stratigraphy of the North and South Coast Limestones.....	53
3	Limestone Cover in Northwestern Puerto Rico	54
4	Seismicity Map of the PRVI Region.....	55
5	The Western Puerto Rico Fault System and Previous work	56
6	Right Lateral Stream Displacement from Mann et al. (2005a)	57
7	Focal Mechanisms SW Puerto Rico	57
8	Long Profile Responses to Base Level Perturbations	58
9	Terrace Classification	59
10	Basin Topography	60
11	Study Area	61
12	Optically Stimulated Luminescence Concept.....	62
13	Strath Surface, Río Culebrinas.....	63
14	OSL Sampling Procedure	63
15	OSL Sample Preparation.....	64
16	Sample Site RC-5.....	65
17	Sample Site RC-6.....	66
18	Sample Site RC-8.....	67
19	Sample Site RC-12.....	68
20	Sample Site RC-7.....	69
21	Sample Site RC-11.....	70
22	Sample Site RC-10.....	71
23	Sample Site RC-9.....	72
24	LOWESS Strontium Seawater Curve	73
25	Specimens of <i>Ostrea sp.</i> and <i>Kuphus incrassatus</i>	74
26	<i>Kuphus incrassatus</i> in thin section and Micromilling	75
27	Sr Isolation Via Colum Chemistry.....	76
28	Long Profile for the Río Culebrinas and Landform	77
29	Linear Regression Plot for Incision Rates.....	78
30	Relative sea level curve last Interglacial-Glacial	79
31	Paleoclimate Proxies for the Caribbean	80
32	Channel Response to Climatic Conditions leading up to the LGM	81
33	Stable Isotope Analysis plot for $\delta^{18}\text{O}$ and $\delta^{13}\text{C}$	82
34	$^{87}\text{Sr}/^{86}\text{Sr}$ values on LOWESS Plot.....	83
35	$^{87}\text{Sr}/^{86}\text{Sr}$ Dates for Limestones in northwestern and southwestern Puerto Rico	84

List of Tables:

1	OSL Results	86
2	Incision Rates.....	87
3	⁸⁷ Sr/ ⁸⁶ Sr ages for Limestones in northern and southern Puerto Rico	88

Appendix

Radial Plot RC-5	90
Radial Plot RC-6	91
Radial Plot RC-8	92
Radial Plot RC-12	93
Radial Plot RC-7	94
Radial Plot RC-11	95
Radial Plot RC-10	96
Radial Plot RC-9	97

PURPOSE

In order to better understand the modern kinematics of the western Puerto Rico fault system (WPRFS) using the Río Culebrinas fault valley as a proxy, Optically Stimulated Luminescence (OSL) dating techniques were used on paleo-fluvial terraces within the river's drainage basin. The ages obtained from different terrace levels provide the first glimpse of the river channel's vertical position over time. Knowing the ages and elevations at which the terraces lie above the modern channel enabled the calculation of incision rates for the system. These incision rates were compared to uplift rates for northwestern Puerto Rico to detect either a decreased or similar vertical component of motion which may be attributed to any ongoing normal style faulting within the basin. This is based on the observation that over 100+ Kyr timescales, a river's incision will match uplift when it is occurring at a steady rate (Merritts & Vincent, 1989). A decreased incision rate will be attributed to accommodation of the accommodation of normal motion on the WPRFS during terrace deposition, whereas an increase in incision may either reflect an increased rate of uplift and/or a response to climate induced disturbances in the systems hydrologic and sediment budget. No increase in rate will indicate modern strike-slip fault motion. This study is unique as it is the first to provide fluvial terrace chronology for the island of Puerto Rico.

$^{87}\text{Sr}/^{86}\text{Sr}$ isotope dating of the marine bivalve *Kuphus incrassatus* and *Ostrea sp.* was used to better understand the onset of the WPRFS. This was accomplished by dating samples from limestone horizons in western Puerto Rico that are interpreted to have been deposited directly after the onset of faulting in the system. The dating of the carbonates complements previous chronostratigraphic studies of the region, highlighting the need for a revision of the

currently accepted chronostratigraphy (Ortega-Ariza, 2009; Ortega-Ariza et al., 2015), whilst confirming the existence of a topographic high in western Puerto Rico during the late Oligocene-early Miocene (Monroe, 1980; Moussa et al., 1987; Renken et al., 2002).

CHAPTER 1

BACKGROUND

1.1 NEO-TECTONIC SETTING & GEOLOGIC HISTORY

Puerto Rico lies along the Northeastern Caribbean Plate Boundary (NCPB) along with Cuba and Hispaniola. Three microplates line this boundary, from east to west these are: The Puerto Rico/Virgin Islands (PRVI), Hispaniola, and Gonave microplates (Jansma & Mattioli, 2005). Multiple neo-tectonic features surround the island (Fig.1). To the southeast of the island is the Anegada Passage, a seismically active deep-water basin and ridge structure separating the PRVI platform from the Lesser Antilles (McCann, 1985; Chaytor & ten Brink, 2014). The system accommodates at least 1.7 mm/yr southeast directed extension (Yang et. al, 2016). Directly south of the island is the Muertos Trough, an east-to-west trending trench and series of imbricated thrust slices of pelagic and turbidite sediments. The trough has been interpreted as a failed subduction zone (McCann, 1985; Mann et al., 2005_b; Granja et al., 2009, 2010). To the west, the Mona Passage is an extensional set of northwest and north-trending normal and oblique faults. The system is accommodating ENE directed extension between the PRVI and Hispaniola microplates (Larue & Draper, 1989; Hippolyte et al., 2005; Chaytor & ten-Brink, 2010; ten Brink & López-Venegas; Yang et al., 2016). To the north, The Puerto Rico Trench covers roughly 800 km east to west and marks the boundary between the PRVI microplate and the North American Plate. GPS data indicates up to $19-20 \pm 3 \text{ mm yr}^{-1}$ of highly oblique (left-lateral) convergence along this boundary (Larue & Draper, 1989; DeMets et al., 2000; Jansma & Mattioli, 2005; ten-

Brink, 2005). In addition to off-shore tectonic motions, the island has been undergoing uplift since the Pliocene (Brocard et al., 2016)

The geology of Puerto Rico records around 150 million years of island-arc accretion and volcanism (Krushensky & Schellekens, 1998). Its basement rocks contain of late Cretaceous - Eocene volcanic and volcanoclastic rocks which represent part of the original Greater Caribbean Arc (Burke, 1988). This north to south trending arc was positioned at the western margin of the Caribbean plate during the Late Cretaceous and migrated eastward as the newly formed Caribbean seafloor moved between the North and South American Plates. West-verging subduction and its associated volcanism (Smith & Schellekens, 1998) ceased during the Late Eocene - Oligocene as the Greater Caribbean Arc collided with the Bahama banks. The change in plate boundary style resulted in the current dominantly left lateral strike-slip boundary along the northern section of the arc (Pindell & Barret, 1990; Van Benthelm, 2013, 2014).

The end of volcanism was coupled with orogenesis which included folding, faulting, and uplift. During this period, large NW trending thrust faults formed throughout the island, the most notable of these being the northern and southern Puerto Rico fault zones (NPRFZ and SPRFZ) (Erikson et al., 1990; Larue et al., 1991). Mountain building was followed by a proposed period of quiescence that lasted from the Late Oligocene until the end of the Pliocene (van-Gestel et al., 1990; Larue & Ryan, 1998; Mann et al., 2005_a). During this time thick limestone sequences accumulated along a stable island platform unaffected by the surrounding tectonic features (Monroe, 1980; van-Gestel et al., 1990). Towards the end of the Miocene- Early Pliocene the island of Puerto Rico had been eroded to near sea level. Large rivers existed but were not transporting as much sediment to the north coast platform as they did in the past (Monroe, 1980).

This period was coeval with a 25° counterclockwise rotation of the PRVI block between ~10-5 Ma. (Reid et al., 1991; Grindlay et al., 2005_a). Rotation was followed by a change in regional tectonic conditions: the once stable island platform was suddenly but steadily arched around 5 Ma, tilting the north coast platform northward 3 - 4° to depths > 4 km in the Puerto Rico Trench (Monroe, 1980, Moussa et al., 1987; Mann et al., 2005_a). Flexure along the crest of this PRVI “arch” is hypothesized as being the source of east-to-west trending half-graben style faulting in the WPRFS thus suggesting the system became active at this time (Mann et al., 2005_a).

The initiation of uplift which followed tilting has been constrained to ~5 Ma by ¹⁰Be-²⁶Al dating of alluvial cave sediments deposited as regional uplift drove water table abandonment across the northern karst terrain (Brocard et al., 2016). Uplift of the island continues to this day and has produced heavily entrenched meanders (~150m) along the largest of the north and west coast rivers (Fig.4) and a series of wave-cut marine terraces (Renken et al., 2002). Radiometric dating of corals from marine terraces located 10 m above modern sea level (Taggart & Joyce, 1989) indicate island-wide uplift is between 0.03 - 0.05 mm/yr over the last 120 Kyr. When this rate is extrapolated to higher undated terraces, their ages coincide with Pleistocene sea level highstands (Taggart & Joyce, 1989). Conversely, ages from younger marine terraces suggest that either sea level was 2 - 3 m higher in the region 1.5 - 2 Kyr before present (BP), or that there has been an increase in the rate of uplift during the Late Pleistocene - Holocene. However, a compilation of Holocene sea level proxies for the Caribbean suggests there has been little regional change over the same time span (Khan et al., 2018), leaving a change in uplift rate as the most viable process.

1.2 NORTH AND SOUTH COAST CARBONATE SEQUENCES

The basement of the island and the Eocene - Oligocene crustal faults are overlain unconformably by thick Oligocene - Pliocene limestone cover sequences (Fig.2) described in depth by Monroe (1980) and are summarized in Renken et al. (2002). These deposits have been the focus of numerous hydro-geologic studies (Román-Más & Lee, 1987; Renken et al., 1994; Rodríguez-Martínez and Hartley, 1994; Tucci & Martínez, 1995; Rodríguez-Martínez 1995, 1997; Troester, 1999; Rodríguez-Martínez and Richards, 2000) and stratigraphic correlation studies (Torres-Vega, 2009; Ortega-Ariza, 2009; Ruidiaz-Santiago, 2013; Ortega-Ariza et al., 2015).

The north coast limestones are relatively un-deformed, trend east to west, and dip 3-8° to the North. At the base of the sequence is the San Sebastián Formation, a Late to Middle Oligocene basal siliciclastic unit representing a change from deep water and non-marine environments to shallow water deposition. The overlying units are characterized by a series of shallowing-upward sequences of relatively pure to chalky limestones (Renken et al., 2002). Classically divided by lithostratigraphy (Monroe, 1980) these are: The Lares Limestone (Late Oligocene - Early Miocene), the Cibao Formation (Mid Miocene), the Aguada (Early - Mid Miocene) and Aymamón (Late Miocene) Limestones, and the Quebradillas Limestone (Late Miocene - Pliocene). The stratigraphic extent of these units is relatively uniform throughout the north coast except in extreme western Puerto Rico where the two oldest units are absent (Fig.3) (Renken et al., 2002). Here the Miocene limestones unconformably overlies the Eocene basement rocks, suggesting that a topographic high existed during the deposition of the older Late Oligocene – Mid Miocene units (Monroe, 1980). The limestones in Rincón and Aguada are

believed to belong to the Cibao Formation as described by Monroe based on their physical and lithological similarities to outcrops in the north coast exposures (Renken et al., 2002). Ages for the Cibao in northern Puerto Rico come from $^{87}\text{Sr}/^{86}\text{Sr}$ analysis of a single specimen of *K. incrassatus* from a core sample in northern Puerto Rico, (Ortega-Ariza et al., 2015) and two dates from a pilot study in extreme western Puerto Rico by Vicens (2016). These analyses yield ages between 15 - 12 Ma.

Although similar in age to their northern counterparts, the south coast limestone cover is less extensive and heavily faulted, making correlations between formations difficult (Monroe, 1980; Renken et al. 2002). The overlying carbonate units are dirtier and chalkier than their northern counterparts and do not share the same faunal assemblages. This suggests that a paleo cordillera-island separated the two depositional environments while the presence of large rivers at that time drained the volcanic Cordillera into the near-shore fringe reefs of the southern nearshore basin (Renken, 2002). Like the north coast limestones, the south coast sequence (Fig.2) is underlain by a dominantly clastic basal unit (Renken et al., 2002): The Juana Díaz Formation (Lower Oligocene - Mid Miocene). The Ponce Limestone (Mid to Late Miocene) rests unconformably on the Juana Díaz Formation and is largely composed of soft to moderately indurated yellowish limestone rich in fossil content (Renken et al., 2002). These deposits are interpreted as being deposited in a near-shore shallow water environment. Overlying the Ponce Limestone are unconsolidated Pliocene - Holocene alluvial and fan delta deposits (Renken et al., 2002) previously described by Monroe (1980) as the Guanajibo Formation.

Chronostratigraphic correlations for the islands of Puerto Rico and Hispaniola by Ortega-Ariza et al. (2015) (Fig.2) and dates from this study suggest that the lithostratigraphic

order and timing of carbonate deposition is in error and that some of the units are time-equivalent in deposition (Fig.2). For the Late Oligocene (28 - 23 Ma) these are the San Sebastián Formation, the Lares Limestone, the Montebello Member of the Cibao Formation, and the Juana Díaz Formation followed by the Mid Miocene - Pliocene Cibao Formation, and the Aguada/Aymamón/ Ponce Limestones. These updated ages highlight a major tectonic event which inhibited carbonate deposition for some time. The beginning of this proposed “event” and hiatus in carbonate deposition is marked by a regional Early Miocene (23 Ma) unconformity observed in both southern Puerto Rico and Hispaniola and is believed to have lasted until the Mid Miocene (16 Ma) as indicated by ages from Ortega-Ariza et al. (2015) and this study.

1.3 SEISMICITY AND FAULTING IN WESTERN PUERTO RICO

Puerto Rico sits at a global scale tectonic boundary capable of producing major earthquakes. The majority of large local M7+ events have occurred offshore (Fig.4) to the northwest of the island along the NCPB and the Mona Passage (Lopez-Venagas et al., 2008). Seismic risk assessment studies for western Puerto Rico by Ascencio (1980) and McCann (1985) have highlighted the danger to the public posed by landward seismicity in western Puerto Rico. These arguments are supported by a growing catalogue of GPS (Fig.4), geophysical, focal mechanism data, and a better understanding of off-shore and landward structural features (Grindlay et al., 2005_b; Hippolyte et al., 2005; Huerfano et al., 2005; Jansma & Mattioli, 2005; Chaytor & ten Brink, 2005; ten Brink & López-Venegas, 2012; Roig-Silva et al., 2014; Yang et al., 2016, Adames, 2017, Solares, 2019). These studies reach consensus that modern stress regimes are exploiting inherited bedrock faults. These stresses are: 1.) ENE oriented compression in northwestern Puerto Rico related to the highly oblique motion occurring along the North

American - Caribbean Plate interface (Jansma & Mattioli; 2005), and 2.) NE - SW extension in southern Puerto Rico related to the opening of the Mona Passage and extension between the PRVI and Hispaniola plates (ten Brink & López, 2012).

The WPRFS (Fig.5) is an east to west trending half-graben system in western Puerto Rico that is interpreted to have been incipient in the Late Miocene- Pliocene under N - S extension related to the Late-Miocene Pliocene rotational event (Larue & Draper, 1990; Mann et al., 2005; Western Geophysical Company of America and Fugro, Inc, 1973). The most prominent of these faults from north to south are the Río Culebrinas valley fault, the Río Grande de Añasco valley and Cerro Goden fault, the Punta Algarrobo/Mayagüez fault zone, the Punta Guanajibo/Punta Arenas fault zone, the South Lajas valley fault, and the North Boquerón Bay-Punta Montalva Fault Zone (Grindlay et al., 2005_b; Roig-Silva et al., 2014; Adames, 2017). The footwall blocks of the system are expressed as the Cadena San Francisco, Monte Grande, and Sierra Bermeja ranges while rivers like the Río Culebrinas, Río Grande de Añasco, and Río Guanajibo flow west along the hanging wall valleys.

Most authors agree that the Cerro Goden fault is a continuation of the SPRFZ which formed as a left-lateral reverse fault during orogenesis in the Eocene (Mann et al., 2005_a), but fail to agree on whether a splay of the SPRFZ continues into the Río Culebrinas basin to the north of this fault (Jansma et al., 2000; Jansma & Mattioli, 2005). In addition, submarine NW trending normal faults imaged by Grindlay et al., 2005_b may continue onshore into the Culebrinas basin (Fig.5). Uncertainties about the current motion along the WPRFS arise from three distinct observations: 1.) Geomorphic features described by Mann et al. (2005) (Fig.6) suggest dominant right-lateral motion. 2.) Focal mechanisms from micro-seismicity in the same region suggest left

lateral shearing at depths associated with plate interactions at the NCPB (Fig.7) (Huérfano et al., 2005). 3.) Quaternary sediments in nearshore seismic profiles show an apparent normal offset (Fig.5) (Chaytor & ten Brink, 2010).

Ample paleoseismic evidence for landward rupture along these faults exists. Radiocarbon dating of liquefaction features along the river valley faults of the WPRFS by Tuttle et al. (2005) recorded ground shaking for multiple large seismic events over the last 500 years. To the south, discernible fault scarps with displaced Holocene sediments occur along the South Lajas valley fault and the North Boquerón Bay-Punta Montalva Fault Zone, both of which have been proven as active thoroughgoing systems (Prentice & Mann, 2005; Roig-Silva et al., 2014; Adames, 2016). Trenching studies in the same area reveal Holocene rupture events occurring around 5 - 10 Kyr BP (Fig.5) (Prentice & Mann, 2005; Piety et al., 2018). These E and ENE trending faults are currently suffering left lateral displacements with some oblique component due to 2 - 3 mm/yr of extension recorded in geodetic studies of southwest Puerto Rico (Jansma & Mattioli, 2005; ten Brink & López-Venegas 2012, Solares, 2019).

1.4 RIVERS AND GEOMORPHIC CHANGE

The erosive power of rivers plays an essential role in developing landscapes. A rivers power to incise and erode a landscape is largely dependent of stream power, defined by Bull (1979) as "the power available to transport sediment load." The discharge of a river and its sediment budget play dominant roles in stream power. In the case where discharge is greater than that needed to transport the sediment budget, then the river will incise, if the sediment budget exceeds that which the river can carry then the channel will aggrade. When the discharge of a

river is enough to transport the amount of sediment being supplied to it the river will neither incise nor aggrade. This type of river is said to be in a graded state and will take on a concave-up longitudinal profile (Fig.8) (Leopold & Bull, 1979).

If a disturbance upsets the balance of the graded state profile, it will accommodate the imparted change by internal adjustments in the watershed's erosive capabilities, sediment flux, and channel morphology (Bull, 1979; 1991; Leopold & Bull, 1979; Schumm, 1993). Disturbances in this balance may be internal or external. External factors such as vertical tectonic forcing and climate-related eustasy have the most profound effects on a river as they are the driving mechanisms behind base level fall. Base level is the lowest elevation to which a river or stream can erode. This reference level may be global such as sea level, or local such as a river flowing into a lake. Even a small amount of base level change may induce either aggradation or incision as the channel adjusts to a new gradient. In the case of alluvium dominated reaches of large rivers the system will respond to these changes in gradient by increasing or decreasing its sinuosity (Schumm et al., 2000). A pronounced fall in base level will drive incision along the whole channel length as it adjusts its profile gradient to the new depositional low (Fig.8) (Leopold & Bull, 1979), leaving behind a series of landforms called fluvial terraces. These fluvial landforms serve as geomorphic markers of change can be used to interpret a rivers response to past climatic and tectonic disturbances (Schumm et al., 2000; Pazzaglia, 2013). In contrast, a rise base level will drive aggradation from the mouth of the river into the floodplain (Fig.8) (Schumm et al., 2000). This aggradation will be coupled with increased degradation in the headwaters to maintain its preferred profile.

1.5 FLUVIAL TERRACES AS GEOCHRONOLOGICAL MARKERS

Fluvial terraces are ubiquitous relicts of previous river channel levels through time and represent a transient response to tectonic and climatic change (Schumm et al., 2000; Wegmann & Pazzaglia, 2002; Pazzaglia, 2013; Hughes, 2016). Terraces are categorized into two end members depending on their thickness and morphology (Pazzaglia, 2013): strath or fill (Fig.9). Strath terraces are characterized by a relatively flat erosional bedrock surface covered in 1 - 5 m of alluvium depending on the size of the basin. These terraces represent the initiation of down cutting in a system. Facies models for strath terraces indicate strath burial by medium to thickly bedded cobbles, which grade upward into beds of gravels and massively bedded sand. Fill terraces are characterized by thick alluvial deposits that represent aggradation and valley filling. Due to their infilling nature, fill terraces may have irregular contacts with the bedrock commonly associated with buried topography. Fill terraces may result from a positive base level change and the need to raise the river channel to maintain profile equilibrium. They may also form in response to climate-induced changes in sediment budget and stream power (Schumm 1973; 1993; Leopold & Bull, 1979; Pazzaglia, 2013).

Geochronological analysis of terraces can be used to gauge a fluvial systems response to vertical tectonic forcing. This is based on the premise that over 100+ Kyr timescales, a river will incise at rates equal to those of regional uplift given that it is occurring at a steady rate (Merritts & Vincent, 1989; Merritts et al., 1994; Schumm, 1993; Burbank et al., 1996; Snyder et al., 2000; 2002; Schaller et al., 2005; Pederson et al., 2006, 2013; Pazzaglia, 2013; Collins et al., 2016; Goren, 2016). Luminescence dating techniques such as Optically Stimulated Luminescence (OSL) have been widely used for dating fluvial terraces as they can be used on loose sand-sized

quartz and feldspar grains common in fluvial deposits (Stokes, 1999). Inferring rates of tectonic driven vertical change can be hampered by climate-driven eustatic forcing (Merritts et al., 1994; Snyder et al., 2000; 2002; Kock et al., 2009_a; Kock et al., 2009_b; Macklin et al., 2012; Limaye & Lamb, 2016; Hughes, 2016) and the response of the system to these may mask the effects of uplift (Hetzl et al., 2006).

Fluvial channels undergo oscillations between periods of aggradation and incision; therefore, the vertical position of a fluvial systems channel may oscillate with time. Therefore, interpretations and comparisons of measured uplift and incision rates are time-dependent and may be biased to the current channel level (Finnegan et al., 2014; Gallen et al., 2015). This dependence on the measured time interval and has been coined the Sadler effect (Sadler, 1981). To remove the uncertainty of the Sadler effect cumulative incision is measured between terrace levels and over at least one glacial-interglacial cycle when possible (Wegmann & Pazzaglia, 2002; Hetzel et al., 2006; Pederson et al., 2006; Pederson et al., 2013; Gallen et al., 2015; Goren, 2016). These rates are representative of cumulative incision for the measured time interval.

1.6 STUDY AREA

The focus of this study is the Río Culebrinas fault valley (Fig.10) and the limestone outcrops in extreme western, and southwestern, Puerto Rico. The Río Culebrinas is a mixed alluvial/ bedrock floored system. Its watershed drains 270 km² of siliciclastic, volcanic, and carbonate bedrock, and is characterized by a set of heavily entrenched meanders and low relief terrace surfaces (Monroe, 1969; McIntyre, 1971). The main channel flows generally east to west from its headwaters in the municipality of Lares to its mouth in the Aguadilla Bay over a maximum relief of ~380 m. Tributaries to the north are relatively short and steep, as they drain a

pronounced east-west trending topographic escarpment along the southern limit of the north coast limestone karst terrain. The escarpment has long been interpreted as an erosional product of differential weathering between the exposed indurated north coast limestone and the poorly lithified San Sebastián Formation (Monroe, 1980) exposed by the original half-graben system. Conversely, the southern tributaries are longer and gentler in gradient as they drain the more homogeneous north-dipping Eocene basement rock of the Cadena San Francisco and Cerro Goden fault. Offshore neo-tectonic features related to extension in the Mona Passage extend inland into the floodplain of the Rio Culebrinas into the basin (Fig.5A) and may be reactivating the older half-graben system as strike slip faults (Hippolyte et al., 2005). The original tilting of the half-graben geology and the topographic escarpment are responsible for the asymmetry of the northern and southern tributaries, which indicate a northward migration of the system in the past due to lateral valley tilt (Schumm et al., 2000).

The extent of the carbonate cover into western Puerto Rico is limited to the upper three units of the north coast carbonate sequence: the Cibao Formation, the Aguada Limestone, and the Aymamón Limestone (Monroe, 1980; Renken et al., 2002) (Fig.3). The unconformity that separates these units from the older Eocene-Oligocene basement is interpreted to have formed as a result of the initiation of the WPRFS and the lowering of a western paleo-highland into a marine environment.

CHAPTER 2

METHODOLOGY

2.1 OPTICALLY STIMULATED LUMINESCENCE DATING

Luminescence dating techniques such as optically stimulated luminescence (OSL) and infrared stimulated luminescence (IRSL) provide a minimum age estimate of the last time a quartz or feldspar mineral grain was exposed to heat or sunlight (Aitkens, 1995;1998). These dating methods are useful as they employ minerals abundant in sedimentary settings (Stokes, 1999). Luminescence in minerals is the release of trapped electrons within their crystal lattices in the form of visible and infrared light. Radioactive minerals may either luminesce naturally or after photo or thermal stimulation, as is the case with quartz and K-feldspar. Luminescence builds in a mineral grain via ionizing radiation from the surrounding material until it is reset by temperature or exposure to sunlight: a process known as bleaching (Fig.12). Radiation may either be derived externally from neighboring radioactive grains, cosmogenic sources, or internally from the natural decay of ^{40}K (Aitkens. 1998; Preusser et al., 2008). This ionizing radiation stimulates the parent nuclei of the mineral grain, raising the electrons out of their valence bands. As they lose energy, they return to their valence state. Not all electrons return to this stable state as they become trapped in defects within the crystal lattice. Examples of these traps in quartz are oxygen vacancies and foreign atoms such as Al^{+3} replacing Si^{+4} .

When mineral grains are stimulated by heat or light under laboratory conditions, these trapped electrons are released as luminescence and can be measured. Ages are obtained by measuring the original luminescence signal known as the paleo dose within the grain, calculating

its equivalent dose (D_E) and relating its intensity to the environmental dose rate (D_R) via the following equation (Aitkens, 1998; Lian, 2007; Nelson et al., 2015):

$$Age = \frac{\text{Equivalent dose } (D_E)}{\text{Dose Rate } (D_R)}$$

The original paleo-dose is measured by preheating the grains to release unstable electrons and isolate the optical component of the luminescence signal. The grains are then stimulated, and the paleo dose is measured. The unit of measurement is in Grays (Gy), which is defined as the absorption of one joule of radiation energy per kg of matter ($1\text{J kg}^{-1} = \text{Gy}$) (Preusser et al., 2008). There are three steps obtain D_E once the paleo dose is measured. These are irradiation, preheating, and stimulation and measurement of the resulting induced luminescence signal. Irradiation of the samples is done via external sources ($^{90}\text{Sr}/^{90}\text{Y}$) with the purpose of creating a latent luminescence signal in the grains by filling all available electron traps whether they are stable or not. The unstable traps are then emptied by heating the samples between 200°C and 300°C , after which the sample is stimulated, and the luminescence produced by that dose measured. In this study, the mineral analyzed by OSL is quartz, stimulated using blue wavelengths (420 - 550 nm) and emission is in the ultraviolet range (Preusser et al., 2008). Measurements are made in increments, increasing the artificially induced irradiation each time. By recording the original observed luminescence signal (D_E) and the rate at which energy is being stored in the grain (D_R), the resulting artificially induced values are used to construct a best-fit line on a regenerative dose-response curve from which the final ages can be inferred (Fig.12). This process is repeated for multiple aliquots ($n = 15 - 50$) of the same sample to remove artifacts of inhomogeneity of the grains physical and chemical characteristics. D_R is

determined by measuring how much ionizing radiation is present in the burial environment of the targeted grains (Aitkens, 1998). This is accomplished by collecting >1 L of surrounding material for high-resolution gamma spectrometry measurements of ^{40}K , ^{238}U , ^{323}Th , and ^{40}Rb and water content analysis. Moisture content is inherently important to quantify as it preferentially attenuates ionizing radiation. The geographic location and elevation also play minor roles in assessing the cosmogenic derived component of radiation.

2.2 SAMPLING PROCEDURE

Once a suitable fill terrace was located (Fig.13, 14) samples were collected using methods described by Nelson et al. (2015). Five to ten centimeters of the sub-vertical outcrop surface was removed to ensure collection of fresh, unbleached grains. Sampling targeted fine-grained sandy layers and lenses while recording the depth from the modern erosional surface of the terrace. Samples were collected by driving 20 - 25 cm long by 4 cm diameter sections of galvanized steel tube (Fig.13) into targeted layers which were then capped at both ends. Before being driven into the deposit, Styrofoam plugs were inserted in the loading end and of the sampling tubes to prevent sediment mixture during transport. Before the removal of the sample, both a 1 L bag and a 120 mL airtight container were filled with material from within a 15 cm radius of the sampling tube (Fig.13). These samples served for dose rate and water content. Samples were shipped to the United States Geological Survey Luminescence Dating Lab in Denver, CO for sample preparation, processing, and analysis by the author of this thesis.

2.3 OSL SAMPLE PREPARATION

OSL samples were opened under subdued dark lab lighting conditions (red spectrum ~600 - 750 nm wavelength). Two to three centimeters of sediment was then removed from both ends as a precaution against light contamination during sampling. Samples were subjected to a 10% HCl bath for 24 hours to remove carbonate components and rinsed in distilled water followed by a 30% H₂O₂ bath over an additional 24 hours to remove organic material. The remaining sediment was then mixed with a deflocculant and wet-sieved, retaining grain sizes between 250 and 90 µm. Once sieved and dried, the remaining coarse-grained quartz components were separated from heavy minerals and feldspars using a Franz magnetic separator and heavy liquid separation using LST (lithium sodium polytungstate, 2.85 ± 0.02 g/mL) (Fig.15) The samples were centrifuged for 5 minutes to aid in mineral separation, and the excess K-feldspar float was drained and stored. The resulting quartz component is bathed in a final solution of 50% HF for 40 minutes to remove any remaining feldspar grains.

2.4 SITES SAMPLED:

The nomenclature used for site samples, description, and terrace chronology is as follows: Sampling sites (Fig.11) are termed RC-# for Río Culebrinas, followed by a number representative of the order in which the sites were located and sampled. The ages or "generation" of the terraces were divided into Q_a for modern floodplain deposits, and Q₁, Q₂, and Q₃ for successively older deposits. Site descriptions are in order of River kilometer. Kilometer 0 is at the river mouth.

Sample RC-5*Fig.16**18.39013, -67.12490**Río Culebrinas km 9.2**Elevation from modern channel 8.4 m*

Site RC-5 is located on private industrial property along the floodplain to the north of the river in Barrio Pueblo in the municipality of Moca. It is one of the fluvial terraces mapped by Monroe (1969) who described the terraces in this area as clay and sand dominant with scattered volcanic pebbles and quartz. The outcrop is a 5 - 6 m near vertical section of alluvial deposits around 11 m above the current channel interpreted as Q₁. It is composed of pebble to cobble-sized clasts with thin lenses of coarse to fine-grained sands and silt dispersed throughout the outcrop. The dominant lithology of clasts is sedimentary and volcanic with a minimal component of visible carbonate component. Samples were taken from one of the sand lenses 2 m below the current erosional surface of the terrace.

Sample RC-6*Fig.17**18.36443, -67.11069**Río Culebrinas km 16.9**Elevation from modern channel 11.8 m*

Site RC-6 is located just upstream of the floodplain to the south of the river between Barrio Marías and Naranjo in the municipality of Moca on private agricultural property. This site was not previously mapped as a terrace and was selected based on slope maps, high-resolution LiDAR-derived DEMs, and field reconnaissance. The site includes of at least two, possibly three paleo surfaces. The uppermost surface is interpreted as a Q₂ bedrock strath terrace with sediment to sample, while the middle and lower surfaces were interpreted as Q₁ and Q_a. These deposits are

dominated by silty sand and sandy silt interbedded with scattered 2 - 15 cm layers of well-rounded sedimentary clasts and a minimal component of igneous material. The layer's dip towards the river at around 10 degrees. Samples were collected from Q₁ along a property access road which cuts through the deposits. Some excavation was required to reach 1m vertical sampling depth from the surface.

Sample RC-8

Fig.18

18.35112, -67.05974

Río Culebrinas km 18.3

Elevation from Channel 24.7 m

Site RC-8 is located on private agricultural property in Barrio Cerro Gordo in the municipality of Moca on the north side of the river. The site was selected using slope maps, LiDAR-derived DEMs, and field reconnaissance. Topographically the site is characterized by two distinct Q₁ and Q₂ terraces. Q₁ was avoided for sampling due to intensive agricultural practices. Samples were taken from an access road-cut at a vertical depth of 1.2 m from the erosional surface of Q₂. The site is characterized by clays and silty clays with thin 0.5 - 5 cm thick beds of angular to sub-angular sand and pebbles with large rounded and sub-angular boulders occurring sporadically throughout the outcrop.

Sample RC-12

Fig.19

18.360996, -67.084227,

Río Culebrinas km 21.2

Elevation from modern channel 34.4 m

Site RC-12 is located on private agricultural property on the south side of the river in Barrio Cerro Gordo in the municipality of Moca and was previously mapped by McIntyre (1970). At least three paleo surfaces characterize the site. Q₁ and Q₂ are two interpreted as fill

terraces. Q₃ was not sampled as it represents a strath surface with no datable material. Q₁ was discarded as it is heavily cultivated. The fill deposits of Q₂ are composed of red silts and clays with 2 - 10 cm thick chaotic beds of sand and pebbles, and 2 - 3cm layers of silty sand overlying a heavily weathered bedrock strath. Samples were taken from a small mass wasting site at the base of Q₂ 1 m below the modern erosional surface.

Sample RC-7

Fig.20

18.35112, -67.05974

Río Culebrinas km 26.9

Elevation from channel 31.0 m

Site RC-7 is located on a shared agricultural plot to the south of the river in Barrio La Plata, Moca and was previously mapped by McIntyre (1970). At least three paleo surfaces characterize the site. The highest surface is interpreted as Q₃ generation bedrock strath surface which was once overlain by fill as there is still some 1 - 15cm of clastic material remaining. The lower two surfaces are interpreted as Q₂ and Q₁ terraces with Q_a occurring within proximity to the main channel. The site is characterized by massive poorly sorted deposits ranging from clay and silt to small-intermediate sized cobbles overlying a heavily weathered strath surface. Clasts are mainly sedimentary with pebble to gravel-sized quartz clasts and less commonly some fragments of calcite within the coarser grained sections. Q₃ and Q₁ were avoided for sampling due to lack of material (Fig.13) and agricultural practices respectively. Samples were taken from Q₂, a massive 2 - 4 m thick bed of well-rounded pebbles with irregularly occurring sand lenses overlying heavily weathered bedrock at a depth of 2.5 m below the modern erosional surface.

Sample RC-11*Fig.21**18.32729, -66.98373**Río Culebrinas km 36.7**Elevation from channel 29.8 m*

Site RC-11 is located on the north side of the main channel in Barrio Hato Arriba, San Sebastián and was selected using slope maps, LiDAR-derived DEMs, and field reconnaissance. The site is characterized by one broad heavily weathered Q₃ surface previously mapped as the San Sebastián Formation by McIntyre (1970). The deposits are composed of a 1 m poorly sorted finning upward layer of cobbles, pebbles, and sands unconformably overlying the basement San Sebastián Formation. A thin layer of gray and red clays separates the fill material from the underlying San Sebastián Formation, which is characterized by alternating layers of conglomerates, clays, and paleosols abundant in caliche. The upper fill is dominated by terrigenous sedimentary clasts of the San Sebastián Formation and less frequently igneous material. Due to the limited exposure samples were collected from the sandiest layers between 0.3 and 0.8 m depth from the modern erosional surface.

RC-10*Fig.22**18.32729, -66.98373**Río Culebrinas km 46.0**Elevation from Channel 30.0 m*

Site RC-10 is located at the base of the headwaters on the south side of the main channel in Barrio Calabazas, San Sebastián. The site is located directly across the river from terraces previously mapped as remnant high terraces by Tobisch & Turner (1971). Topographically the site is characterized by one broad surface interpreted as a Q₁ generation terrace resting on bedrock strath. The deposit is composed of massive beds of pebbles, sands, and silts which fine

upwards. These massive layers overlay a 20 - 30 cm basal layer of sand and sub-angular gravel. Clasts show little to no weathering and are dominated by terrigenous sedimentary clasts and some carbonate fragments. Samples were taken at a vertical depth of 3 m from the surface above the basal layer targeting fine-grained sand.

RC-9

Fig.23

18.32991, -66.97509

Río Culebrinas km 47.6

Elevation from channel 15.6 m

Site RC-9 is located at the base of the headwaters on the north side of the main channel in Barrio Piedras Blancas, municipality of San Sebastián. The site was selected using slope maps, LiDAR-derived DEMs, and field reconnaissance. The location is characterized by one paleo surface interpreted as a Q₁ fill terrace. The deposits are dominated by sandy silt interbedded with irregularly spaced beds of clay and small pebbles. The deposits gently dip downstream to the modern flow direction. Clasts show little to no weathering rinds and are of mixed terrigenous and volcanoclastic origin. Samples were taken from a vertical depth of 1 m from the modern erosional surface below a distinct layer of white and gray clay.

2.5 STRONTIUM ISOTOPE GEOCHRONOLOGY

$^{87}\text{Sr}/^{86}\text{Sr}$ is a reliable tool for chronostratigraphy and has been successfully used to date shallow water marine bivalves by comparing measured skeletal $^{87}\text{Sr}/^{86}\text{Sr}$ values to the standard strontium seawater reference curve empirically developed by McArthur (2001) using pre-existing data and literature review (Fig.24). Marine waters are well mixed when compared to meteoric and formation waters, therefore the amount of strontium in these waters is constant (8

ppm) (Tucker & Wright, 1990). Both Sr^{2+} and Ca^{2+} share the same charge and have similar atomic radii. Because of this Sr^{2+} is incorporated naturally in place of Ca^{2+} in the shells and skeletons of marine organisms, preserving the original $^{87}\text{Sr}/^{86}\text{Sr}$ ratio of the ocean waters in which it was precipitated. There are four naturally occurring stable isotopes of strontium: ^{84}Sr , ^{86}Sr , ^{87}Sr , and ^{88}Sr . The first two isotopes are not part of any decay chain and remain constant in marine waters over time. ^{87}Sr is generated by the decay of ^{87}Rb with a half-life of 4.89×10^{10} yr. ^{86}Sr is stable and does not undergo isotopic fractionation. The long half-life of ^{87}Sr and the insignificant amount of ^{87}Rb marine water (120 ppb) produces very little in-situ ^{87}Sr over the residence period of Sr in the oceans (4 - 5 Ma), which leads to a constant value for $^{87}\text{Sr}/^{86}\text{Sr}$ in the oceans at any given time (Tucker & Wright, 1990). Nonetheless, changes in the $^{87}\text{Sr}/^{86}\text{Sr}$ ratio have occurred over the millennia (Burke et al., 1982; Koepnick et al., 1985) and are attributed to varying sources of continental runoff where Rb concentrations are much higher, and hydrothermal alteration of basalts at seafloor spreading centers (Tucker & Wright, 1990).

$^{87}\text{Sr}/^{86}\text{Sr}$ isotope dating has been used to provide improved chronographic resolution on the Oligocene-Pliocene carbonates in Hispaniola, Puerto Rico, and Panama (Ramirez, 2006; Ruidiaz-Santiago, 2013; McNeil et al., 2012; Ortega-Ariza, 2009; Ortega-Ariza et al., 2015; Vicens, 2016) by dating Low-Mg bivalves such as *Ostrea sp.* and *Kuphus incrassatus*. This dating method is used in this study to verify the age of the carbonate cover in extreme western and southwestern Puerto Rico. Over 100 specimens of *Kuphus incrassatus* and *Ostrea sp.* (Fig.25) were collected from outcrops in western and southwestern Puerto Rico for $^{87}\text{Sr}/^{86}\text{Sr}$ isotope analysis of their powdered skeletons. Both species present ideal candidature for $^{87}\text{Sr}/^{86}\text{Sr}$ dating due to their Low-Mg calcite shells which are relatively stable and resistant to diagenesis

(Veizer et al., 1983; McArthur, 1994). Once collected viable samples were chosen visually using transmitted light (TL) microscopy to identify any visible re-crystallization of the original skeleton (Fig.26). Once unaltered segments of the skeletons were located and drilled, 450 - 500 μg of skeletal powder was collected for $\delta^{13}\text{C}$ and $\delta^{18}\text{O}$ stable isotope analysis to verify whether or not the samples have been geochemically altered since deposition (Lloyd, 1964; Tucker, 1990; Tucker & Wright, 1990; Patterson & Walter, 1994). $\delta^{18}\text{O}$ values are indicative of the waters from which the carbonates were precipitated. Meteoric waters characteristic depleted $\delta^{18}\text{O}$ values. This is due to isotopic fractionation during the hydrologic cycle. As seawater is evaporated it retains more of the lighter isotope. Once airborne, the higher vapor pressure of ^{16}O forces the heavier ^{18}O into water droplets where it is preferentially depleted in ^{18}O through precipitation (Tucker & Wright, 1990). $\delta^{13}\text{C}$ measures the ratio between $\delta^{13}\text{C}$ & ^{12}C . These values are used to determine primary productivity and the environment where an organism fed (Tucker & Wright, 1990). Biotic processes in flora and fauna preferentially sequester ^{12}C . This leads to depleted $\delta^{13}\text{C}$ values less than -7 ‰, which are indicative of near shore environments with large inputs of organic carbon (Tucker & Wright, 1990).

The stable isotope analysis was performed at the Gas Analysis Stable Isotope (GASI) lab in the Department of Geology at the University of Puerto Rico, Mayagüez using a Thermo-Finnigan MAT 253 isotope ratio mass spectrometers. Viable samples were then analyzed for $^{87}\text{Sr}/^{86}\text{Sr}$ via isotope dilution-thermal ionization mass spectrometry (ID-TIMS) at the University of North Carolina Chapel Hill's Isotope Geochemistry Lab using a VG Sector 54 TIMS.

2.6 SAMPLE PREPARATION AND THIN SECTIONS

Samples of *Kuphus incrassatus* were cut perpendicular to their long axis with a Rigid® tile saw and checked for visible recrystallization, fractures, and thickness of shell (Fig.24). Shells must be over 1 mm thick to be suitable for micro mill powder collection. Any specimens that do not satisfy these criteria were discarded. Viable specimens were embedded in epoxy to improve the cohesiveness of fragile samples during subsequent procedures and left overnight to harden. Hardened samples were then cut again, retaining one end for sampling while the other was thin sectioned to provide a mirror view of the surface to be sampled. Specimens to be thin sectioned were polished with 240, 400, and 600 grit sandpaper on a Buhler Ecomet III polisher and then glued with optical cement to frosted thin section slides and cured under ultraviolet light. Samples were then thin sectioned using a Buehler PetroThin machine with digital adjustments to a standard thickness of 30 μm .

2.7 STRONTIUM ISOLATION AND LOADING FOR ID-TIMS:

Samples were dissolved in 550 μL 3.5 M HNO_3 and left to sit overnight to dissolve all carbonate components. Once dissolved, samples were centrifuged at 9×10^3 rpm for 8 minutes to separate any remaining solids. Elemental Sr was isolated from the powdered samples by column chemistry (Fig.27) using Sr Specific resins via the following procedure. Before sample loading columns were rinsed in ultra-pure Type 1 water (18.2 $\text{M}\Omega \cdot \text{cm}$ at 25 $^\circ\text{C}$). A Sr specific resin was then added up to the neck of the reservoir. The columns were flushed twice with 21 mL of H_2O . Once rinsed, the resin was preconditioned with 450 μL of HNO_3 . 500 μL of sample was loaded into each column via pipette after centrifuge and rinsed three times with 30 μL 3.5 M HNO_3 and then four times with 360 μL 3.5 M HNO_3 . Sr was then eluted with two rinses of 450 μL H_2O and

retrieved in a separate beaker and prepared for drying and loading with 30 μL H_3PO_4 . Samples were then dried at 125°C for 2 - 3 hours until dry. Once the elemental Sr component was isolated it was then mounted on the heating element of the VG Sector 54 TIMS: a 1 mm wide rhenium filament on two reusable posts. While mounting sample, the posts and filament are placed on a loading bench to provide electrical current to heat the filament and dry it. The loading of the standard (NBS 987) and samples is the same: 1 μL of standard NBS 987 or sample bead was added to 1 μL HCl and 1 μL TaF_5 tantalum fluoride. The dissolved sample was then retrieved with a pipette and placed in the center of the filament. Before mounting the standard and sample on the filament, the two outer thirds of the filament were coated in paraffin with the mounting bench set at ~ 1 A, leaving the center third for mounting. This paraffin dam inhibits the sample from rolling around the filament before it is dry. An oscillating current between 1 - 2.5 A was applied to the filament through mounting bench to dry sample bead while avoiding melting the paraffin dam. Once mounted, the samples were loaded onto the turret and into the ID-TIMS.

CHAPTER 3

RESULTS AND DISCUSSION

3.1 RÍO CULEBRINAS TERRACE AGES

For this study, OSL analysis was carried out on select fill terrace samples from the Río Culebrinas basin. Dates obtained from different terrace elevations were used to estimate incision rates for the Río Culebrinas. Samples were collected from near vertical exposures targeting original sedimentary layers, avoiding zones disturbed by bioturbation or reworking. Potential terrace sites were evaluated using geologic maps (Monroe, 1969; McIntyre, 1971; Tobisch & Turner, 1971), high-resolution LiDAR-derived DEMs, and extensive fieldwork. Due to the relatively low inclination of these surfaces when compared with the surrounding topography, many of these have been preferentially farmed over the last century. In many places intensive agricultural practices for vegetables, sugar cane, plantains, and root crops common in the tropics, coupled with intense chemical weathering have either reworked the upper meter of alluvium or led to the erosion most of the terrace fill cover down to the bedrock (Fig.13). These factors significantly limited the number of viable deposits for dating.

OSL ages for fluvial terraces within the Río Culebrinas basin (Table 1) were derived using the age equation (Eq1) (Aitkens, 1998; Lian, 2007; Nelson et al., 2015). D_E values were measured from single-grain aliquots to maximize the number of runs using a Risø automatic OSL -IRSL reader. Values were determined using the single aliquot-regenerative (SAR) procedure described in Murray & Wintle (2003) for improved accuracy (Pagonis et al., 2011). D_R for sediments surrounding the individual samples was calculated using protocol by Murray et

al. (1987) via high-resolution gamma spectrometry measurements for ^{40}K , ^{238}U , ^{323}Th , and ^{40}Rb . D_R contributions from cosmogenic sources were addressed using methods by Prescott & Hutton (1994). Age modeling used both CAM (central age model) to determine the dispersion of D_E values in single grain analysis and MAM (minimum age model) to highlight any significantly bleached grains (Galbraith et al., 1999) (Appendix A). Either the central age model (CAM) or minimum age model (MAM) was used to calculate D_E values depending on the scatter and distribution of individual D_R values when plotted on radial plots (Galbraith, 1999) and field observations.

Ages reveal at least three generations of terraces (Table 1, Fig.28). Sites RC-5, RC-6, RC-9, and RC-10 are interpreted as Q_1 generation terraces that date between 11 - 13 Kyr BP. All but one of these sites, RC-10 is found at elevations between 8 and 15 m above the modern channel. RC-10 is considered an outlier as it sits at almost 30 m above the current channel and may be related to the retreat of a nearby knickpoint (Pazzaglia, 2013) or a change in bedrock geology (Fig.8), Sites RC-7, RC-8, and RC-12 correspond to Q_2 generation terraces, dating between 19 - 22 Kyr BP. These deposits are found between 25 - 35 m above the modern channel (Fig.28). Site RC-11 - a single deposit dated at 65 ± 5.1 Kyr BP is inferred as a Q_3 generation terrace and is found at similar elevations to Q_2 . RC-11 displays a striking two-component population in ages (Appendix A). This suggests that the terrace was overridden or flooded with younger sediment before base level made a significant downfall, leaving the terrace stranded. A less apparent two-component age population is also present in both Q_1 and Q_2 terraces (RC-12, RC-9, and RC-5).

3.2 INCISION RATES

Overall incision rates were calculated for each generation of the terrace by plotting the landform heights above the modern channel against their ages (Table 2). A simple best fit linear regression was applied to these plots, where the slope of the line represents the average incision for each group (Fig.29). With respect to the modern channel, incision rates for Q₁ and Q₂ are 1.36 and 1.46 ± 0.10 mm/yr respectively and a long-term incision rate of 0.37 ± 0.03 mm/yr for Q₃. To derive accurate incision rates which take into consideration the Sadler Effect imparted by the cut-and-fill nature of the system, the incision was measured between Q₂ - Q₁, and Q₃ - Q₁. Cumulative incision between Q₂ - Q₁, is ~12 m, giving an average rate of 2.4 mm/yr between ~12 - 22 Kyr BP. Incision between the sole sampled Q₃ deposit dated and Q₂ deposits was not possible because they are found at the same elevations. Incision between the single datum for Q₃ - Q₁ is 12 m between 12 - 65 Kyr, giving a long-term rate of ~0.22 mm/yr.

3.3 IMPLICATIONS: TECTONICS

All the calculated incision rates for the Río Culebrinas are orders of magnitude higher than the 120 Kyr uplift rate of 0.03 - 0.05 mm/yr obtained from the 10 m marine terraces in Taggart & Joyce (1989). If the obtained incision rates were lower than the regional uplift rate, it could be assumed that the Río Culebrinas is flooring an active downthrown normal fault hanging wall block and that incision is being inhibited by local base level rise as. Assuming these rates are a product of uplift, this would imply that vertical land motion has accelerated during the last 65 Kyr. Evidence of accelerated uplift is suggested by the youngest marine terraces, found at 2 - 3 m above modern sea level, which have been dated to ~1.5 Kyr BP (Taggart & Joyce, 1989). Holocene sea level rise for the Caribbean demonstrates that sea level was at or near modern

datum by 1.5 Kyr BP (Khan et al., 2018), suggesting that the short-term incision rates are not likely to be a product of higher sea level. The long term incision rate (0.37 ± 0.03 mm/yr) calculated from the 65 Kyr Q₃ terrace is an order of magnitude greater than the long term uplift rate (0.03 - 0.05 mm/yr) and may tentatively be explained as a lag response or “catching up” of the system to some past perturbation.

This proposed forcing potentially related to the 65 Kyr terrace may be attributed to a variety of internal and external factors. Delayed incision may have been caused by a response to drainage network reorganization. For example, a period of internal drainage to a local non-marine base level followed by a connection with the ocean may lead to an increase in incision once the system breaks through and adjusts to a new lower base level. Elevated incision rates may also be related to stream piracy as stream power is raised by a rapidly increasing drainage network. The most probable case is that this proposed lag period may be attributed to periods of intense channel aggradation brought on by glacial and interglacial cycles (Bull, 1991) due to the cut-and-fill style of the Río Culebrinas system during the last 65 Kyr. The timing of the phase of aggradation can be discerned by comparing the results of this study with uplift rates of 0.6 - 1.0 m per 20 Kyr (Taggart & Joyce, 1989). Corrected long term incision rates indicate 4 - 5 m of incision per 20 Kyr. The discrepancy between rates suggests that the system is undergoing a lag response to a rapid base level fall occurring between 80 - 100 Kyr BP. This coincides with a global fall in sea level at the end of the last interglacial period (Fig.30) (Lambeck & Chapell, 2001), after which channel incision may have been inhibited by large influxes of sediment coupled with insufficient and erratic discharge within the system attributed to cooler and drier conditions in the region (Bull, 1991; Wegmann & Pazzaglia, 2002; Warken, 2018).

In conclusion, downward vertical movement occurring along the Río Culebrinas fault valley could not be discerned within the internal and external dynamics of the basin. Downward movement may have ceased as suggested by laterally consistent Quaternary valley fill thickness in seismic profile MCS ID-131-D (Fig.5B). The elevated rates of incision suggest that the system is undergoing a lag response due to past disturbances in its discharge and sediment supply prior to Q₂ deposition, and an increased uplift in the late Holocene as demonstrated by the accelerated rate of incision between Q₂ - Q₁ and marine terraces in western Puerto Rico (Taggart & Joyce, 1989).

3.4 IMPLICATIONS: PALEOCLIMATE

In the humid tropics, the last glacial maximum (LGM) has been characterized by a 50% reduction in rainfall and generally drier savannah-like conditions for the Sahel region, Central, and northern South America (Thomas & Thorpe, 1995). Globally, climatic conditions leading up to the LGM 80 - 22 Kyr BP were relatively arid and are characterized by reduced stream power and channel aggradation (Bull, 1991). Paleoclimate records from speleothems in northern Puerto Rico and Cuba (Fig.31) suggest that during the lead up to the LGM (Fig.30) the regional climate was drier and up to 2 - 4 °C cooler than today (Warken, 2017). Drier conditions directly affect vegetation cover, increasing the sediment load to system. They also affect stream power by decreasing the average discharge of the system, rendering it unable to transport the increasing amount of available sediment, driving channel aggradation (Bull, 1991) (Fig.32).

The Pleistocene-Holocene transition following the LGM is characterized by periods of intense climate variability and mass wasting events as the climate became wetter and rainfall increases outpaced vegetation recuperation (Thomas & Thorpe, 1995). Large paleo floods have

been globally recognized as occurring during a brief cooling period between 11 & 13 Kyr BP referred to as the younger and older Dryas (Thomas & Thorpe, 1995; Kock et al., 2009b; Keigwin et al., 2018). This short cooling triggered aggradational phases in rivers worldwide (Bull, 1991) and was followed by a return to warm humid conditions around 9 Kyr BP. This return to warmer conditions lead to the establishment of tropical forests by 7 Kyr BP, increasing fluvial incision by a combination of increasing stream power and the addition of sediment stored by the previous glacial conditions (Bull, 1991; Thomas & Thorpe, 1995). Both Q₁ and Q₂ generation terraces fall within these two distinct periods: Q₂ generation terraces date to precisely the end of the LGM, while the Q₁ generation terraces date to the younger and older Dryas.

This climatic interpretation can explain the apparent increase in incision and landform heights (Fig.28). The onset of colder drier conditions associated with glacial periods began around 80,000 yr BP. These conditions triggered an aggradational phase or “incision hiatus” in the system that lasted until the climax of the LGM around 22,000 yr BP. Landslide deposits along the escarpment to the north of the system supplied large amounts of clays and gravels to the system. Once glacial conditions began to wean, the return to warmer tropical conditions and climate change induced extreme precipitation events which triggered two waves of incision separated by brief periods of channel aggradation during the Older and Younger Dryas. It can be assumed then that the system is now adjusting to base level changes imparted by the significant eustatic changes associated with glacial cycles and with increased Holocene uplift in northwestern Puerto Rico.

3.5 $\delta^{13}\text{C}$ $\delta^{18}\text{O}$ STABLE ISOTOPE ANALYSIS OF KUPHUS INCRASSATUS AND OSTREA SP.

Of the 100+ specimens collected from 11 sites, 20 fell within the acceptable isotopic ranges for their modern marine counterparts (Table 3, Fig.33) (Lloyd, 1964; Tucker & Wright, 1990). $\delta^{18}\text{O}$ values ranged between -3.79‰ and -0.59‰ for $\delta^{18}\text{O}$, while $\delta^{13}\text{C}$ values ranged between -9.09‰ and -0.32‰. Fifteen of these specimens showed depleted $\delta^{13}\text{C}$ values but were not discarded for analysis. Depleted $\delta^{13}\text{C}$ values have been interpreted by Patterson & Walter (1994) to be a product of modified seawater in the organism's original habitat. This modification may be due to hypersaline lagoon settings with restricted seawater flow and environments near an input of fresh water. These depleted $\delta^{13}\text{C}$ values have been recorded in *Kuphus* skeletons present in other limestone units representing near shore, coastal lagoon, and fluvial; environments in both Puerto Rico and Hispaniola. In Puerto Rico (Fig.2) these are the San Sebastián Formation, parts of the Cibao Formation, and within the Ponce Limestone in Southern Puerto Rico (Ruidiaz-Santiago, 2013; Ortega-Ariza et al., 2015).

3.6 $^{87}\text{Sr}/^{86}\text{Sr}$ ISOTOPE ANALYSIS OF KUPHUS INCRASSATUS AND OSTREA SP.

Strontium Isotope analysis of skeletal powders of the marine bivalve species *Kuphus incrassatus* and *Ostrea sp.* (Table 3) from carbonate rocks in northwestern Puerto Rico returned ages between 11.45 ± 1.1 Ma and 15.95 ± 0.3 Ma based on the strontium seawater curve (McArthur, 2001) (Fig. 29,30). These results agree well with those obtained by Ortega-Ariza (2015) and Vicens (2016) and constrain the deposition of the rocks these fossils inhabited to the middle to late Miocene (Fig.2). This places the unit's stratigraphic position to the end of the Middle Cibao Formation and Aguada Limestone, interpreted as time equivalent deposits (Fig.2).

Field observations of the texture and composition of the rocks, as well as the fossils present (the presence of clastic material, terrigenous clays, chalky limestones, and the abundance of oyster beds in some of the locations), suggest the limestones in western Puerto Rico are part of the Cibao Formation, rather than the “pure” Aguada Limestone. Although the Cibao Formation, Aguada Limestone, and Aymamón Limestone are at least partially contemporaneous in their deposition, they represent a transition from the terrestrial/fluvial influenced environments in western Puerto Rico to those unaffected by nearshore sedimentation to the east respectively (Renken et al., 2002). It is hypothesized that the origin of the increase in clastic material westward is the product of a local highland in the area during that time (Fig.3) (Monroe, 1980; Renken et al., 2002). A pilot study of cobbles of fluvial origin underlying the limestones in western Puerto Rico tentatively suggest that their origin is in southwestern Puerto Rico (Vicens, 2016).

Carbonate fossil ages from sites in southern and southwestern Puerto Rico correlate well with those obtained by previous workers (Ruidiaz-Santiago, 2013; Ortega-Ariza et al., 2015). Ages based on $^{87}\text{Sr}/^{86}\text{Sr}$ from two samples of *Kuphus incrassatus* and *Ostrea sp.* collected at Playa Jaboncillo, Guánica (KF-JB) resulted between 15.50 ± 0.25 Ma and 15.70 ± 0.3 Ma, which date to the base of the Ponce Limestone. Ages based on $^{87}\text{Sr}/^{86}\text{Sr}$ for limestones in Guayanilla (Fig.29, KF-GY) obtained in this study range between 10.15 ± 0.75 Ma and 9.75 ± 0.70 Ma. Samples collected from stratigraphic intervals believed to be in the Ponce Limestone and located in the extreme southwestern corner of the island (Fig.29, KF-PS) returned dates between 6.15 ± 0.5 Ma and 6.40 ± 0.5 Ma, 6.15 ± 0.5 Ma. These samples were collected 10 m above sea level

and represent the youngest numerically verified stratigraphic position (this study) for the Ponce Limestone (Fig.2).

The ca. 15 Ma limestones in extreme western Puerto Rico are up to 500 m lower than their projected stratigraphic elevations from the similarly dated exposures of the Cibao Formation in northern Puerto Rico (this study KF-8). These discrepancies highlight off-shore crustal features in seismic profile MCS-50, (Fig.5A) (Chaytor & ten-Brink, 2010) and confirm the extension of these features into northwestern Puerto Rico. Although these features do extend landward into the Río Culebrinas fault valley, regional seismic profiling and basin stratigraphy indicate a near cessation of normal movement along the WPRFS. This interpretation is derived from the apparent evening out of younger reflectors in seismic profile MCS-151-D (Fig.5B) which suggest a termination in normal faulting, while old reflectors overlying the top of the hanging-wall dip to the north and decrease in and pinch out southward, indicating valley tilting to the north. The age discrepancies between KF-PS and those to the east in Guanica and Guayanilla may be due to downward movement imparted by the thoroughgoing North Boquerón Bay-Punta Montalva Fault Zone. This suggests that normal, N-S extensional fault motion may have continued for quite some time in south-western Puerto Rico and is being re-activated under local NE-SW extension.

These results indicate that subsidence associated with incipient north - south oriented extension along the WPRFS half-graben was already underway in the early Miocene and developed enough to lower the previously exposed non-carbonate basement rocks of a local highland into a marine environment. The course(s) of the north flowing river(s) responsible for the clastic material in western Puerto Rico (Vicens, 2016) ceased during the initiation of half-

graben style faulting marked by the transition from conglomerate to carbonate deposition. The asymmetry of the interpreted Miocene reflectors in MCS Line ID-131-D indicates that the system was active during deposition of these units, constraining the origins of the system to the beginning of carbonate deposition at around 15 Ma.

CHAPTER 4

CONCLUSIONS

Two controls dominate alluvial terrace deposition, abandonment, and incision in the humid tropics: Terrace deposition is controlled by climate induced changes in the rivers hydrology and sediment supply and are deposited during periods of cooler drier glacial conditions where discharge is erratic and insufficient to mobilize material deposited in and around the channel (Bull, 1991). Fluvial incision and terrace abandonment occur during wet humid interglacial conditions and high stream power. The rate of incision is controlled by tectonic uplift and will accommodate any vertical movement suppressed by periods of river aggradation.

Incision rates show no detectable signature of downward vertical motion along the Río Culebrinas fault valley. This correlates well with the laterally consistent Quaternary valley fill in seismic profiles, indicative of a cessation in down-slip movement. Micro seismicity occurring along these crustal features suggests that they may be re-activated under current regional stresses producing left-lateral strike slip motion similar to the NCPB. Previous studies show that the WPRFS in southwestern Puerto Rico is accommodating strike slip motion with a minor vertical component in the Holocene (Prentice & Mann, 2005; ten-Brink & López-Venegas, 2012). The cessation of half-graben extension may be related to the kinematic inversion from subsidence to uplift occurring around 5 Ma (Taggart & Joyce, 1989; Brocard et al., 2016).

Cumulative fluvial incision rates calculated from terraces within the Río Culebrinas fault valley range between 0.22 - 0.37 mm/yr for the older pre LGM deposits (Q₃), and between 1.36 -

2.60 mm/yr for younger terraces deposited during and after the LGM (Q₁ - Q₂). Although these rates are orders of magnitude higher than the 120 Kyr uplift rate of 0.03 - 0.05 mm/yr, cumulative incision between Q₁, Q₂, and the modern channel produce incision rates (Fig.29) that approach the tentative increase in uplift of ~2 mm/yr suggested by the 2 - 3 m marine terraces in northwestern Puerto Rico (Taggart & Joyce, 1989).

The discrepancy between the long term uplift and the long term incision rates may tentatively be described as a product of delayed landscape adjustment, as the system responds to climate induced changes in the system's hydrologic and sediment balance leading up to the LGM. Climate-induced forcing would have caused accelerated channel aggradation, initiated by cooler and drier conditions leading up to and during the LGM (Bull, 1991). This is supported by the similar vertical distribution and the cut-and-fill nature of Q₂ and Q₃ terraces which were deposited during this period (Fig.28). Local paleoclimate records indicate that during the last glacial period the climate in Puerto Rico was 2 - 4°C cooler than present (Warren, 2017) (Fig.31). Paleoclimate records reveal that precipitation was variable, but generally less frequent during this time (Thomas & Thorpe, 1995; Warren, 2017) leading to a decrease in the river's capacity to mobilize and transport its bed load, driving channel aggradation (Fig.32).

⁸⁷Sr/⁸⁶Sr isotope geochronology of limestone fossils in northwestern and southwestern Puerto Rico indicate a depositional age of Early to Late Miocene (16 - 6 Ma). Lithological and biostratigraphical markers in limestones in northwestern Puerto Rico indicate that they are indeed part of the Cibao Formation described in more eastern outcrops and validate the theory of the existence of a topographic high in western Puerto Rico prior to 15 Ma. It can be concluded that tectonic subsidence associated with the initiation of half-graben style extensional features

was incipient in the Early Miocene. This is contradictory to the theory that the Miocene was a time of tectonic quiescence for the region, and that the faulting was coeval to supposed arching of the PRVI microplate at 5 Ma.

Strontium isotope chronostratigraphy of limestones in western Puerto Rico by Ortega-Ariza et al. (2015) and this study (Fig.2) highlight a major hiatus in carbonate deposition occurring between 23 - 16 Ma. This break may tentatively be linked to an unknown regional tectonic event as it is also observed in Hispaniola. These results imply that Oligocene - Pliocene carbonate deposition was more complex than originally modelled (Monroe, 1980; Renken et al., 2002) and that more detailed chrono- and litho-stratigraphic studies are needed to better understand the depositional chronology of limestones and tectonic history of the region during the Late Oligocene - Miocene.

References:

- Adames, A.R., 2017, Geomorphic and Geophysical Characterization of the North Boquerón Bay-Punta Montalva Fault Zone, Master's Thesis, University of Puerto Rico Mayagüez, Department of Geology, 190 p.
- Aitken, M.J., 1985. Thermoluminescence Dating. Academic Press, 359 p.
- Aitken, M.J., 1998. An Introduction to Optical Dating. Oxford Science Publications, Oxford, UK, 267 p. ISBN 9780191589270.
- Asencio, E., 1980, Western Puerto Rico seismicity: U.S. Geological Survey Open-file Report 80-192, 135 p.
- Brocard, G.Y., Willenbrig, J.K., Miller, T.E., Scatena, F.N., 2016, Relict landscape resistance to dissection by upstream migrating knickpoints, *Journal of Geophysical Research: Earth Surface*, 22 p., DOI: 10.1002/2015JF003678
- Brocard, G.Y., Willenbrig J.K., Scatena F.N., Johnson A.H. (2015): Effects of a tectonically-triggered wave of incision on riverine exports and soil mineralogy in the Luquillo Mountains of Puerto Rico, *Applied Geochemistry*, DOI: 10.1016/j.apgeochem.2015.04.001, 13 p.
- Burbank, D. W., Leland, J., Fielding, E., Anderson, R.S., Brozovic, N., Reid, M.R., Duncan, C., 1996, Bedrock incision, rock uplift, and threshold of hillslopes in the northwestern Himalayas, *Nature*, 379, p. 505-510.
- Burke, K., 1988, Tectonic evolution of the Caribbean: *Annual Reviews*, no. 16, p. 201–30.
- Carbo, Andres, Cordoba, D., Martin Davila, J., ten Brink, U., Herranz, P., Von Hildebrandt, C., Payero, J., Munoz, Martin, A., Pazos A., Catalan, M., Granja, Jose Luis, Gomez, M., 2005, Survey explores active tectonics in northeastern Caribbean, *Eos, Transactions, American Geophysical Union* 86 (51), 537p.
- Burke, W.H., Denison, R.E, Hetherington, E.A, Koepnick, R.B., Nelson, H.F., Otto, J.B., 1982, Variaton of Seawater $^{87}\text{Sr}/^{86}\text{Sr}$ through Phanerozoic time, *Geology* 10, p. 516-519.
- Bull, W.B., 1979, Threshold of critical power in streams, *Geologic Society of America, Bull.*, 90, p. 453 – 454.
- Bull, W.B., 1991, *Geomorphic Responses to Climatic Change*, Blackburn Press, 326 p., ISBN-10:1-932846-21-2.
- Chaytor, J.D., and ten Brink, U.S., 2010, Extension in Mona Passage, Northeast Caribbean, *Tectonophysics*, v. 493, p. 74-92.
- Chaytor, J.D., ten Brink, U.S., 2014, Event sedimentation in low-latitude deep-water carbonate basins, Anegada passage, northeast Caribbean, *Basin Research*, doi: 10.1111/bre.12076

- Collins, B.D., Montgomery, D.R., Schanz, S.A., Larsen, I.J., 2016, Rates and mechanisms of bedrock incision and strath terrace formation in a forested catchment, Cascade Range, Washington, *Geological Society of America Bulletin*, 19 p., doi:10.1130/B31340.1
- DeMets, C., Jansma, P.E., Mattioli, G., Dixon, T.H., Farina, F., Bilham, R., Calais, E., Mann, P., 2000, GPS geodetic constraints on Caribbean-North America plate motion, *Geophysical Research Letters*, V. 27, NO. 3, p. 437-440.
- Erikson, J.P., Pindell, J.L., and Larue, D.K., 1990, Mid-Eocene–Early Oligocene sinistral transcurrent faulting in Puerto Rico associated with formation of the northern Caribbean plate boundary zone: *Journal of Geology*, v. 98, p. 365–384.
- Finnegan, N.J., Schumer, R., and Finnegan, S., 2014, A signature of transience in bedrock river incision rates over timescales of 104–107 years: *Nature*, v. 505, p. 391–394, doi:10.1038/nature12913.\
- Galbraith, R.F., Roberts, R.G., Laslett, G., Yoshida, H., Olley, J.M., 1999. Optical dating of single and multiple grains of quartz from Jinmium rock shelter, northern Australia: Part I, experimental design and statistical models. *Archaeometry* 41(2), p. 339-364.
- Gallen, S.F., Pazzaglia, F.J., Wegmann, K.W., Pederson, J.L., Gardner, T., 2015, The dynamic reference frame of rivers and apparent transience in incision rates, *Geology*, 4 p., doi:10.1130/G36692.1
- Gilles Y. Brocard, G.Y, Jane K. Willenbring, Thomas E. Miller, Frederik N. Scatena (2016): Relict landscape resistance to dissection by upstream migrating knickpoints. *Journal of Geophysical Research.*, DOI: 10.1002/2015JF003678
- Glover, L. III., 1971, *Geology of the Coamo area, Puerto Rico, and its relation to the volcanic arc trench association*: U.S. Geological Survey Prof. Paper 636, 102 p.
- Granja, J.L., U.S., Brink, A., Carbo, A., Munoz, M. Gomez, 2009, Morphotectonics of the central Muertos thrust belt and Muertos Trough (northeastern Caribbean), *Marine Geology*, no. 263, 1-4, p. 7-33.
- Granja, B., Muñoz-Martin, A., ten-Brink, U.S., Carbó-Gorosabel, A., Estrada, P.L., Martín-Dávila, J., Córdoba-Barba, D., Morollón, M., 2010, Gravity Modeling of the Muertos Trough and tectonic implications (north-eastern Caribbean), *Marine Geophysical Research*, Vol. 31, p. 263-283., doi: 10.1007/s11001-010-9107-8
- Grindlay, N.R., Mann, P., Dolan, J.F., van Gestel, 2005_a, Neotectonics and subsidence of the northern Puerto Rico-Virgin Islands margin in response to the oblique subduction of high-standing ridges, *Geological Society of America Special Paper* 385, p. 31-60.
- Grindlay, N.R., Abrams, L.J., Del Greco, L., Mann, P., 2005_b, Towards an integrated understanding of Holocene fault activity in western Puerto Rico: Constraints from high-resolution seismic and sidescan sonar data, *Geological Society of America Special Paper* 385, p. 139-160.

- Goren, L., 2016, A theoretical for fluvial channel response time during time-dependent climatic and its inverse applications, *Geophysical Research Letters*, 43, p. 10,753–10,763, doi:10.1002/2016GL070451.
- Hetzl, R., Niedermann, S., Tao, M., Kubil, P.W., Strecker, M.R., 2006, Climatic versus tectonic control on river incision at the margin of NE Tibet: ¹⁰Be exposure dating of river terraces at the mountain front of the Qilian Shan, *Journal of Geophysical Research*, Vol. 111, 13 p., F03012, doi:10.1029/2005JF000352
- Hippolyte, J., Mann, P., Grindlay, N.R., 2005, Geologic evidence for the prolongation of active normal faults of the Mona rift into northwestern Puerto Rico, *Geological Society of America Special Paper 385*, p. 161-171.
- Huérffano, V., von Hillebrandt-Andrade, C., Baez-Sanchez, G., 2005, Microseismic activity reveals two stress regimes in southwestern Puerto Rico, *Geological Society of America Special Paper 385*, p. 81-110.
- Hughes, K., 2016, River response to climate change in the Wet Tropics, northeast Queensland Australia, PhD Thesis, School of Geography, Planning and Environmental Management, University of Queensland, Australia, 211 p.
- Jansma, P.E., and Mattioli, G.S., 2005, GPS results from Puerto Rico and the Virgin Islands: Constraints on tectonic setting and rates of active faulting, *Geological Society of America Special Paper 385*, p. 13-30.
- Keigwin, L.D., Klotsko, S., Zhao, N., Reilly, B., Giosan, L., Driscoll, N.W., 2018, Deglacial floods in the Beaufort Sea preceded Younger Dryas cooling, *Nature Geoscience* Vol 11, 599-604, 8 p.
- Khan, N.S., Ashe, E., Horton, N.P., Dutton, A., Kopp, R.E., Brocard, G., Engelhart, S.E., Hill, D.F., Peltier, W.R., Vane, C.H., Scatena, F.N., 2017, Drivers of Holocene sea level in the Caribbean, *Quaternary Science Reviews* 115, p 12-36, DOI: 10.1016/j.quascirev.2016.08.032
- Kock, S., Kramers, J.D., Preusser, F. & Wetzel, A. 2009a: Dating of Late Pleistocene terrace deposits of the River Rhine using uranium series and luminescence methods: potential and limitations. *Quaternary Geochronology*. p. 363-373. doi: 10.1016/j.quageo.2009.04.002
- Kock, S., Huggenberger, P., Preusser, F., Rentzel, P., Wetzel, A., 2009b, Formation and evolution Of the Lower Terrace of the Rhine River in the area of Basel, *Swiss Journal of Geosciences*, 102, p. 307-321, doi:10.1007/s00015-009-1325-1.
- Koepnick, R.N., Burke, W.H., Denison, R.E., Hetherington, E.A, Nelson, H.F., Otto, J.B. & Waite, L.E., 1985 Construction of the seawater ⁸⁷Sr/⁸⁶Sr curve for, the Cenozoic and Cretaceous: supporting data. *Chem. Geol.* 58, p. 55-81.
- Krushensky, R.D., Schellekens, J.H., 1998, Geology of Puerto Rico, in *Geology, Geochemistry, Geophysics, Mineral Occurrences and Mineral Resource Assessment for the Commonwealth of Puerto Rico*, USGS Open-File Report 98-88, 337 p.

- Laó-Dávila, D.A., Llerandi-Román, P. A., 2015, Structural analysis of hanging wall and footwall blocks within the Río Guanajibo fold-and-thrust belt in Southwest Puerto Rico: *Int. J. Earth. Sci.*, Vol 106, Iss. 1, 6 p., doi: 10.1007/s00531-015-1290-z.
- Larue, D.K., Ryan, H. F., 1998, Seismic reflection profiles of the Puerto Rico Trench: Shortening between the North American and Caribbean plates, in Lidiak, E. G., and Larue, D. K., eds., *Tectonics and Geochemistry of the Northeastern Caribbean*, Boulder, Colorado, Geological Society of America Special Paper 322, p. 193–209.
- Larue, D.K., Draper, G., 1989, Extensional Tectonism in the Mona Passage, Puerto Rico and Hispaniola: A Preliminary Study, *Transactions of the 12th Caribbean Geological Conference*, St. Croix, U.S.V.I., p. 223-230
- Larue, D.K., Pierce, P., and Erikson, J., 1991, Cretaceous intra-arc summit basin on Puerto Rico, in Gillezeau, K. A., ed., *Transactions, 2nd Geological Conference of the Geological Society of Trinidad and Tobago: Port-of- Spain, Trinidad, April 3–8*, p. 184–190.
- Lambeck, K., Chappell, J., 2001, Sea Level Through the Last Glacial Cycle, *Science*, Vol. 292, 9 p.
- Leopold, L.B., and Bull, W.B., 1979, Base Level, Aggradation and Grade, in *American Philosophical Society Proceedings*, v.123, no.3, p.168-202.
- Lian, O.B., 2007. Luminescence Dating, in: *Encyclopedia of Quaternary Science*. Elsevier. 3576 p. 1491-1505, <https://doi.org/10.1016/B0-44-452747-8/00057-0>
- Limaye, Ajay B.S., Lamb, M.P., 2016, Numerical model predictions of autogenic fluvial terraces and comparison to climate change expectations, *Journal of Geophysical Research: Earth Surface*, Vol. 121, doi:10.1002/2014JF003392
- Lopez-Venegas, A.M., ten Brink, U.S., Geist, E., 2008, Submarine landslide as the source for the October 11, 1918 Mona Passage tsunami: Observations and modeling, *Marine Geology*, Vol. 254, n. 1-2, 12 p., doi: 10.1016/j.margeo.2008.05.001.
- Lloyd, R. M. 1964. Variations in the oxygen and carbon isotope ratios of Florida Bay mollusks and their environmental significance, *Journal of Geology*, Vol. 72: p. 84–111.
- Maier, K. L.; Klaus, J. S.; McNeill, D. F.; and Budd, A. F., 2007, A late Miocene low-nutrient window for Caribbean reef formation, *Coral Reefs* 26, p. 635–639.
- Mann, P., Prentice, C.S., Hippolyte, J., Grindlay, N., Abrahms. L.J., Lao-Davila, D., 2005_a, Reconnaissance study of Late Quaternary faulting along Cerro Goden fault zone, western Puerto Rico, *Geological Society of America Special Paper* 385, p. 115-137.
- Mann, P., Hippolyte, J.C., Grindlay, N.R., Abrams, L.J., 2005_b, Neotectonics of southern Puerto Rico and its offshore margin, *Geological Society of America Special Paper* 385, p. 173 - 214.
- Macklin, M.G., Lewin, J., Woodward, J.C., 2012, The fluvial record of climate change, *Philosophical Transactions of the Royal Society*, 370, p. 2143–2172, doi:10.1098/rsta.2011.0608

- Mallinson, D., 2008. A Brief Description of Optically Stimulated Luminescence Dating, <http://core.ecu.edu/geology/mallinsond/OSL>.
- McArthur, J.M. 1994. Recent trends in strontium isotope stratigraphy. *Terra Nova* 6:331–358.
- McArthur, J.M., Howarth, R.J., Bailey, T.R., 2001, Strontium isotope stratigraphy: LOWESS version 3: best fit to the marine Sr-isotope curve for 0-509 Ma and accompanying look-up for deriving numerical age, *Journal of Geology*, Vol. 109, p. 155-170.
- McArthur, J.M., Howarth, R.J., Shields, G.A., 2012, Strontium Isotope Stratigraphy, *in* *The Geologic Timescale*, Chapter 7, p. 128-129.
- McCann, 2002, Microearthquake Data Elucidate Details of Caribbean Subduction Zone, *Seismological Research Letters*, Vol. 73, No. 1, 8 p.
- McCann, W.R., 1985, On the earthquake hazards of Puerto Rico and the Virgin Islands: *Seismological Society of America Bulletin*, v. 75, p. 251–262.
- McIntyre, D.H., 1971, Geologic Map of the Central La Plata Quadrangle, Puerto Rico, U.S. Geological Survey Miscellaneous Investigations Map I-660, scale 1: 20,000.
- McNeill, D. F., Klaus, J. S., Budd, A. F., Lutz, B. P., and Ishman, S. E. 2012. Late Neogene chronology and sequence stratigraphy of mixed carbonate-siliciclastic deposits of the Cibao Basin, Dominican Republic. *Bull. Geol. Soc. Am.* Vol. 124, p. 35–58. <https://doi.org/10.1130/B30391.1>
- Merritts, D.J., and Vincent, K.R., 1989, Geomorphic response of coastal streams to low, intermediate, and high rates of uplift, Mendocino triple junction region, northern California: *Geological Society of America Bulletin*, v. 101, p. 1373–1388, doi:10.1130/0016-7606(1989)101<1373:GROCST>2.3.CO;2.
- Merritts, D.J., Vincent, K.R., Wohl, E.E., 1994, Long river profiles, tectonism, and eustasy: a guide to interpreting fluvial terraces, *Journal of Geophysical Research*, Vol. 88, No.B7, p. 14031-14050.
- Monroe W.H., 1969, Geologic Map of the Aguadilla Quadrangle, Puerto Rico, U.S. Geological Survey Miscellaneous Investigations Map I-569, scale 1: 20,000.
- Monroe W.H., 1980, Geology of the Middle Tertiary Formations of Puerto Rico, Geological Survey Professional Paper 953, 98 p.
- Murray, A.S., Marten, R., Johnston, A., Martin, P., 1987, Analysis for naturally occurring radionuclides at environmental concentrations by gamma spectrometry, *Journal of Radioanalytical and Nuclear Chemistry* 115(2), p. 263-288.
- Murray, A.S., Wintle, A.G., 2003, The single aliquot regenerative dose protocol: improvements in reliability, in *Radiation measurements*, No. 37, p377-381.
- Moussa, M.T., Seiglie, G.A., Meyerhoff, A.A., Taner, I., 1987, The Quebradillas Limestone (Miocene-Pliocene), northern Puerto Rico, and tectonics of the northeastern Caribbean Margin, *Geol. Soc. Am. Bul.* V. 99, p. 427-439.

- Nelson, M.S., Harrison, J.G., Johnson, J.A., Rittenour, T.M., Feathers, J.K., Mahan, S.A., 2015, User Guide for Luminescence Sampling in Archaeological and Geological Contexts, *Advances in Archaeological Practice* 3(2), p. 166-177, doi:10.7183/2326-3768.3.2.166
- Ortega-Ariza, D.L., 2009, Establishing A High-Resolution Sequence Stratigraphy & Sea Level Curve for Tertiary Limestones, Puerto Rico, Master's Thesis, University of Puerto Rico Mayagüez, Department of Geology, 198 p.
- Ortega-Ariza, D.L., Franseen, E.K., Santos-Mercado, H., Ramirez-Martinez, W.R., Core-Suarez, E.E., 2015, Strontium Isotope Stratigraphy for Oligocene-Miocene Carbonate Systems in Puerto Rico and the Dominican Republic: Implications for Caribbean Processes Affecting Depositional History, *Journal of Geology*, v. 123, no. 6, p. 539-560.
- Pagonis, V., Baker, A., Larsen, M., Thompson, Z., 2011, Precision and accuracy of two luminescence techniques for respective dosimetry: SAR-OSL and SAR-ITL, *Nuclear Instruments and Methods in Physics Research B*, 269, p. 653-663, doi: 10.1016/j.nimb.2010.10.029
- Patterson, W.P., and Walter, L. M. 1994. Depletion of ^{13}C in seawater ΣCO_2 on modern carbonate platforms: significance for the carbon isotopic record of carbonates, *Geology*, Vol. 22, p. 885–888.
- Pazzaglia, F.J., 2013, Fluvial terraces, in Shroder, J.F., ed., *Treatise on geomorphology Volume 9: Fluvial geomorphology*: San Diego, Academic Press, p. 379–412, doi:10.1016/B978-0-12-374739-6.00248-7.
- Pederson, J.L., Anders, M.D., Rittenhour, T.M., Sharp, W.D., Gosse, J.C., Karlstrom, K.E., 2006, Using fill terraces to understand incision rates and evolution of the Colorado River in eastern Grand Canyon, Arizona, *Journal of Geophysical Research*, Vol. 111, F02003, doi:1029/2004JF000201, 10p.
- Pederson, J., Burnside, N., Shipton, J., Rittenhour, T., 2013, Rapid river incision across an inactive fault- implications for patterns of erosion and deformation in the central Colorado Plateau, *Lithosphere* Vol. 5, p. doi: 11.1130/L282.1 513-520, doi: 11.1130/L282.1
- Piety, L.A., Redwine, J.R., Derouin, S.A., Prentice, C.S., Kelson, K.I., Klinger, R.E., Mahan, S., 2018, Holocene Surface rupture on the Salinas Fault and Southeastern Great Southern Puerto Rico Fault Zone, South Coastal Plain of Puerto Rico, *Bulletin of the Seismological Society of America*, Vol. 108, No. 2, 22 p. doi: 10.1785/0120170182
- Pindell, J. L., and Barrett, S. F., 1990, Geological evolution of the Caribbean region: a plate tectonic perspective, in Dengo, G., and Case, J. E., eds., *The Caribbean region*: Boulder, Colorado, Geological Society of America, *The Geology of North America*, v. H, p. 405-432.
- Prentice, C.S., Mann, P., 2005, Paleoseismic study of the South Lajas fault: First documentation of an onshore Holocene fault in Puerto Rico, *Geological Society of America Special Paper* 385, p. 215-222.

- Preusser, F., Degering, D., Fuchs, M., Hilgers, A., Kadereit, A., Klasen, N., Krbetschek M., Richter, D., Spencer, J.Q.G., 2008, Luminescence dating: basics, methods, and applications, *Eiszeitalter und Gegenwart Quaternary Science Journal*, Vol. 57, 1-2, p. 95-149.
- Ramírez, W. R., Johnson, C., Martin vez, M., Torres, M., Ortiz, V.; and Velez, J. 2006. Strontium isotope stratigraphy from *Kuphus incrassatus*, Cenozoic limestones, Puerto Rico. Abstract. In *Geol. Soc. Am. Annual Meeting, Abstracts with Program*, 39: 90.
- Reid, J., Plumley, P.W., and Schellekens, J.H., 1991, Paleomagnetic evidence for Late Miocene counterclockwise rotation of north coast carbonate sequence, Puerto Rico: *Geophysical Research Letters*, v. 18, p. 565–568.
- Renken, R.A., Ward., I.P., Gómez-Gómez, F., 1994, Potentiometric Surfaces of the Upper and Lower Aquifers, North Coast Limestone Aquifer System, Puerto Rico, U.S. Geological Survey Open File Report 93-499, 15 p.
- Renken, R.A., Ward., I.P., Gómez-Gómez, F., Rodríguez-Martínez, J., 2002, Geology and hydrogeology of the Caribbean islands aquifer system of the Commonwealth of Puerto Rico and the U.S. Virgin Islands, U.S. Geological Survey Professional Paper 1419, ISBN 0-607-99361-8, 139 p.
- Roberts, R.G., Galbraith, R.F., Yoshida, H., Laslett, G.M., Olley, J.M., 2000, Distinguishing dose populations in sediment mixtures: a test of single-grain optical dating procedures using mixtures of laboratory-dosed quartz, Vol. 32, Issues 5–6, p. 459-465.
- Robinson, E. 2004. Zoning the White Limestone Group of Jamaica using larger foraminiferal general a review and proposal. In Donovan, S. K., ed. *The Mid-Cainozoic White Limestone Group of Jamaica. Cainozoic Res.* 3, p. 39–75.
- Rodríguez-Martínez, J., 1997, Characterization of Springflow in the North Coast Limestone of Puerto Rico Using Physical, Chemical, and Stable Isotopic Methods, U.S. Geological Survey Water-Resources Investigations Report 97-4122, 53 p.
- Rodríguez-Martínez, J., Richards, R.T., 2000, Detection of Conduit-Controlled Groundwater Flow in Northwestern Puerto Rico Using Aerial Photograph Interpretation and Geophysical Methods, U.S. Geological Survey Water-Resources Investigations Report 00-4147, 45 p.
- Rodríguez-Martínez, J., 1995, Hydrogeology of the North Coast Limestone Aquifer System, U.S. Geological Survey Water-Resources Investigations Report 94-4249, 22 p.
- Rodríguez-Martínez, J., Hartley, J.L., 1994, Geologic and Hydrologic Data Collected at Test Holes NC-6 and NC-11, Hatillo and Isabella, Northwestern Puerto Rico, U.S. Geologic Survey, Open-File Report 93-465, 39 p.
- Román-Más, A., Lee, R.W., 1987, Geochemical Evolution of Waters Within the North Coast Limestone Aquifers of Puerto Rico: A Conceptualization Based on a Flow Path in the Barceloneta Area, U.S. Geologic Survey Water-Resources Investigations Report 86-4080, 28 p.

- Roig-Silva, C.M., Joyce, J., Ascencio, E., 2013, The Northwest Trending North Boquerón Bay-Punta Montalva Fault Zone: A Through Going Active Fault System in Southwestern Puerto Rico, *Seismological Research Letters*, Vol. 84, No. 3, 13 p., doi: 10.1785/0220120115
- Ruidiaz-Santiago, C. M. 2013. Facies distribution model and sequence stratigraphic model of mid Tertiary rocks exposed in east side of Guanica Bay, Puerto Rico. MS thesis, University of Puerto Rico, Mayaguez, 125 p.
- Sadler, P.M., 1981, Sediment accumulation rates and the completeness of stratigraphic sections, *Journal of Geology*, v. 89, p. 569–584, doi:10.1086/628623.
- Schaller, M., Hovius, N., Willet, S.D., Ivy-Ochs, S., Synal, H.-A., Chen, M.-C., 2005, Fluvial bedrock incision in the active mountain belt of Taiwan from in situ-produced cosmogenic nuclides, *Earth Surface Processes and Landforms*, 30,995-971, DOI: 10.1002/esp.1256, 17 p.
- Schumm, S.A., 1973, *Geomorphic thresholds and complex response of drainage systems*, *Fluvial Geomorphology*, Publications of Geomorphology, State University of New York, Binghamton, p. 299-310.
- Schumm, S.A., 1993, River Response to Baselevel Change: Implications for Sequence Stratigraphy, *Journal of Geology*, Vol. 101, P. 279-294.
- Smith, A. L., Schellekens, J. H., 1998, Batholiths as markers of tectonic change in the northeastern Caribbean, in Lidiak, E. G., and Larue, D. K., eds., *Tectonics and Geochemistry of the Northeastern Caribbean*, Boulder, Colorado, Geological Society of America Special Paper 322, p. 99–222.
- Snyder, N.P., Whipple, K.X., Tucker, G.E., and Merritts, D.J., 2000, Landscape response to tectonic forcing: Digital elevation model analysis of stream profiles in the Mendocino triple junction region, northern California: *Geological Society of America Bulletin*, v. 112, p. 1250–1263,
- Snyder, N.P., Whipple, K.X., Tucker, G.E., Merritts, D.J., 2002, Interactions between onshore bedrock-channel incision and nearshore wave-base erosion forced by eustasy and tectonics, *Basin Research*, Vol. 14, p 105-127.
- Solares, M.M., 2019, *New Constraints on Crustal Deformation within the Puerto Rico-Virgin Islands Microplate Using Two Decades of GPS Data*, Unpublished MS Thesis, Department of Geology, UPRM, 129 p.
- Stokes, S., (1999). Luminescence dating applications in geomorphological research. *Geomorphology* 29(1), 153-171.
- Taggart, B.E, and Joyce, J., 1989, Radiometrically dated terraces on Northwestern Puerto Rico, in Larue, D.K., and Draper, G., eds., *Transaction of the 12th Caribbean Conference*, St. Croix, U.S.V.I, Miami-Caribbean Geological Society.
- ten Brink, U., 2005, Vertical Motions of the Puerto Rico trench and Puerto Rico and their causes, *Journal of geophysical Research*, Vol. 110, 16 p., doi:10.1029/2004JB003459

- ten Brink, U., López-Venegas, A.M., 2012, Plate interactions in the NE Caribbean Subduction zone from continuous GPS observations, in *Geophysical Research Letters*, Vol. 39, doi:10.1029/2012GL051485, 6 p.
- Thomas, M.F., Thorp, M., 1995, Geomorphic Response to Rapid Climatic and Hydrologic Change during the Late Pleistocene and Early Holocene in the Humid and Sub-Humid tropics, *Quaternary Science Reviews*, Vol 14, p 193-207, doi: 0277-3791/95.
- Torres, M.C., 2009, A fluid inclusions study of Puerto Rico Tertiary dolomite, Master's Thesis, University of Puerto Rico Mayagüez, Department of Geology, 123 p.
- Troester, J.W., 1999, Geochemistry and Hydrogeology Framework of the Saline-Freshwater Interface and the Calculation of Net Recharge in the Dorado Area, North-Central Puerto Rico, U.S. Geological Survey Water-Resources Investigations Report 98-4030, 36 p.
- Tucci, P., Martínez, M.I., 1995, Hydrology and Simulation of Ground-Water Flow in the Aguadilla to Río Camuy Area, Puerto Rico, U.S. Geological Survey Water-Resources Investigations Report 95-4028, 39 p.
- Tucker, M.E., 1990. Diagenetic processes, products and environments. In Tucker, M. E., and Wright, V. P., eds. *Journal of Geology Carbonate sedimentology*, Oxford, Blackwell Science, p. 314–364.
- Tucker, M.E., Wight, V.P., 1990, *Carbonate Sedimentology*: Oxford, Blackwell Science Ltd, 482 p.
- Tuttle, M.P., Schweig, E.S., Prentice, C.S., Moya, J.C., Tucker, K.B., 2005, Liquefaction induced by historic and prehistoric earthquakes in western Puerto Rico, *Geological Society of America Special Paper* 385, p. 263-276.
- Tobisch O.T., Turner M.D., 1971, *Geologic Map of the San Sebastián Quadrangle, Puerto Rico*, U.S. Geological Survey Miscellaneous Geologic Investigations Map I-661, scale 1: 20,000.
- Vail P.R., Mitchum R.M Jr., Todd R.G., Widmier J.M., Thompson S. III, et al. 1977, Seismic stratigraphy and global changes of sea level, See Payton 1977, p. 49-212.
- van Benthem, S., Govers, R., Spakman, W., Wortel, R., 2013, Tectonic evolution and mantle structure of the Caribbean, *Journal of Geophysical Research: Solid Earth*, Vol 118, 3019-3036, doi:10.1002/jgrb.50235
- van Benhtem. S., Govers, R., Wortel, R., 2014, What drives microplate motion and deformation in the northeastern Caribbean plate boundary region, *Tectonics*, 33,850-873, doi: 10.1002/2013TC003402
- van Gestel, J.P, Mann, P., Grindlay, N.R., Dolan, J.F., 1990, Three-phase tectonic evolution of the northern margin of Puerto Rico as inferred from integration of seismic reflection, well, and outcrop data, *Marine Geology*, 161, p. 257-286.
- van Gestel, J.P., Mann, P., Dolan, J.F., and Grindlay, N.R., 1998, Structure and tectonics of the upper Cenozoic Puerto Rico–Virgin Islands carbonate platform as determined from

- seismic reflection studies: *Journal of Geophysical Research*, v. 103, p. 505–30, doi: 10.1029/98JB02341.
- Veizer, J. 1983. Trace elements and isotopes in sedimentary carbonates. In Reeder, R. J., ed. *Carbonates: mineralogy and chemistry*. *Rev. Mineral.* 11., p. 265–299.
- Vicens, E.C., 2016, *Petrology and Stable Isotope Analyses of Kuphus incrassatus samples from Rincón, Puerto Rico*, Undergraduate Research, University of Puerto Rico Mayagüez, Department of Geology, UPRM. 24p.
- Ward, W. C.; Scharlach, R. A.; and Hartley, J. R. 2002, *Geology of the north coast ground-water province of Puerto Rico*, In Renken R. A. et al., eds. *Geology and hydrogeology of the Caribbean-islands aquifer system of the commonwealth of Puerto Rico and the U.S. Virgin Islands*. U.S. Geological Survey Professional Paper 1419, p. 45–76.
- Warken, S.F., 2017, *Potentials and limitations of multi-proxy records in speleothem research*, Ph. D Thesis, Faculties for the Natural Sciences and for Mathematics, Ruperto-Carola University of Heidelberg, Germany, 284 p.
- Wegmann, K.W., Pazzaglia, F., 2002, *Holocene strath terraces, climate change, and active tectonics: The Clearwater River basin, Olympic Peninsula, Washington State*, *GSA Bulletin*, v. 114; no. 6; p. 731–744, DOI: 10.1130/0016-7606(2002)114<0731:HSTCCA>2.0.CO;2
- Western Geophysical Company of America and Fugro, Inc., 1973, *Geological-geophysical reconnaissance of Puerto Rico for siting of nuclear power plants: San Juan, Puerto Rico*, The Puerto Rico Water Resources Authority, 127 p.
- Yang, L., Wang, G., Huérfano, V., von Hillebrandt-Andrade, C.G., Martínez-Cruzado, J.A., 2016, *GPS geodetic infrastructure for natural hazards study in the Puerto Rico and Virgin Islands region*, *Natural Hazards*, DOI 10.1007/s11069-016-2344-7, 26 p.

Figures

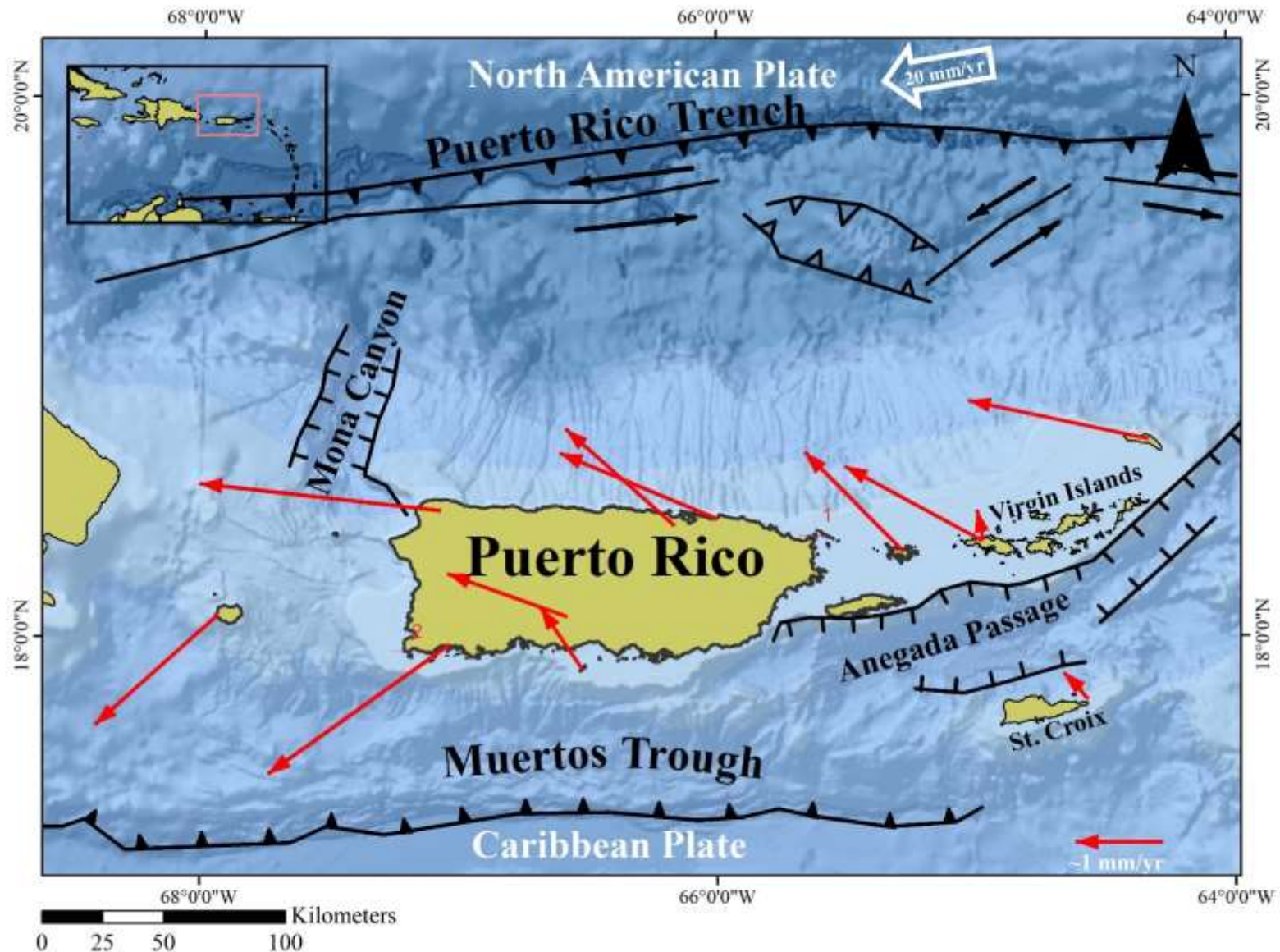


Figure 1: Geographic and Tectonic setting of Puerto Rico (modified from Granja et al., 2010). Extensional features like the Aneгада and Mona Passage lie to the east and west respectively. To the north is the major tectonic plate boundary between the North American and Caribbean plates, accommodating $20 \pm 3 \text{ mm yr}^{-1}$ of highly oblique convergence. South of the island is the Muertos, a failed subduction zone. Red arrows represent GPS site movement with respect to a fixed Caribbean Plate reference from ten Brink & López Venegas (2012).

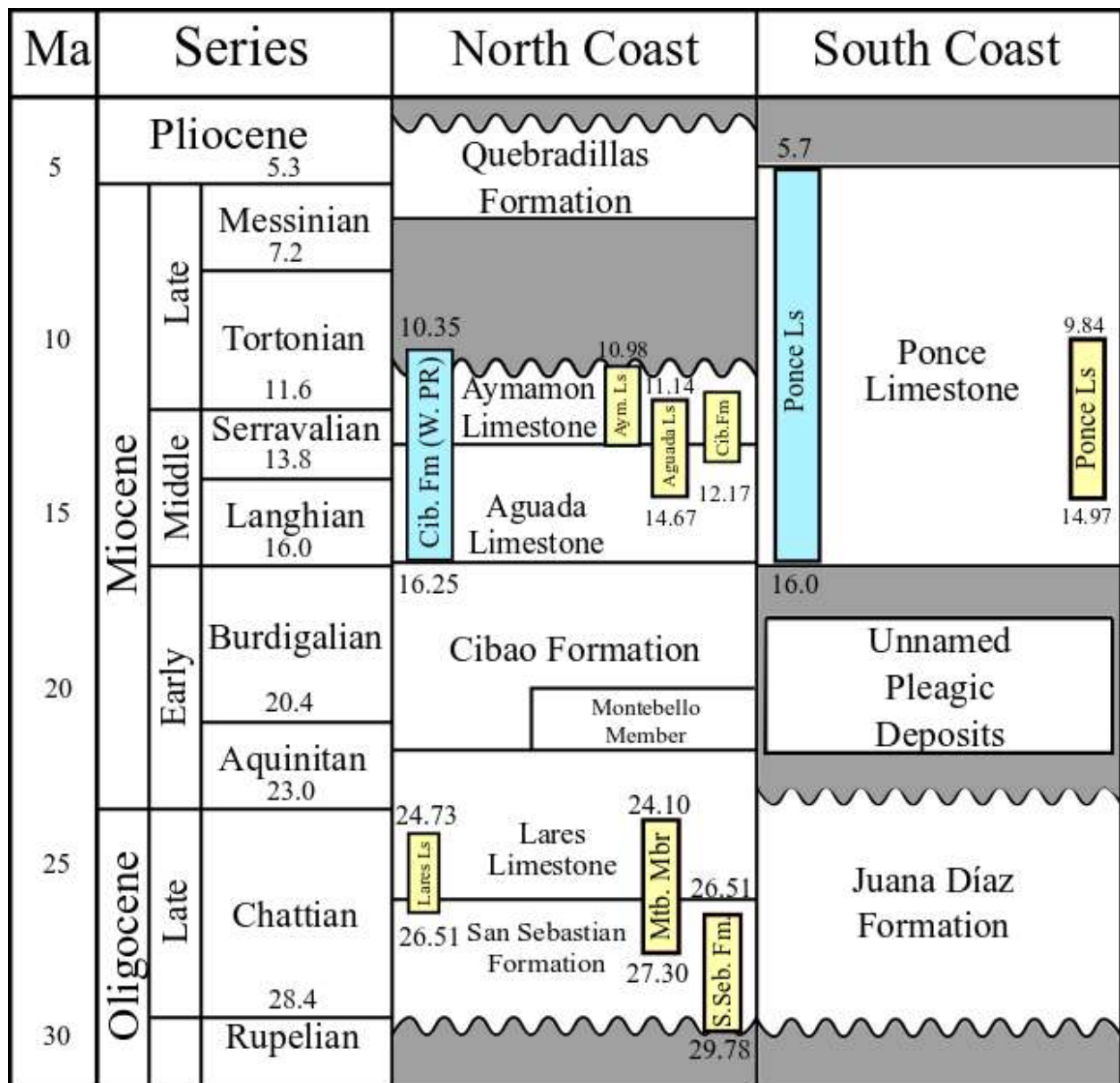


Figure 2: Lithostratigraphic correlations between the North and South coast limestone units with chronostratigraphy by Ortega-Ariza et al. (2015) (yellow rectangles) and this study (blue rectangles). Maximum and minimum age error included in bar. Stratigraphic column modified from Ortega-Ariza et al. (2015). North Coast stratigraphy from Renken et al. (2002), South Coast stratigraphy off Ward et al. (2002). Ages by Ortega-Ariza et al. (2015) and this study indicate that the Aymamón-Aguada Limestones and the late Cibao Formation were deposited coevally in northern Puerto Rico and are contemporaneous with the Ponce Limestone in southwestern Puerto Rico.

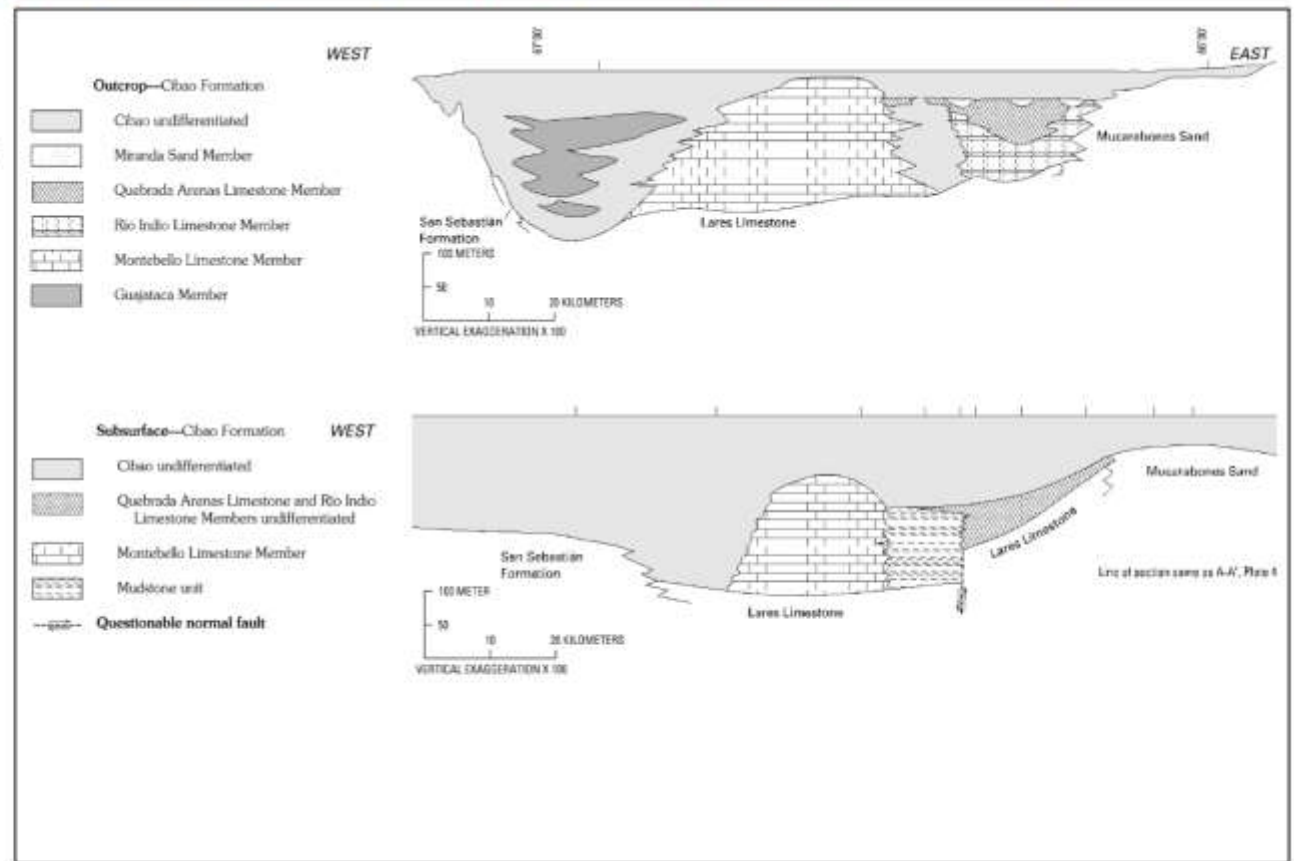
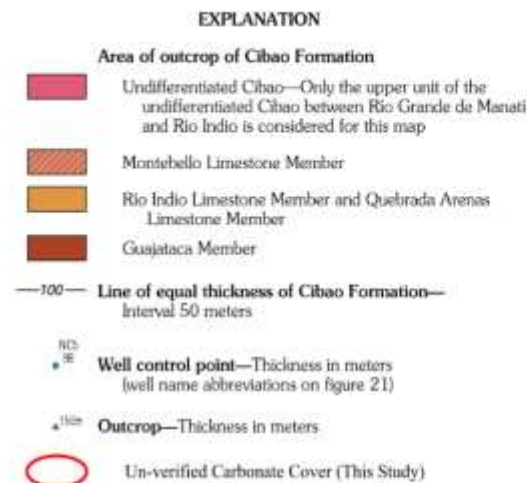
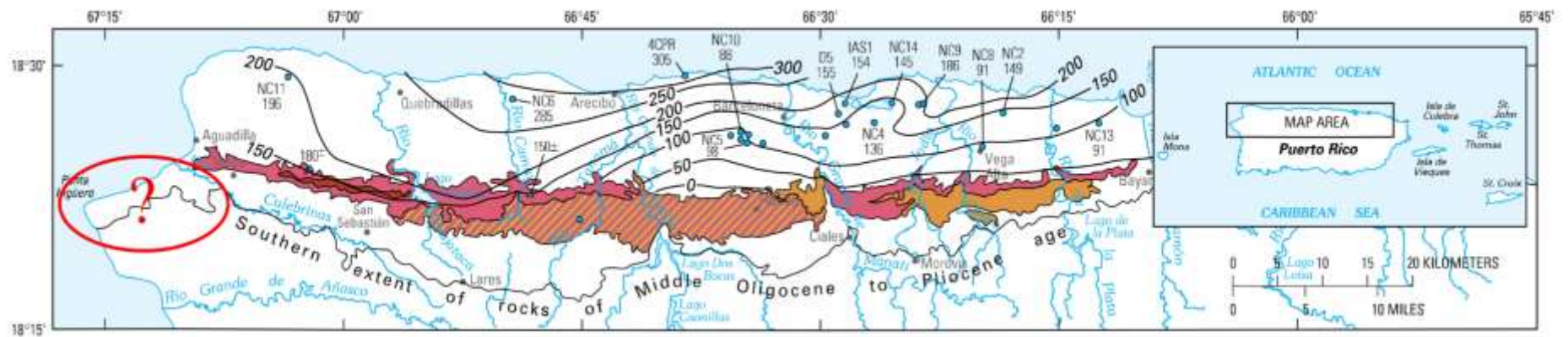


Figure 3: *Top:* Map of the outcrop extent of the Cibao Formation and its Members and the southernmost limit of Tertiary carbonate rocks in northern Puerto Rico. *Right:* East - West profiles showing outcrop thickness at the surface and subsurface. In extreme western Puerto Rico, the lower two limestone units The Lares Limestone and San Sebastian Formation are both absent and the Cibao Formation Rests unconformably on Eocene-Oligocene basement rocks. Image modified from Renken et al. (2002).

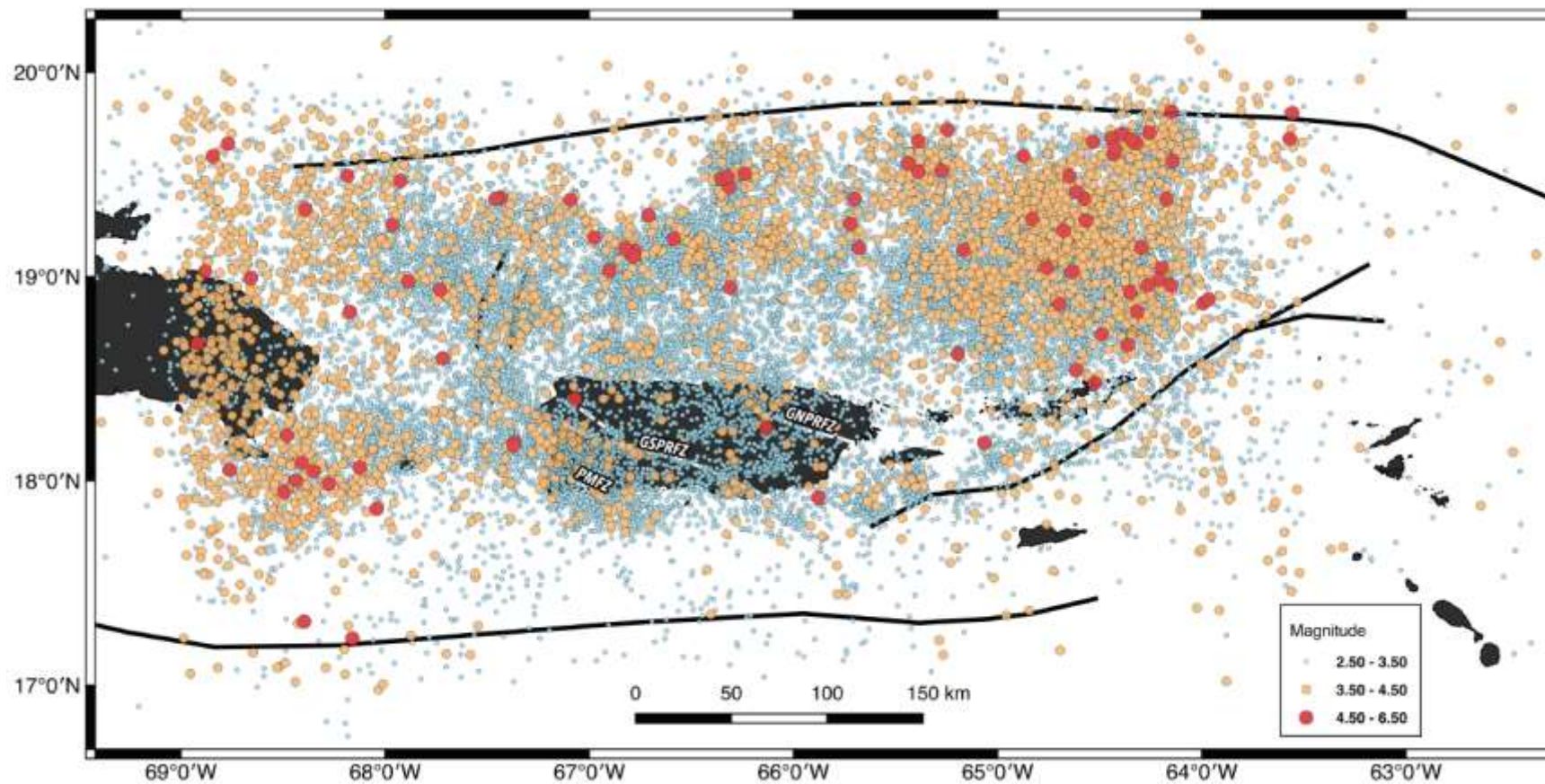


Figure 4: Seismicity map of the PRVI region showing seismic events between 1994 - 2017 (magnitude 2.5 - 6.6). Figure from Solares (2019). *GN/SPRFZ* = Great Northern Puerto Rico Fault Zone and Great Southern Puerto Rico Fault Zone and *PMFZ* = North Boquerón Bay–Punta Montalva Fault Zone.

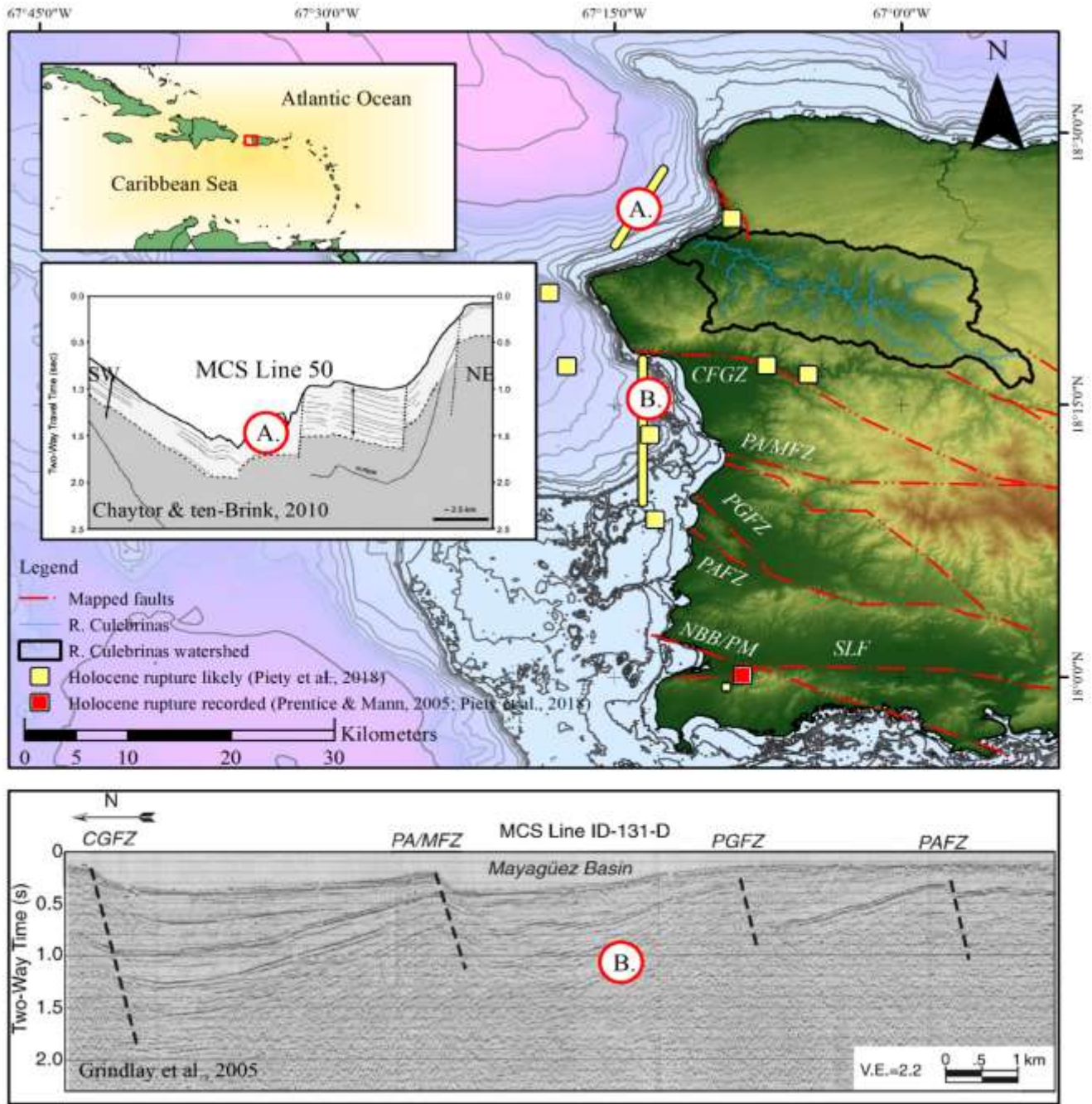


Figure 5: Summary map of faulting in western Puerto Rico. A.) MCS Line 50 shows north-tilted carbonate cap overlying tilted basement rocks of downthrown block. Faults extend into northwestern Puerto Rico and the target area of this study. B.) MCS Line-131-D shows half-graben style faulting South of study area along the Cerro Goden (*CFZ*), Punta Algarrobo/ Mayaguez (*PA/MFZ*), Punta Guanajibo (*PGFZ*), and Punta Arenas Fault Zones (*PAFZ*). Basin fill becomes more symmetrical in thickness in younger Holocene-Pleistocene sediments suggesting a cease in vertical movement in recent times. Trenching and geophysical studies in southwestern Puerto indicate Holocene rupture in at least two sites along the South Lajas Fault (*SLF*) and the North Boquerón Bay-Punta Montalva Fault Zone (*NBBPM*).

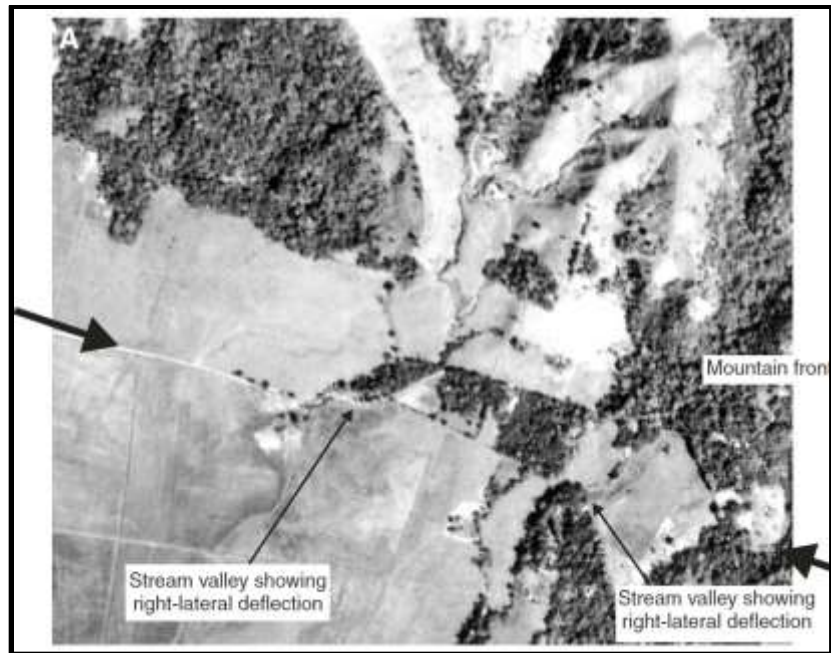


Figure 6: 2001 aerial photo from Mann et al. (2005_a) showing right-lateral displacement of streams along the inferred trace of the Cerro Goden Fault of the WPRFS.

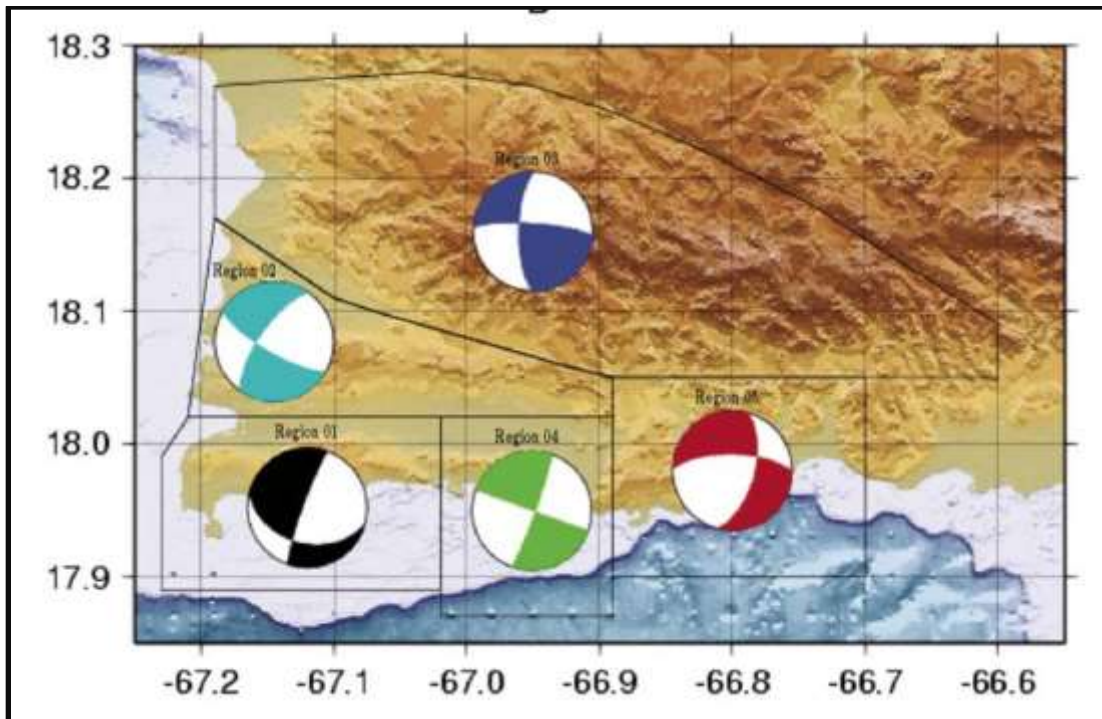


Figure 7: Composite focal mechanisms computed for southwestern Puerto Rico showing left-lateral dominant motion, Image from Huerfano et. Al (2005).

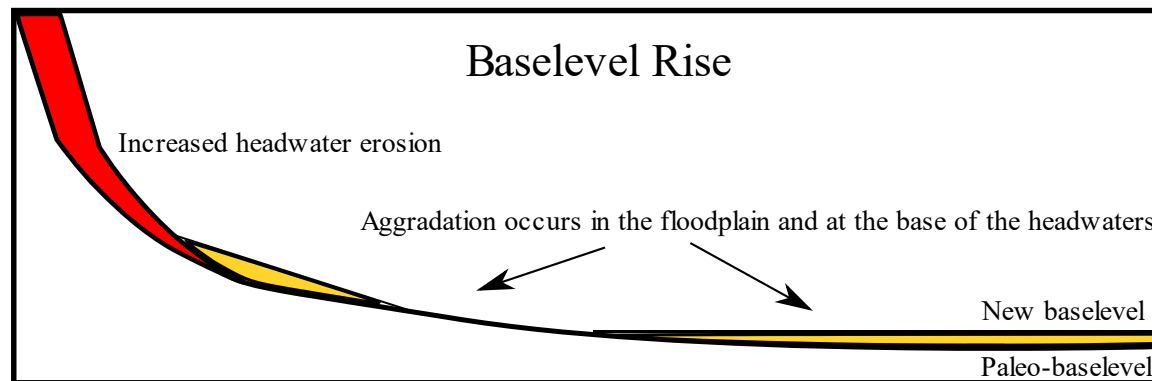
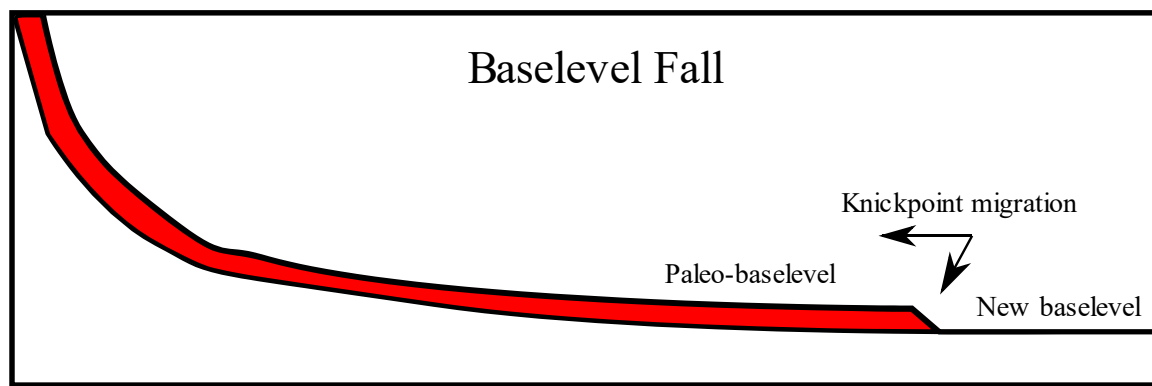
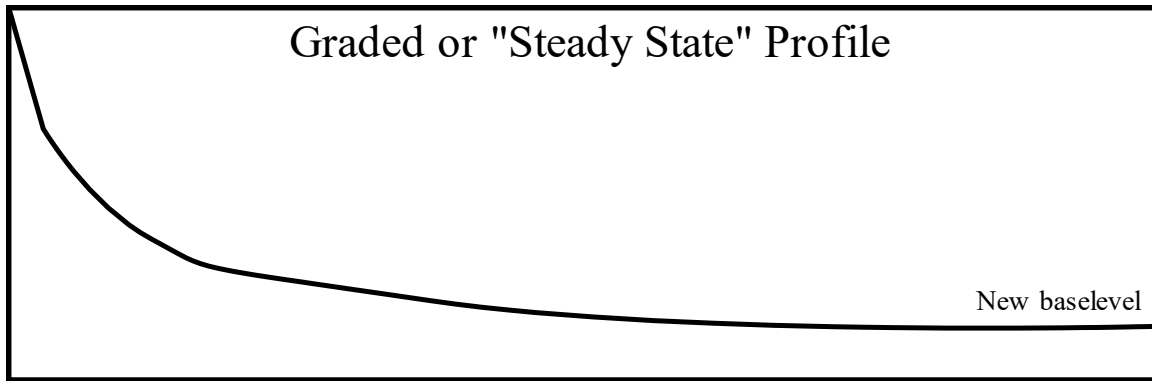


Figure 8: Vertical channel response to changes in base level. *Top:* Profile shows a graded state for systems in equilibrium where the total sediment budget is equal to that which the system can transport, *Middle:* Profile adjustment to the effects of base level fall, Knickpoints migrate upstream from the mouth of the river and incision occurs along most of the channel. *Bottom:* Profile adjustment to base level rise. Incision is heightened in the headwaters, Aggradation occurs at the base of the headwaters there is a change in slope, hence less energy for transport, and in the flood plain reaches.

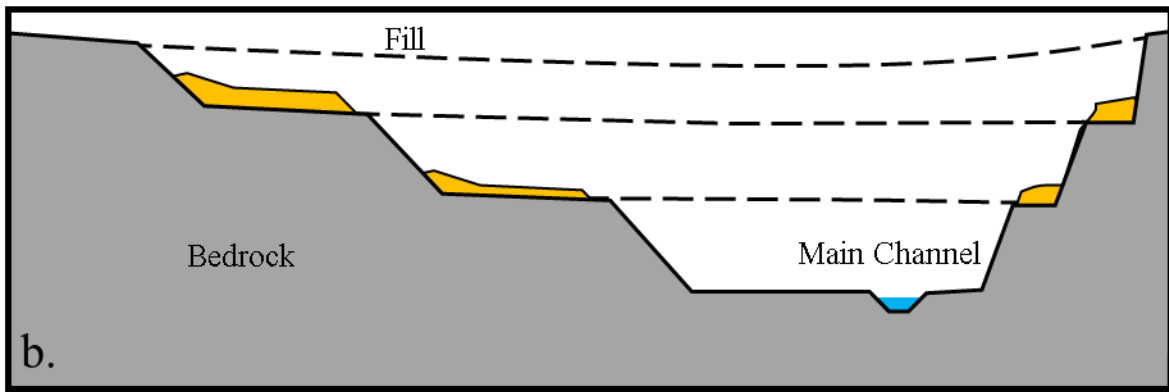
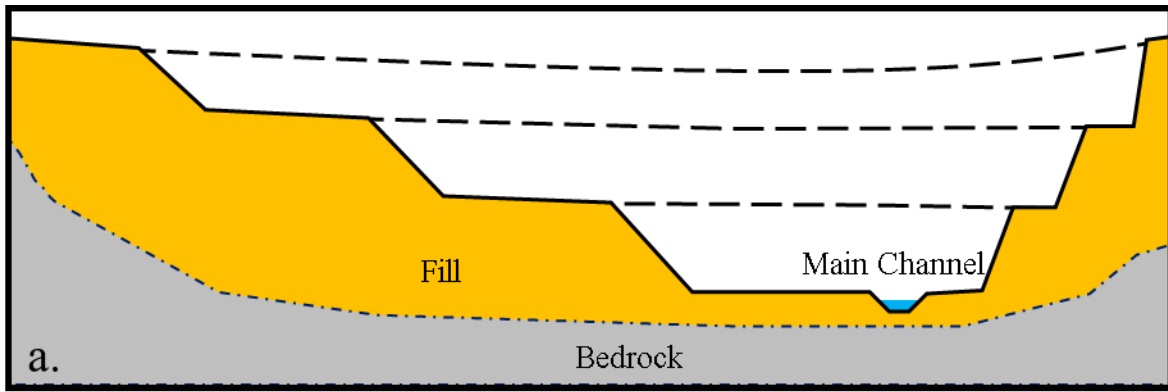


Figure 9: a.) Fill Terrace, characterized by loose alluvial deposits representing periods of aggradation followed by vertical incision, and b.) Strath Terrace, characterized by little to no alluvium overlying bedrock planation surfaces. Strath terraces represent periods of stability and lateral erosion via meanders and cut-banks.

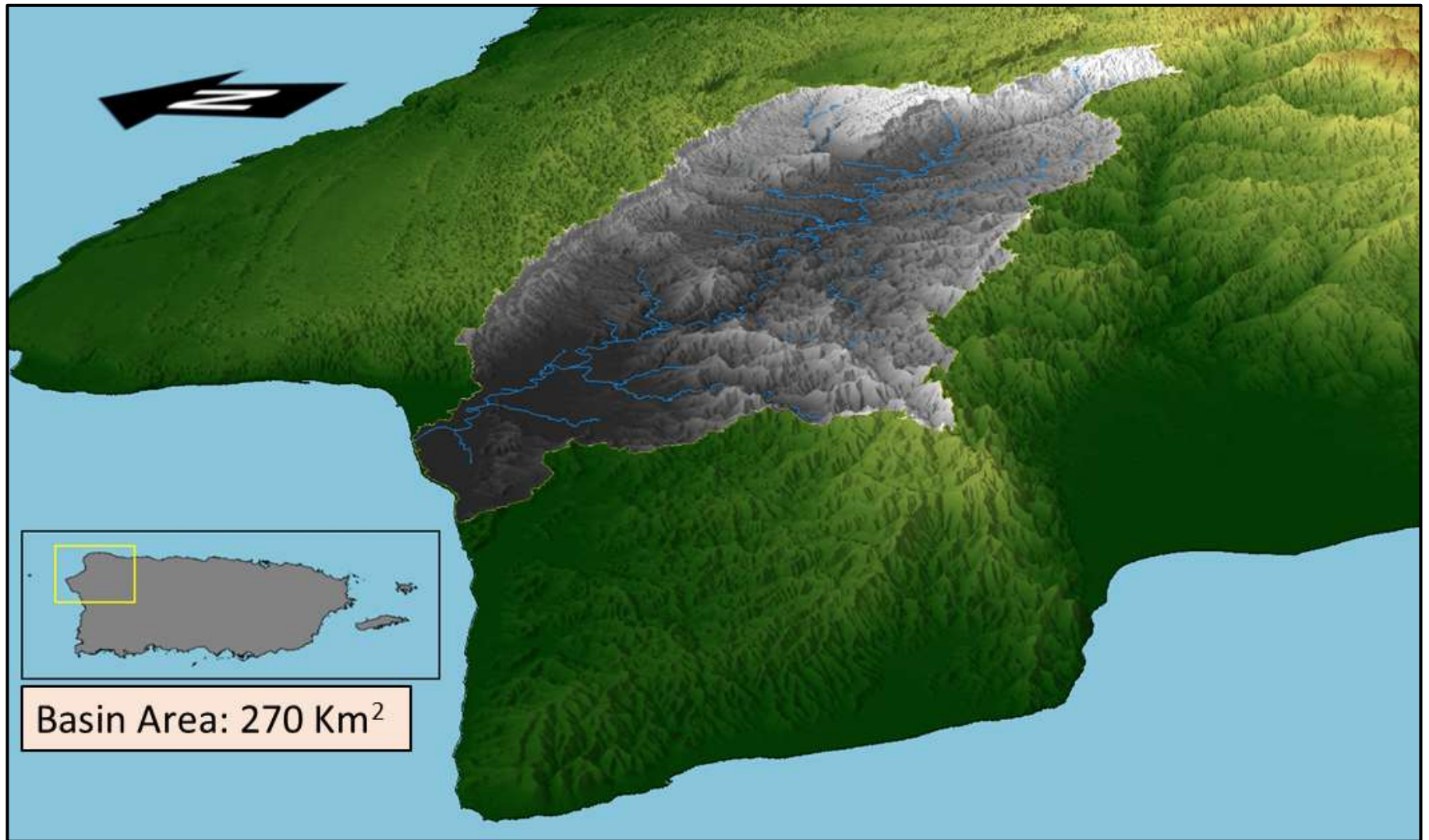


Figure 10: DEM derived 3D topographic model of the Río Culebrinas Basin showing the main channel of the river and its tributaries.

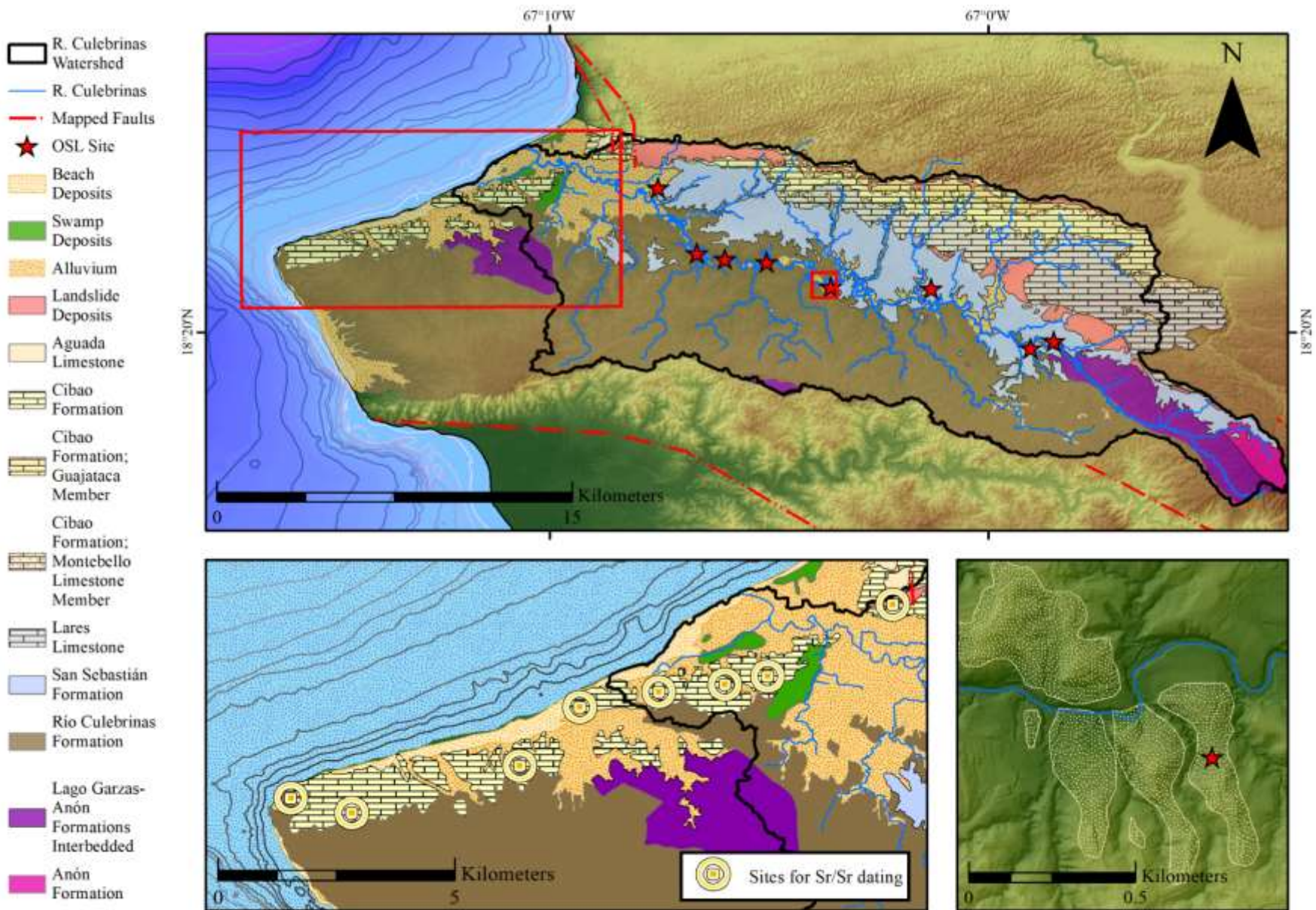


Figure 11: (Top) Map showing the extent of the study area and the Río Culebrinas Basin. Locations of OSL sites are marked as red stars. Red dashed lines show mapped fault traces to the ESE and WNW. Bottom right: Fluvial terraces mapped by McIntyre (1971). Bottom left: Carbonate cover in extreme western Puerto Rico believed to be coeval with the initiation of N-S extension along the WPRFS

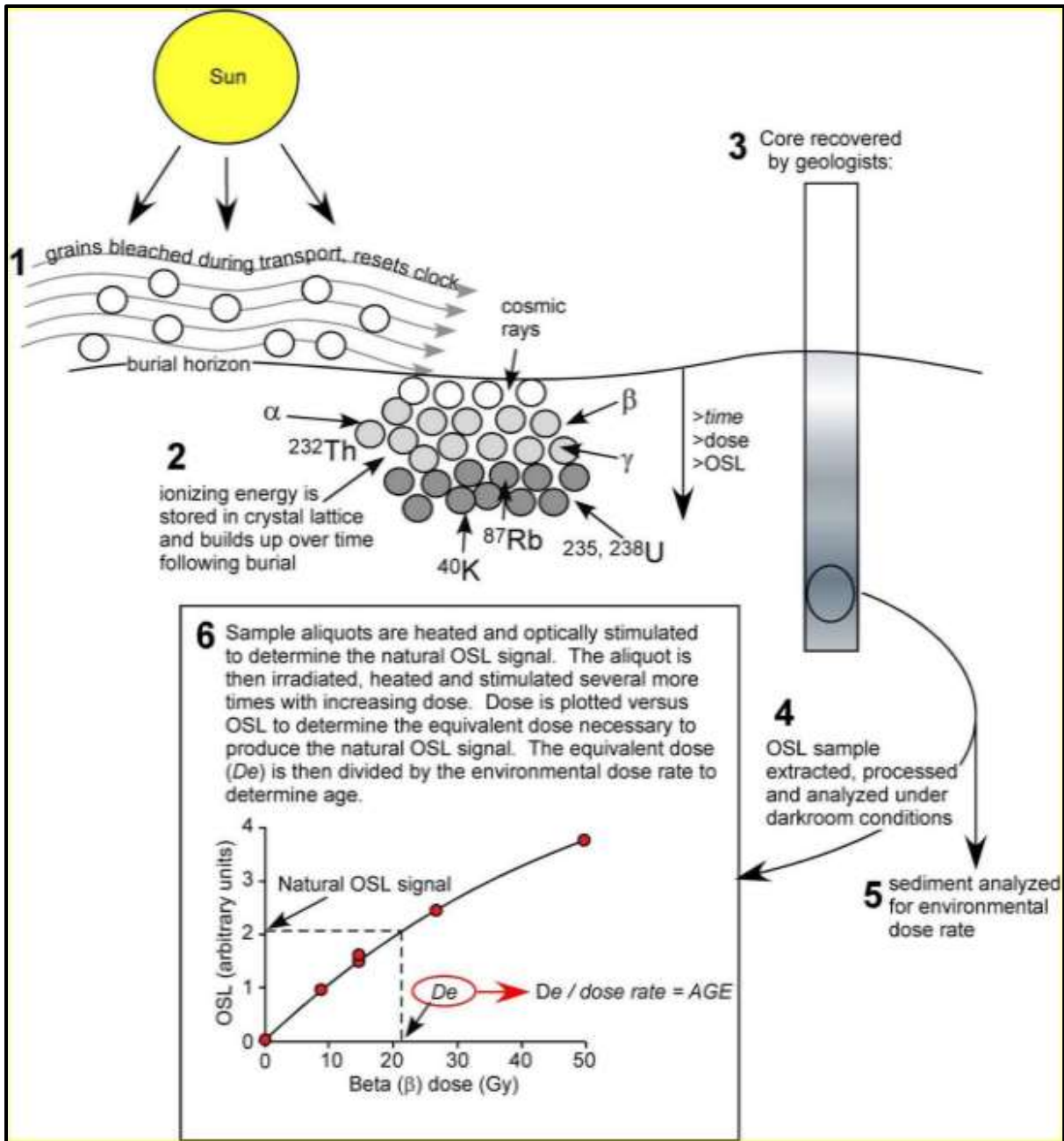


Figure 12: Luminescence Dating Technique flow chart from Mallinson (2008).



Figure 13: Bedrock strath surface (RC-7) characteristic of most Q₃ and some Q₂ terrace surfaces. These surfaces were not datable using the methods employed in this study.



Figure 14: Sampling tube in site RC-7. Circle shows area where dose rat and water content samples were taken.

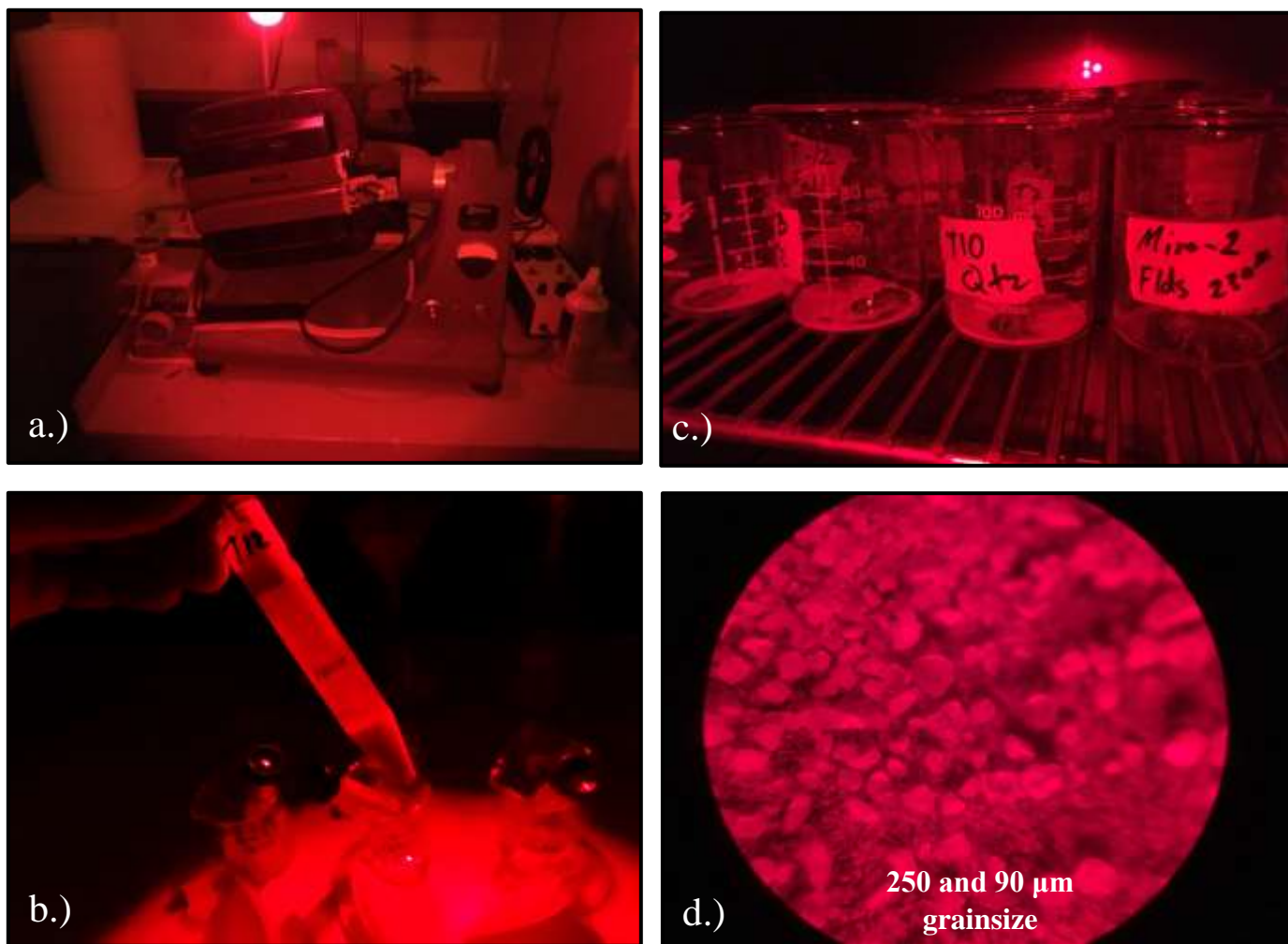


Figure 15: a.) Franz Magnetic Separator, b.) heavy liquid separation via lithium sodium polytungstate, 2.85 ± 0.02 g/mL, c.) semifinal product. K-Feldspar float is retained in case of insufficient quartz yields, d.) close-up of fine to very fine-grained mineral grains. The remaining feldspars are dissolved in HF bath; the clear quartz grains are used for analysis.

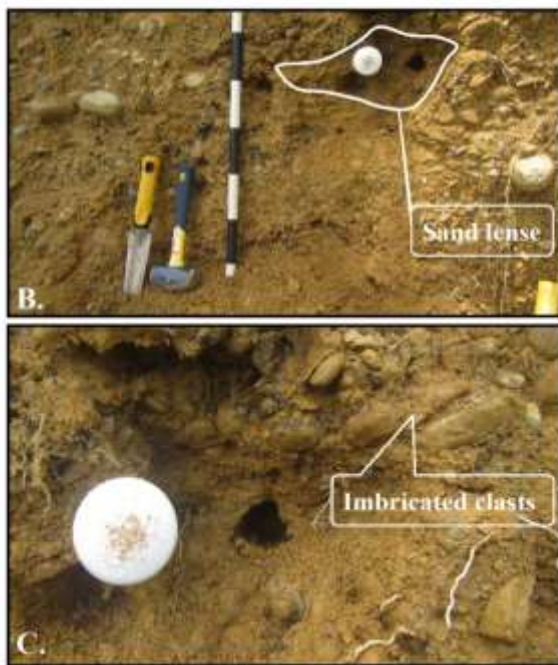
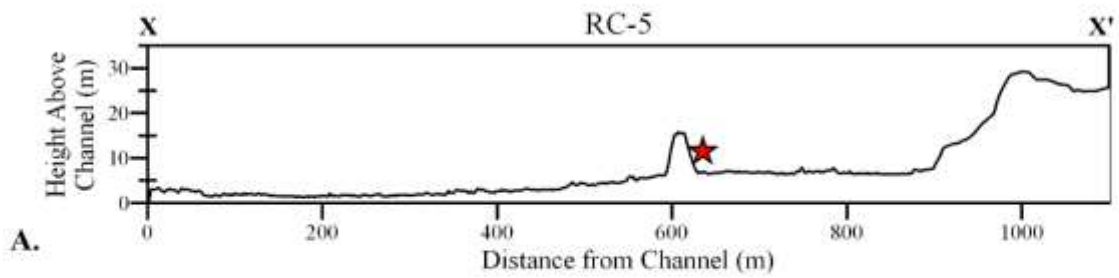
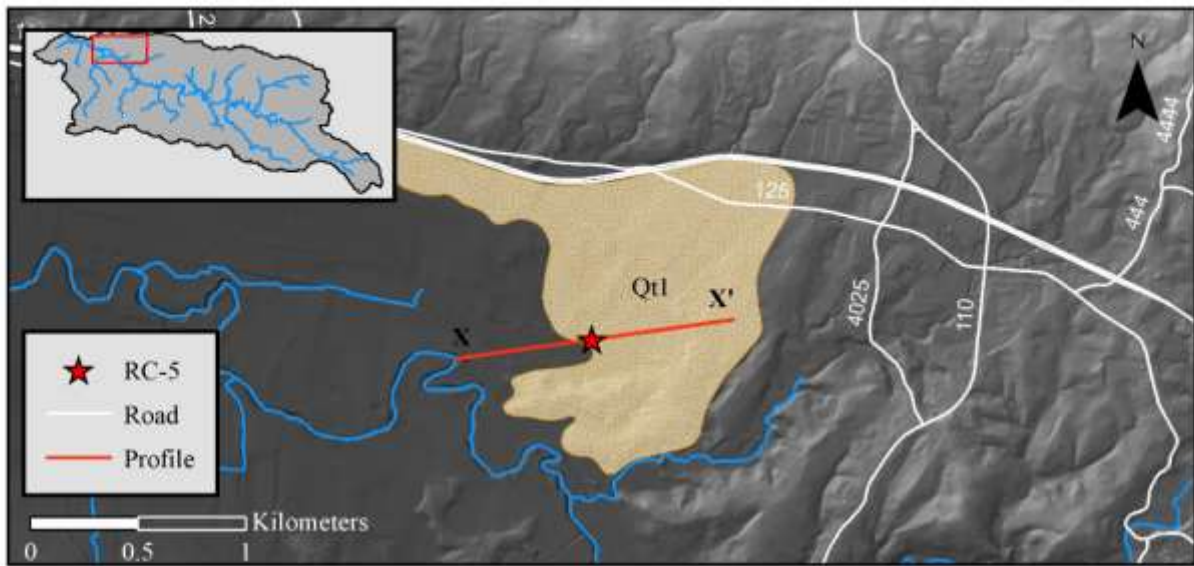


Figure 16: Site RC-5

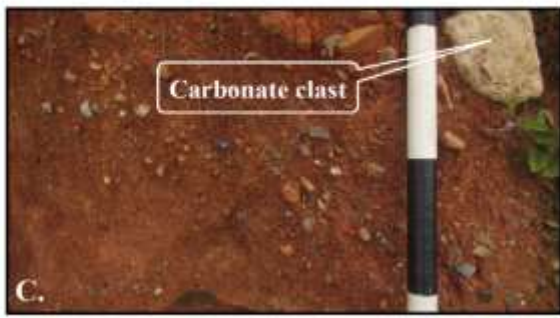
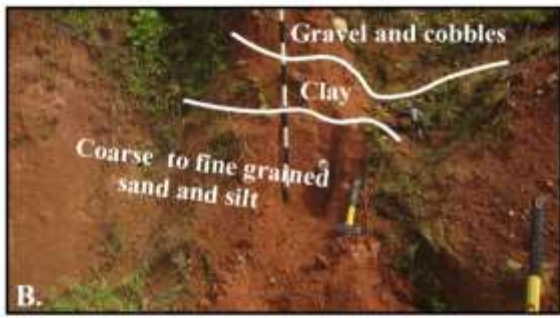
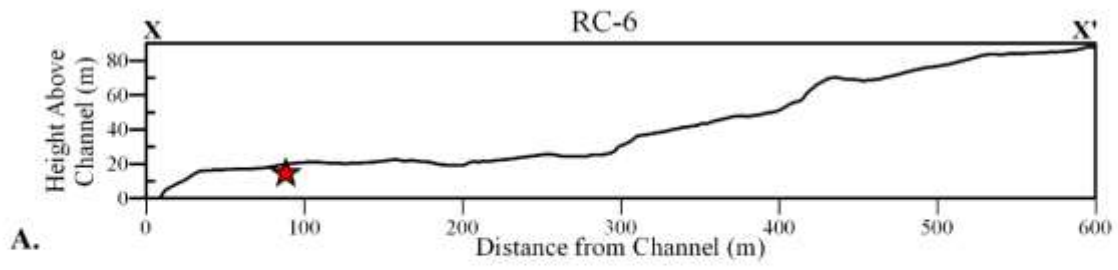
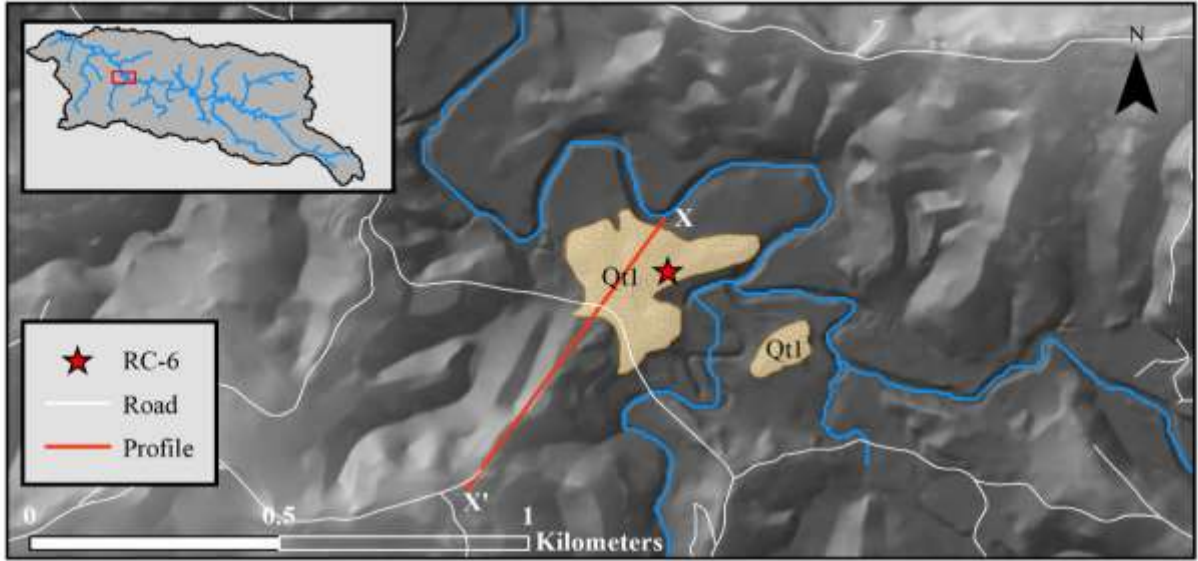


Figure 17: Site RC-6

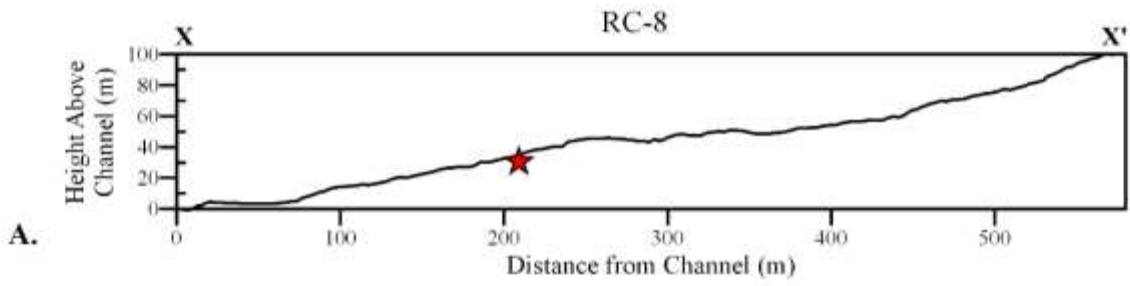
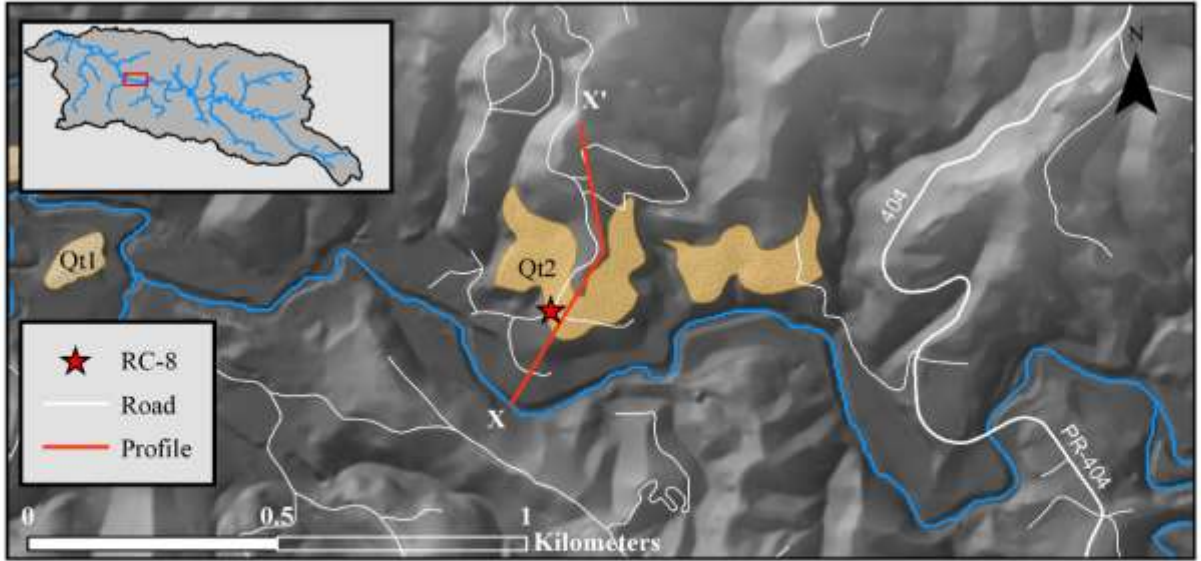
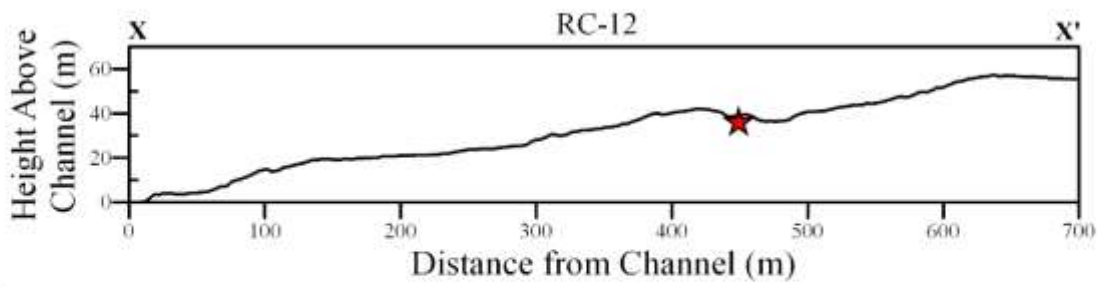
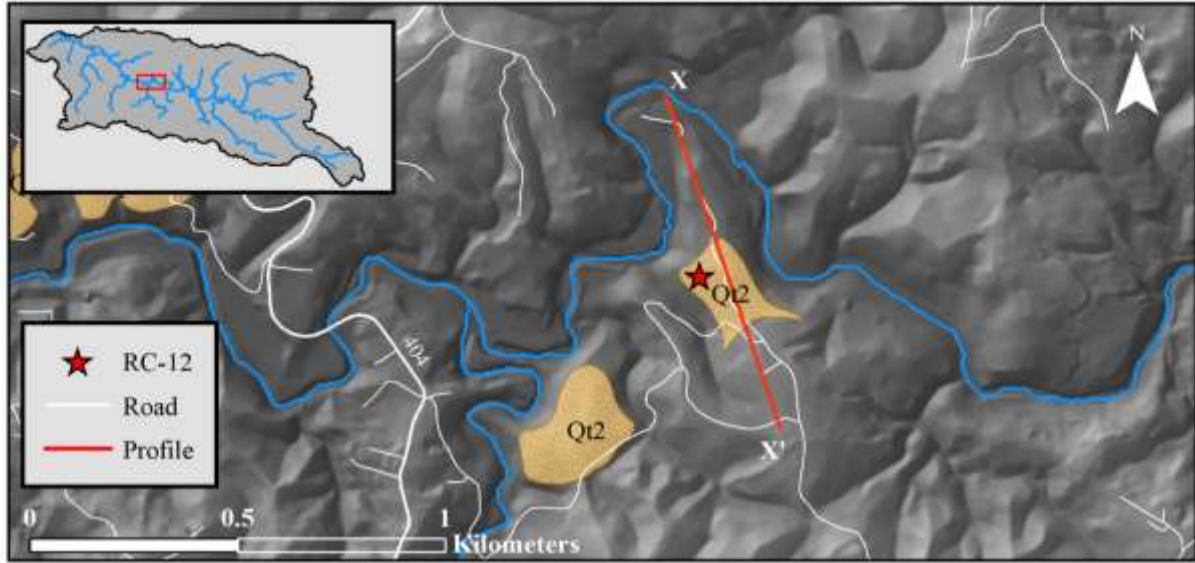


Figure 18: Site RC-8



A.

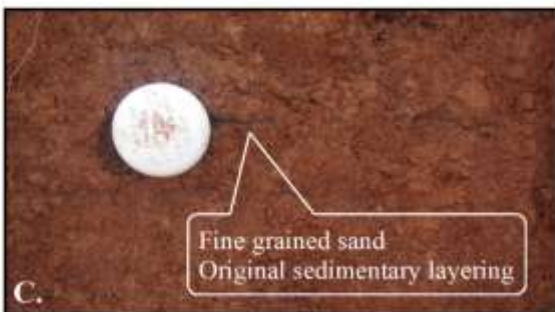


Figure 19: Site RC-12

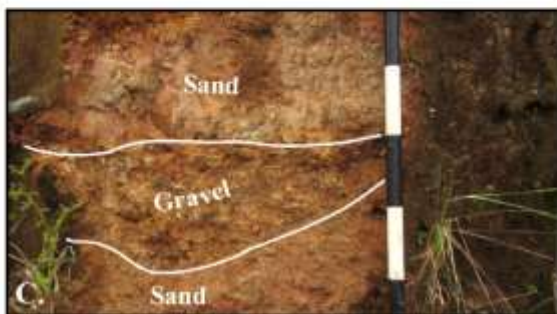
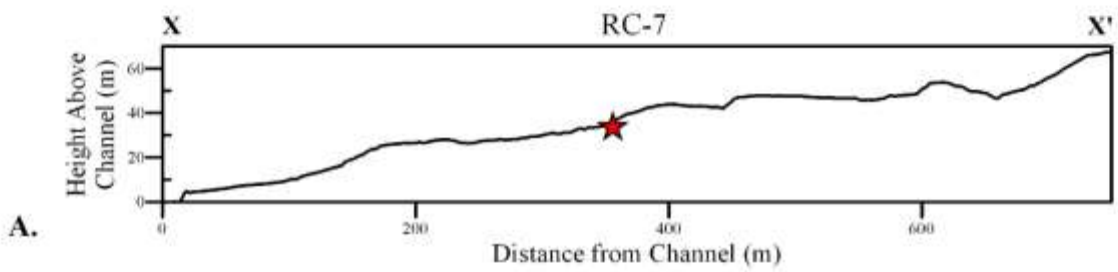
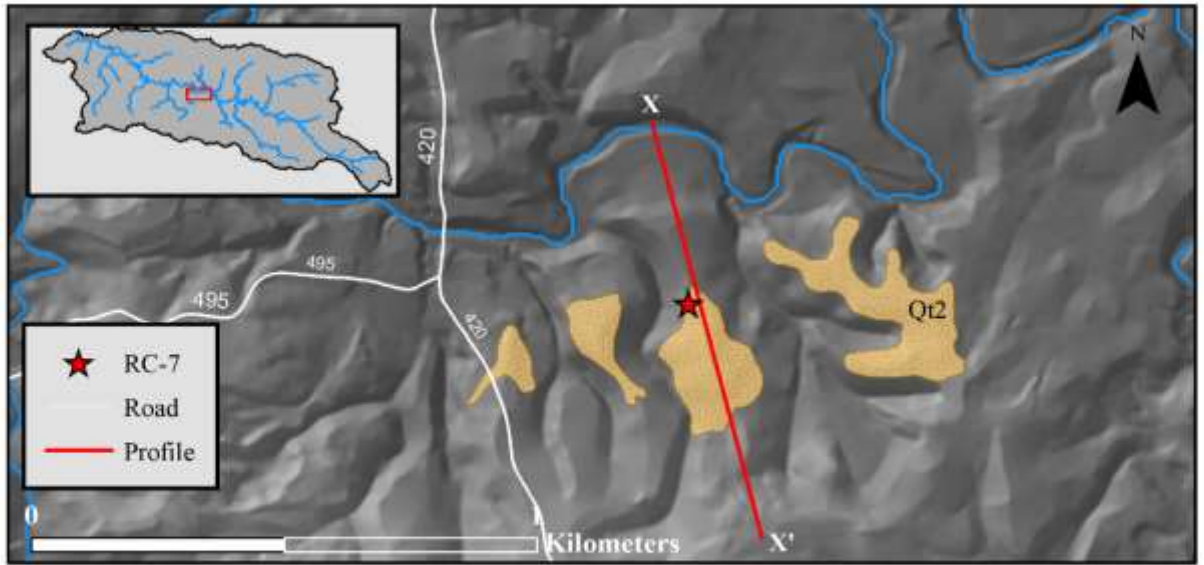


Figure 20: Site RC-7

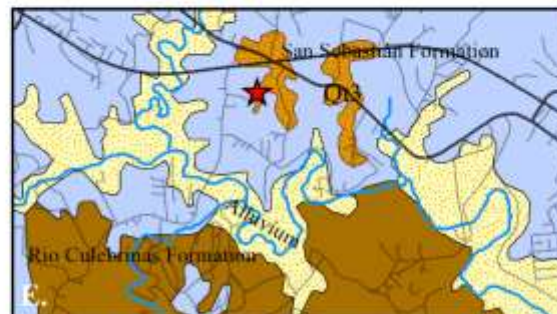
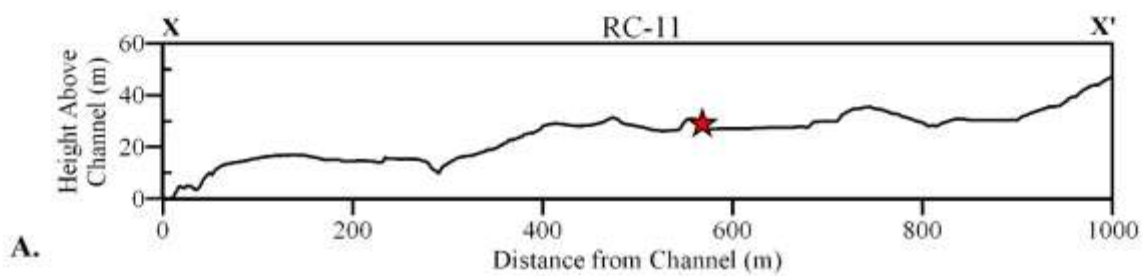
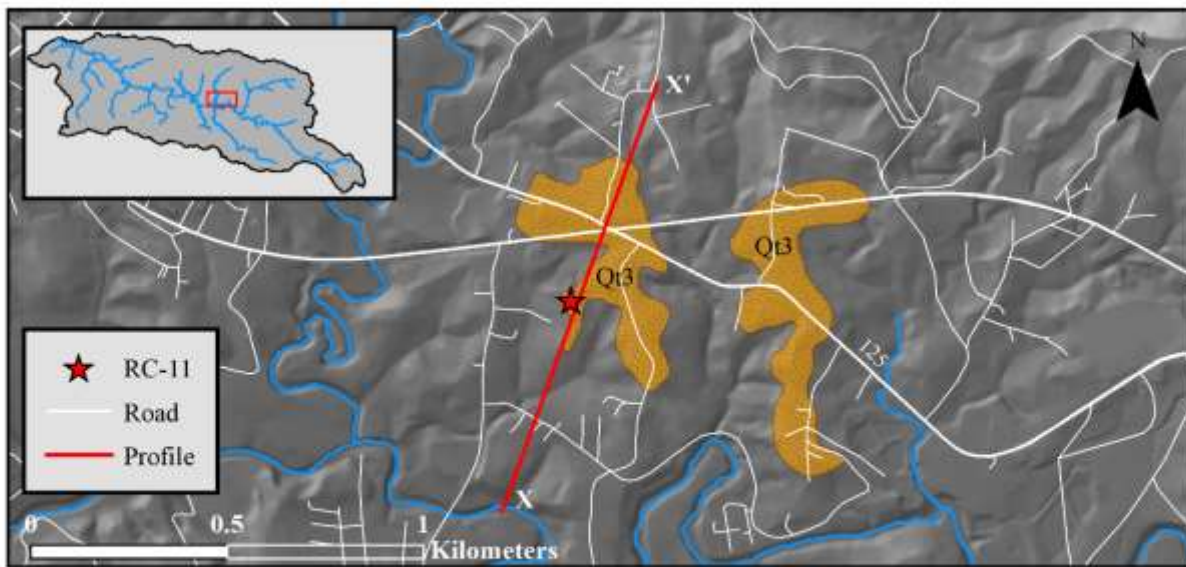


Figure 21: Site RC-11

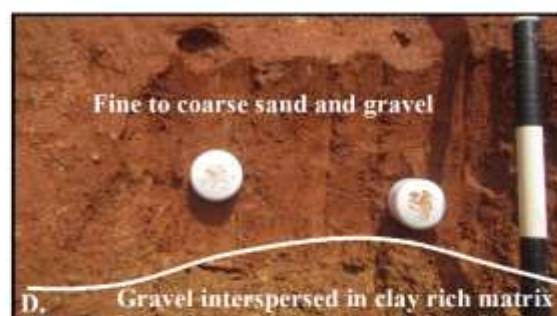
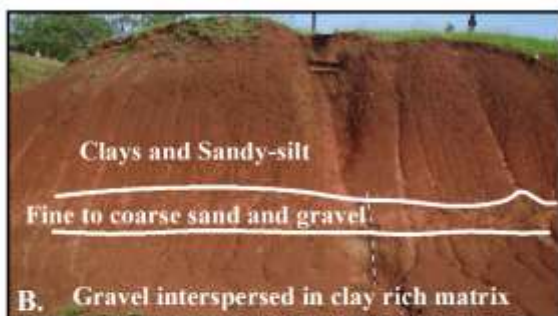
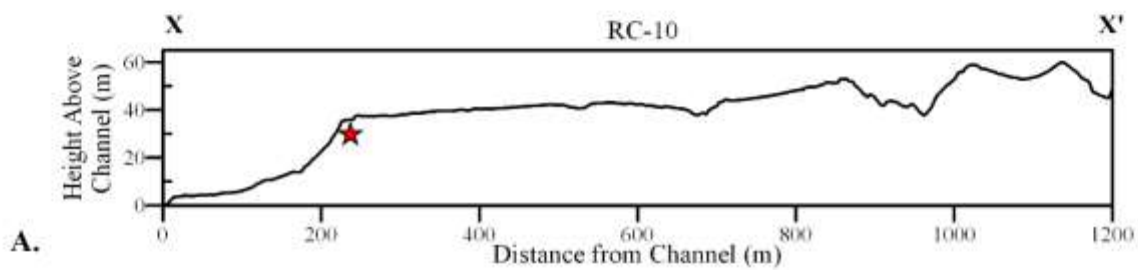
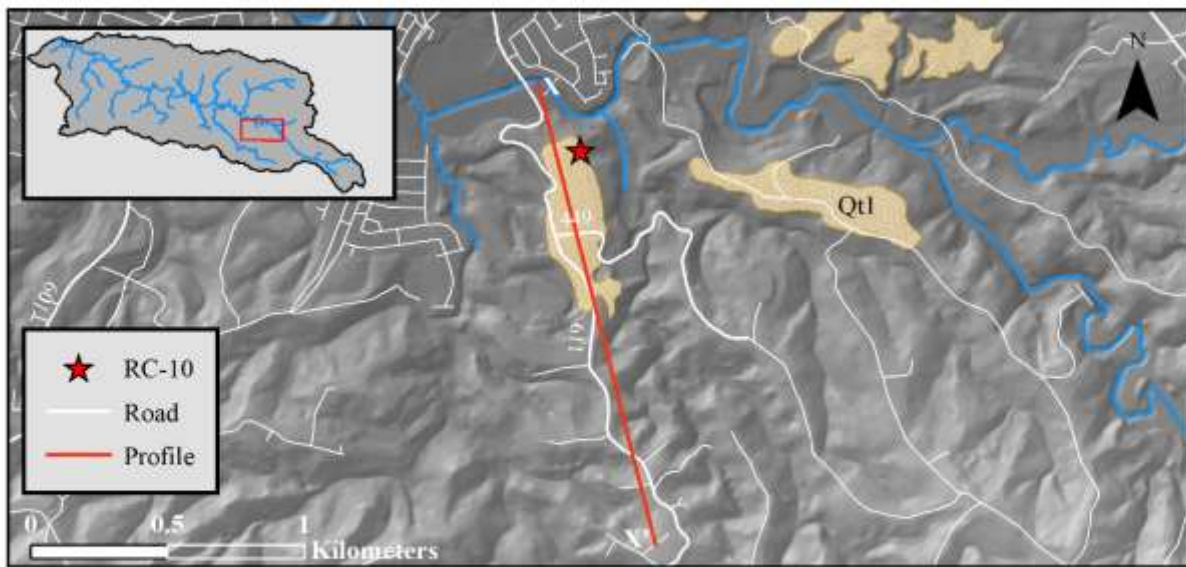


Figure 22: Site RC-12

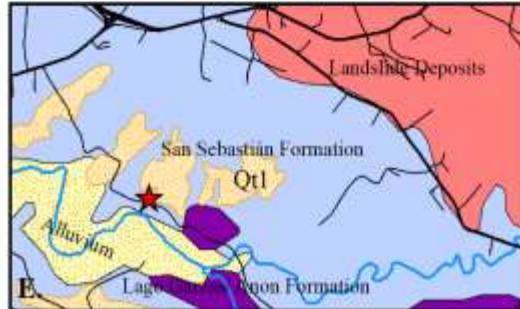
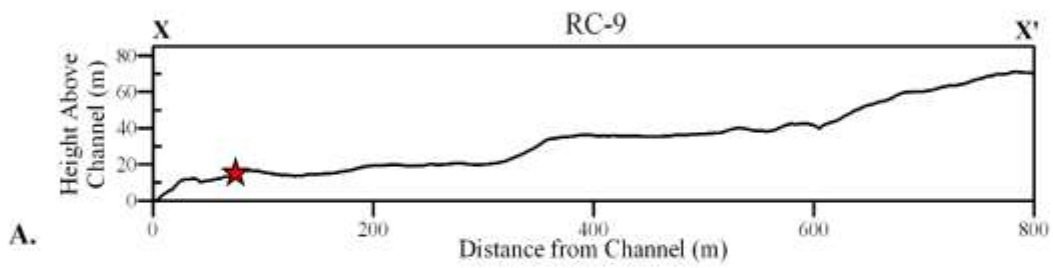
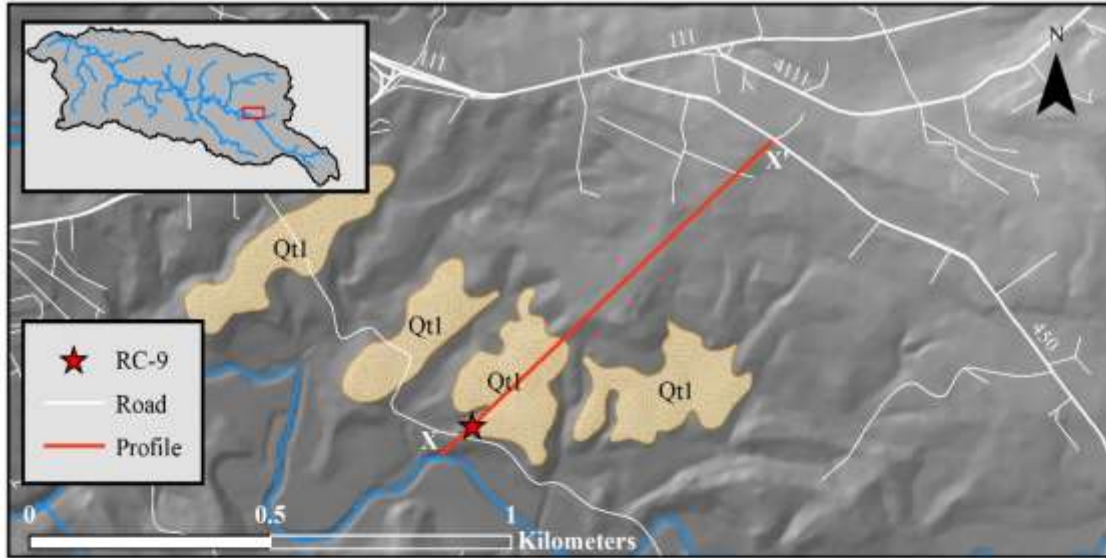


Figure 23: Site RC-9

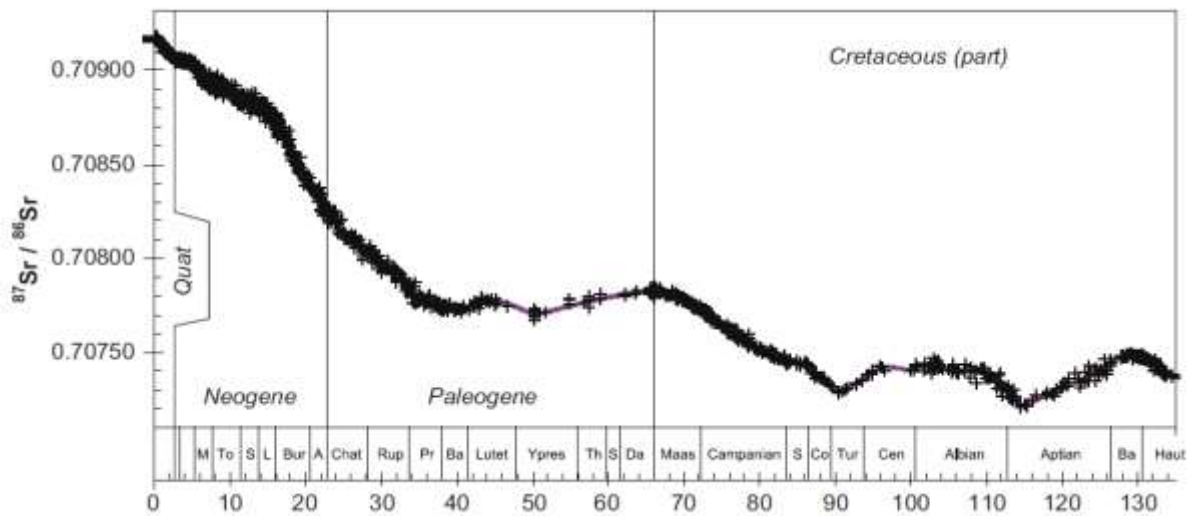
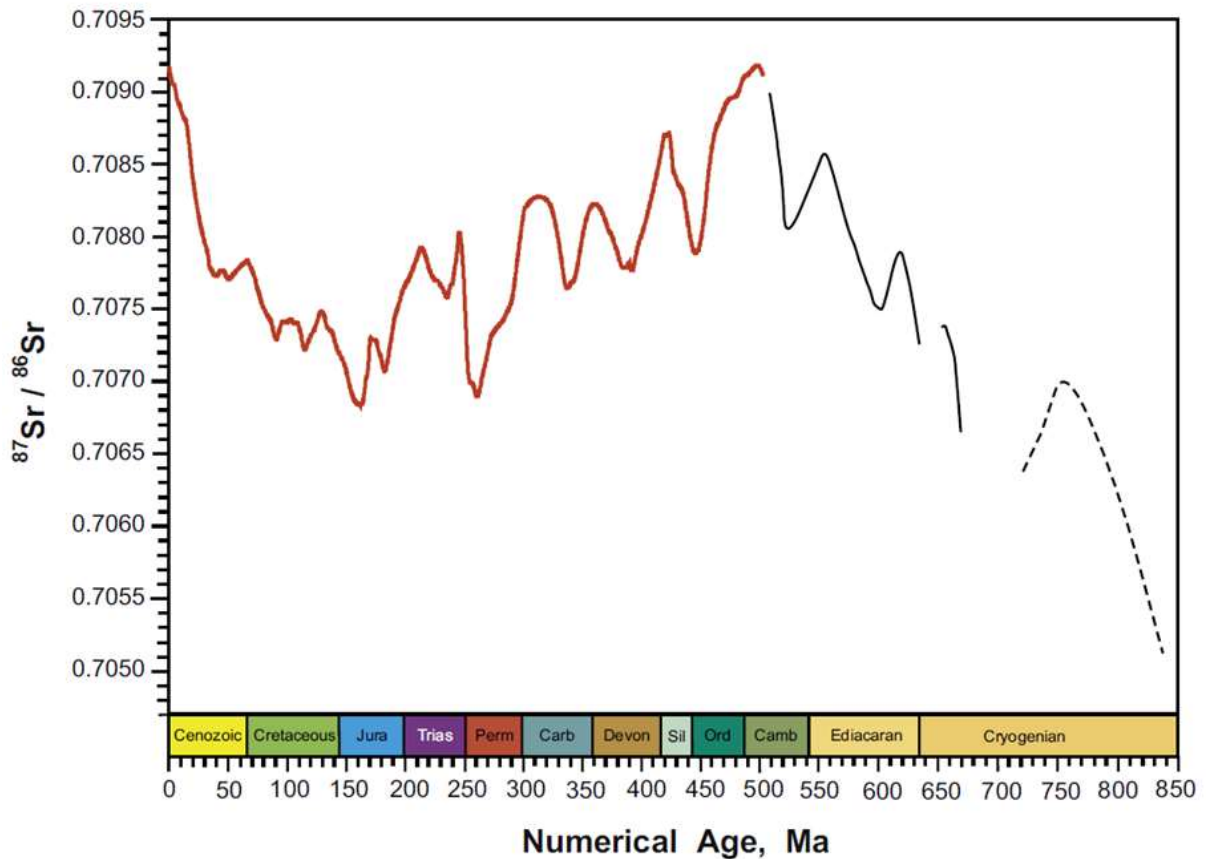


Figure 24: Strontium Seawater Curves from McArthur et al. (2012) for ~800 Ma (*top*), and the last 130 Ma (*bottom*)



Figure 25: *Top:* specimens of *Ostrea sp.* at site KF-GY, *bottom:* Specimens of *Kuphus incrassatus*. Note the tube-like appearance of *K. incrassatus*.

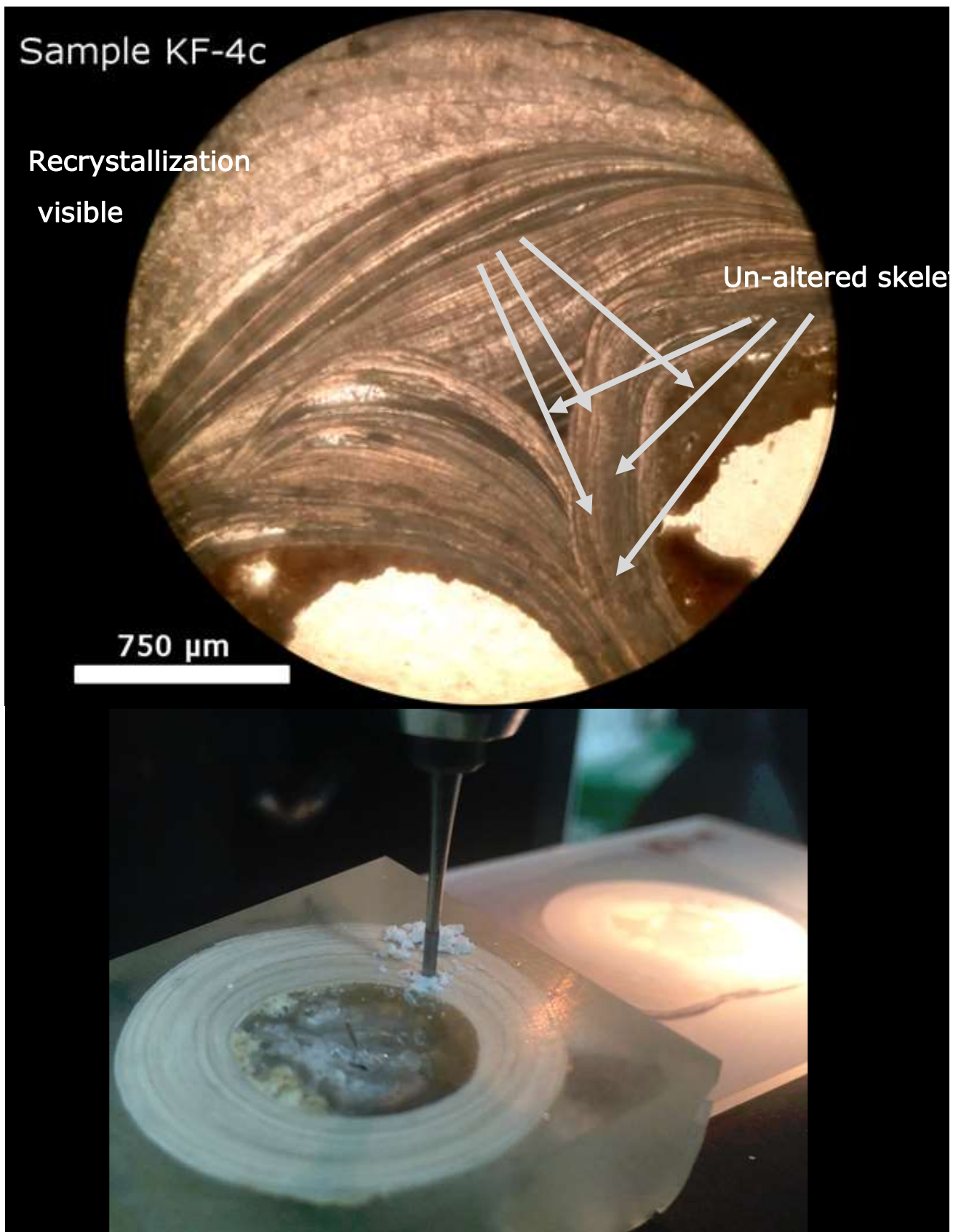


Figure 26: Thin section analysis and drilling of *Kuphus incrassatus*. Thin section microscopy (*top*) is used to help identify recrystallization in samples and select drill sites within the unaltered segments of the skeleton rim. Drilling was done with a computer aided 1mm diamond carbide drill (*bottom*)



Figure 27: Strontium separation via column chemistry at the Geochronology Isotope Geochemistry Lab, UNC Chapel Hill. Sr was separated using Sr specific rosin. The rosin works by preferentially bonding with Sr ions under certain condition and will release the bound ions once rinsed with H₂O

Fluvial lanform height and generation for the Río Culebrinas

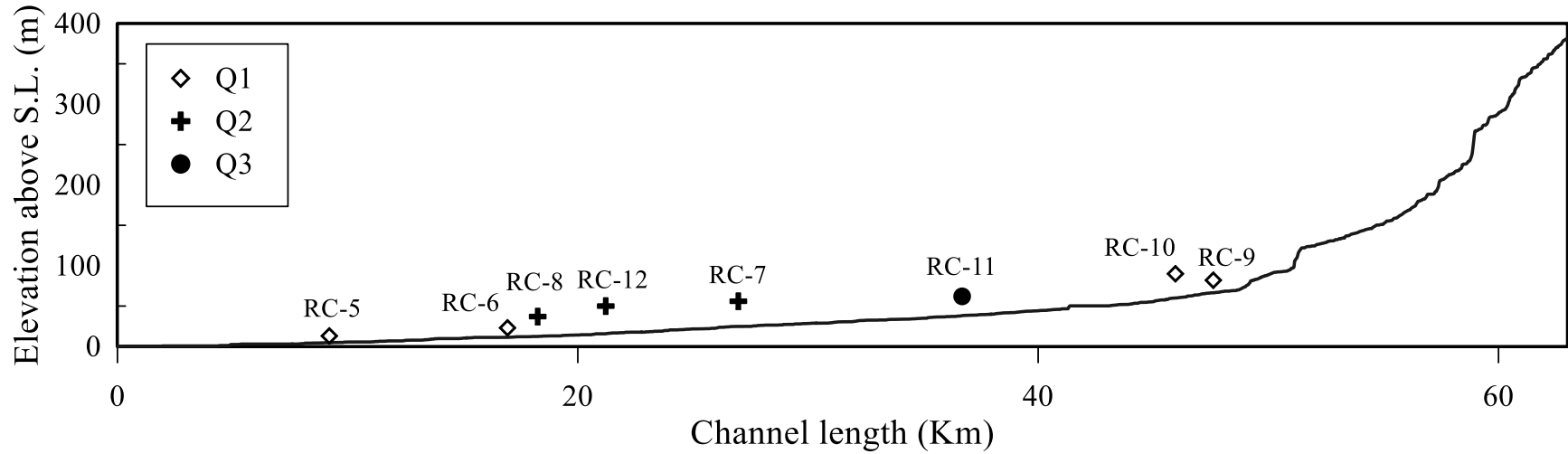


Figure 28: Long river profile for the Río Culebrinas showing three generations of fill terraces occurring at 11-13 Kyr BP (Q₁), 19-22 Kyr BP (Q₂), and 65 Kyr BP (Q₃). Q₃ is found at the same elevations above the current channel as some of the Q₁ and Q₂ terraces.

Fluvial Incision of the Río Culebrinas Western Puerto Rico

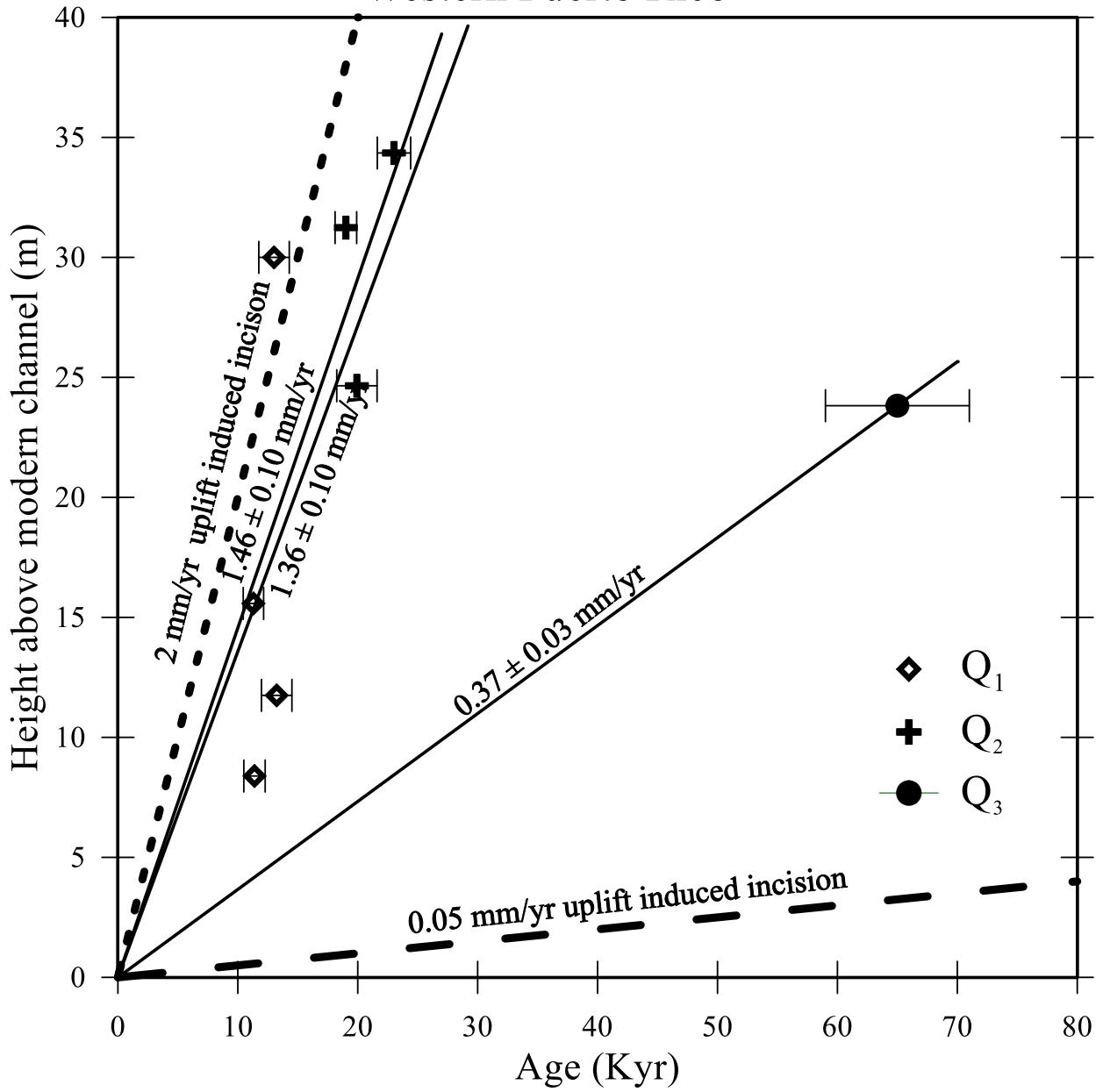


Figure 29: Linear regression plot for incision rates with respect to the Modern Channel. Uplift rates from Taggart & Joyce (1898) are plotted as dashed lines.

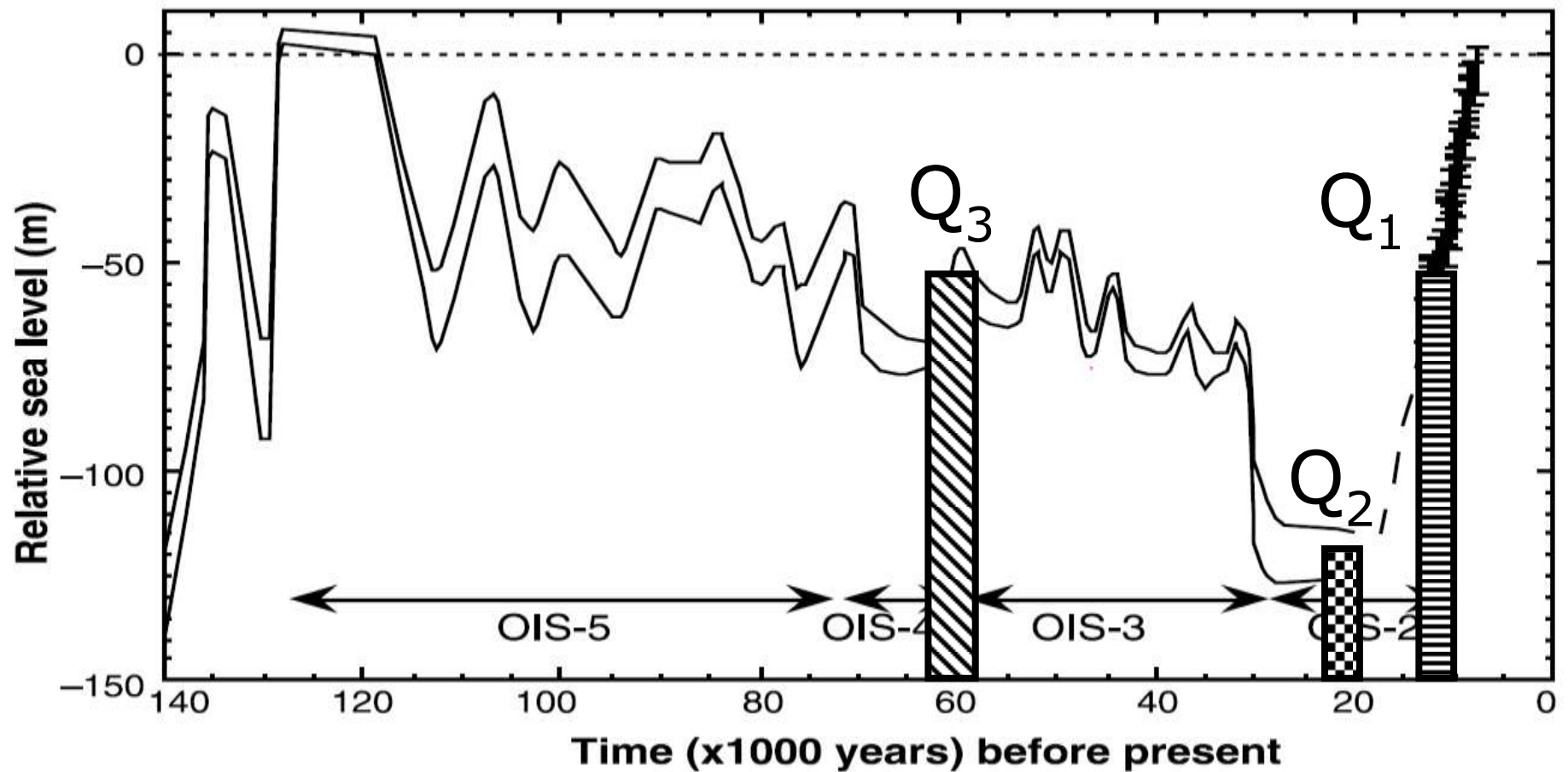


Figure 30: Relative sea level curve from Lambeck & Chapell (2001) modified with age ranges of fluvial terraces from this study showing climate control on terrace deposition. Q₃ terraces mark the onset of cooler and drier conditions associated with glacial conditions. Q₂ terraces were deposited during the Last Glacial Maximum (LGM). Q₁ terraces represent a transition from cool dry climates to warm humid interglacial conditions and mark a small reversal in this warming trend known as the Younger Dryas (Thomas & Thorpe, 1995; Kock et al., 2009b; Keigwin et al., 2018).

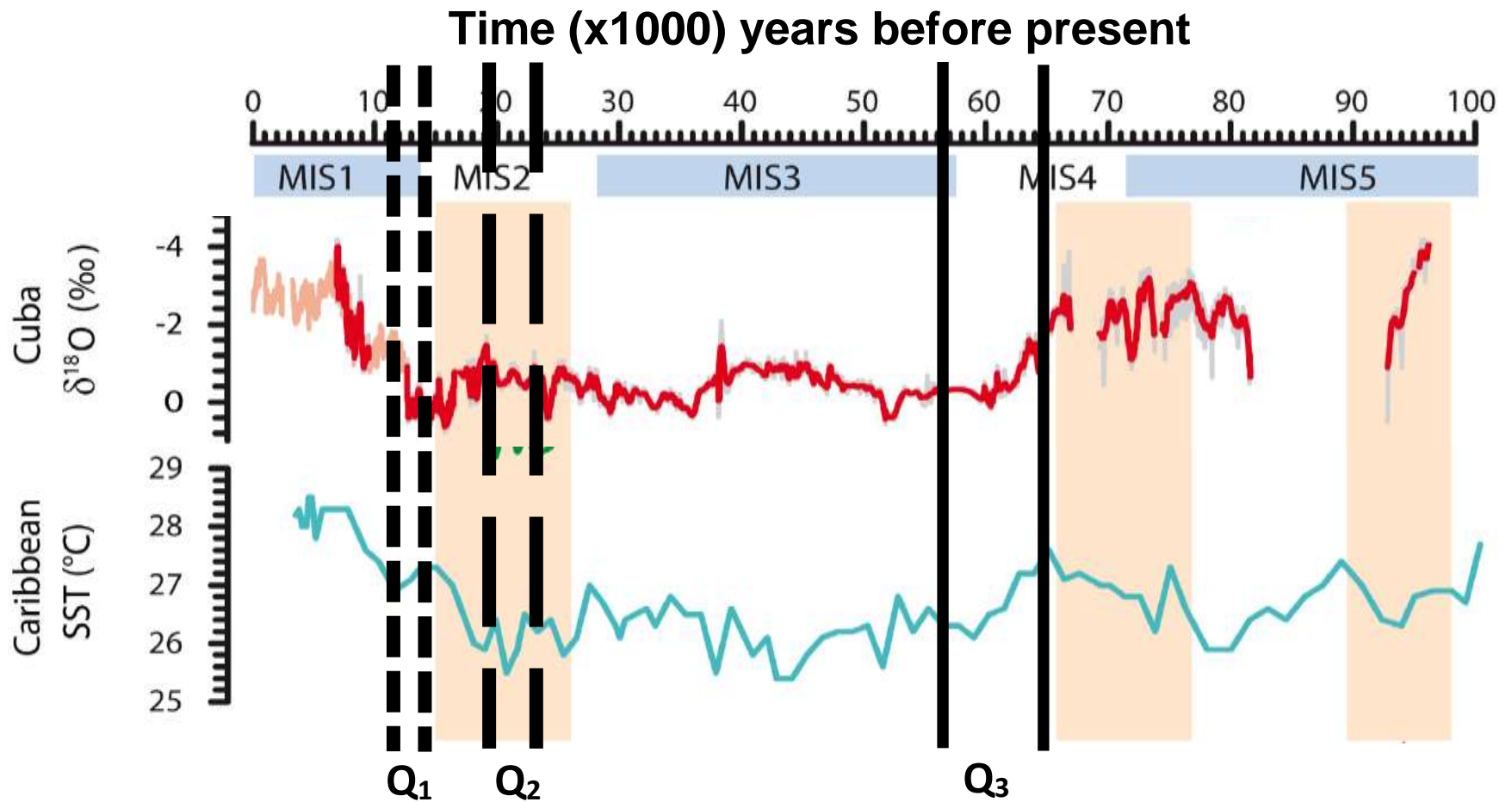


Figure 31: Speleothem $\delta^{18}\text{O}$ data from Cuba and Caribbean Sea Surface Temperatures (SST) for the Caribbean. Figure modified from Warken (2017). Speleothem CM $\delta^{18}\text{O}$ values (raw composite record: light grey, 5p RM: red line, Warken, 2017) together with the Holocene speleothem $\delta^{18}\text{O}$ record from Fenster et al. (2013) (light red). Depleted $\delta^{18}\text{O}$ values in speleothem and paleoclimate records indicate increased precipitation and temperature.

Channel response to climatic forcing over the last 65 Kyr

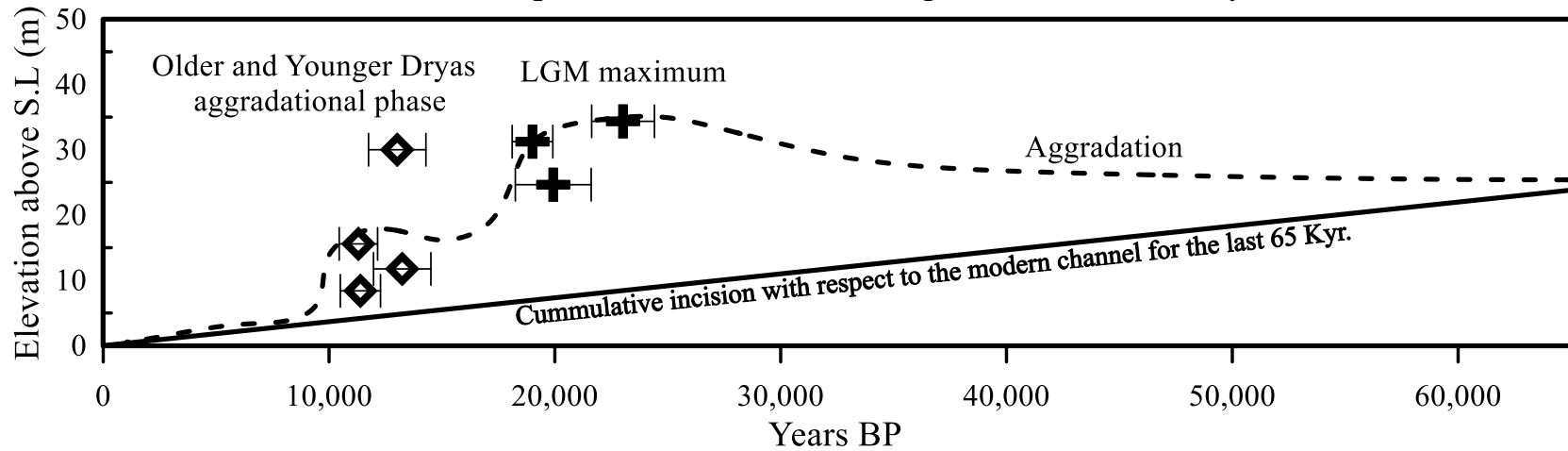


Figure 32: Landform heights above the current channel superimposed on the trend of cumulative incision. Slope of the line is the long-term incision rate with respect to the modern channel. Dashed line shows potential river channel position over the last 65 Kyr. The long lived aggradational trend of the system since 65 Kyr may be a product of drier cooler climates in the region. During this period, precipitation events were infrequent but intense, delivering large amounts of material to the channel yet producing too little discharge to transport it. This aggradational period came to an abrupt stop sometime between 15-19 Kyr BP as the planet began to warm following maximum glacial conditions during the LGM. This new trend in incision was driven by an increasing intensity of precipitation and discharge events which mobilized material that had accumulated in and around the channel during the preceding glacial conditions

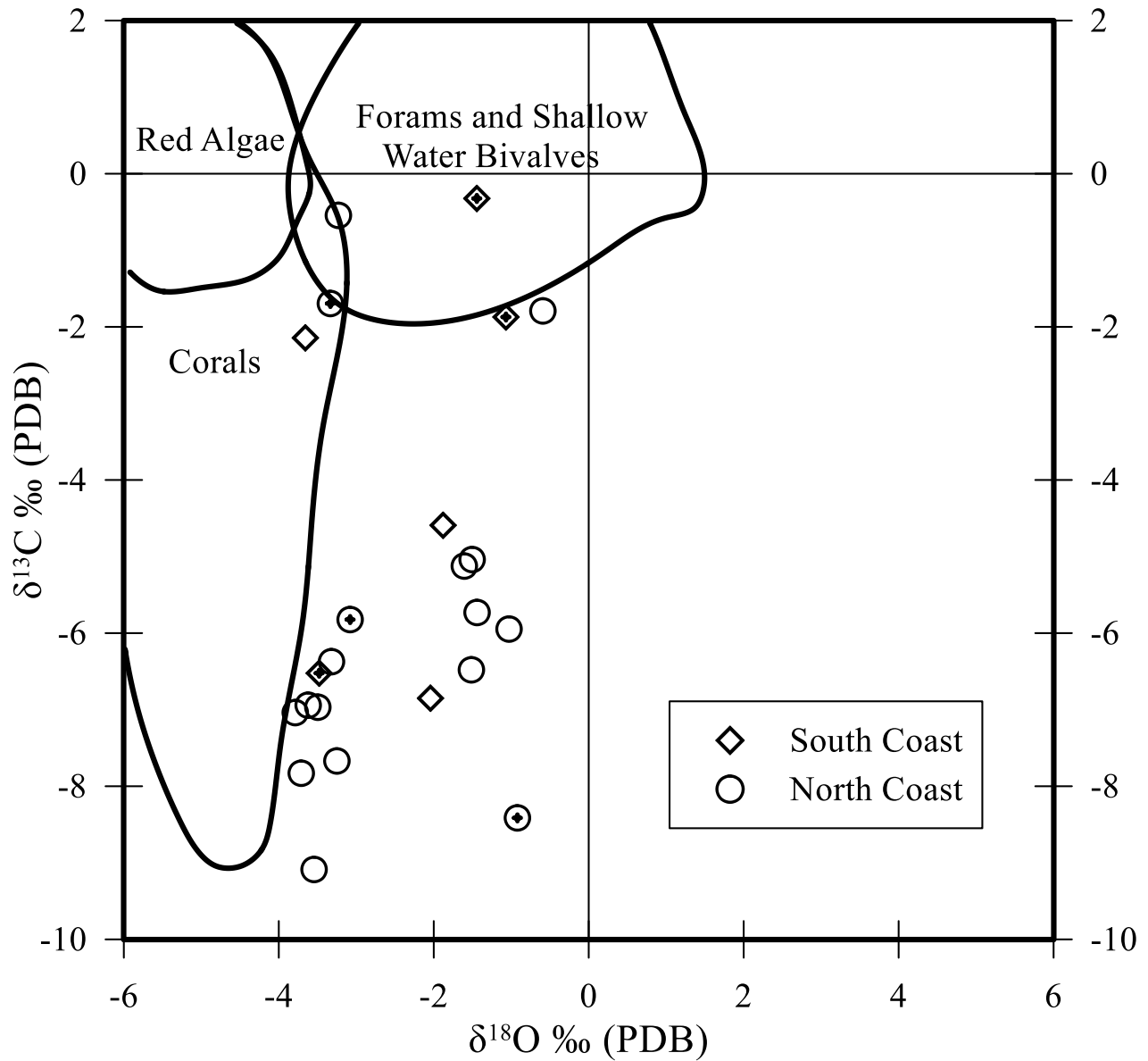


Figure 33: $\delta^{18}\text{O}$ vs $\delta^{13}\text{C}$ stable isotope analysis results from *Kuphus incrassatus* and *Ostrea sp.* showing sample distribution and value fields for unaltered skeletons of shallow marine organisms (Tucker & Wight, 1990). Samples with depleted $\delta^{13}\text{C}$ values suggest restricted environments (Lloyd, 1964; Patterson & Walter, 1994) and were not discarded for analysis. Symbols with dot represent samples of *Ostrea sp.*

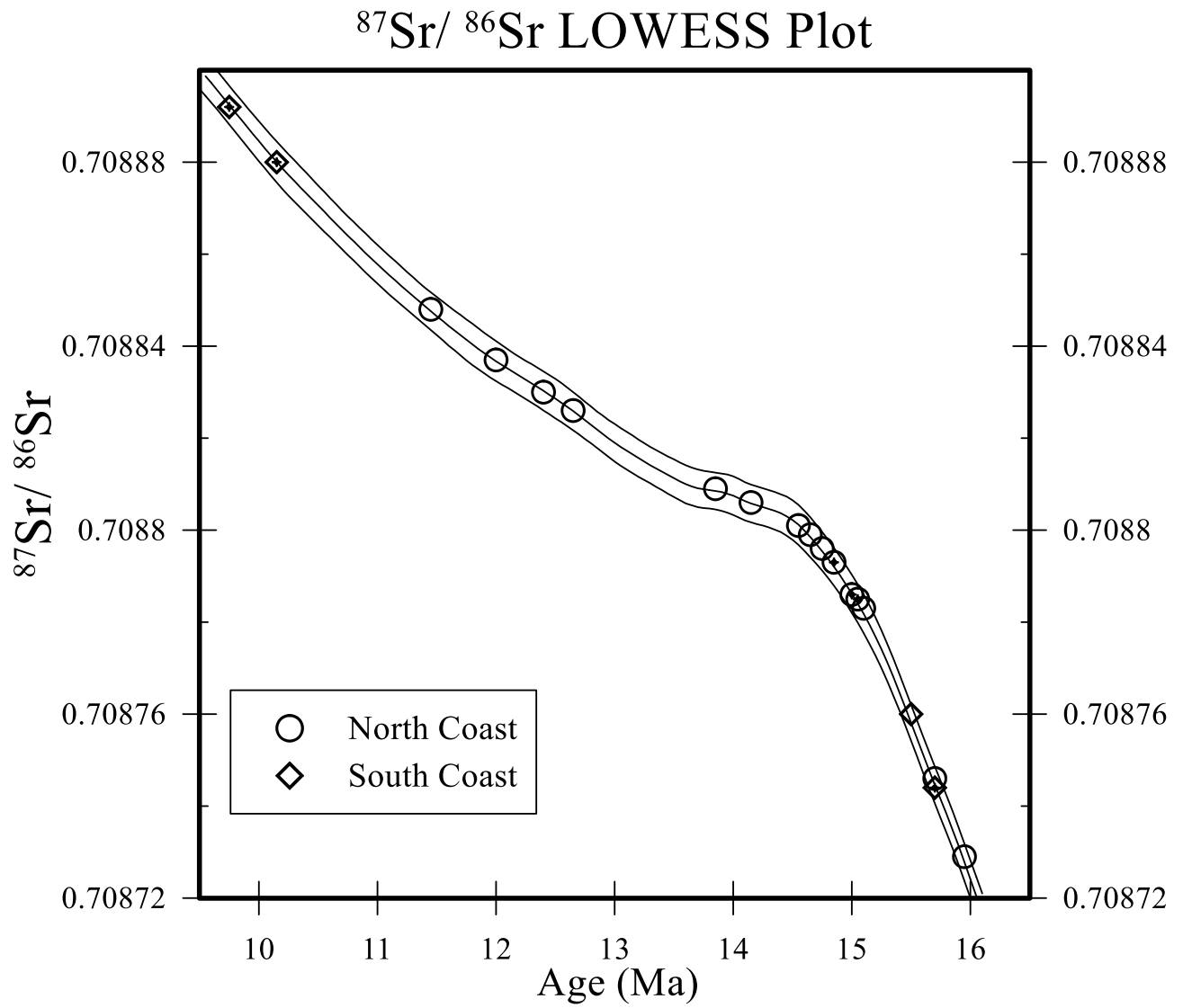


Figure 34: LOWESS Plot. Final reported ages include both analytical errors and the maximum and minimum values of the McArthur Sr-Seawater curve (McArthur, 2001). Samples from extreme northwest PR cluster around 15 Ma, while samples from the southwest coast range from 6 to 14 Ma. Symbols with dot represent samples of *Ostrea sp.*

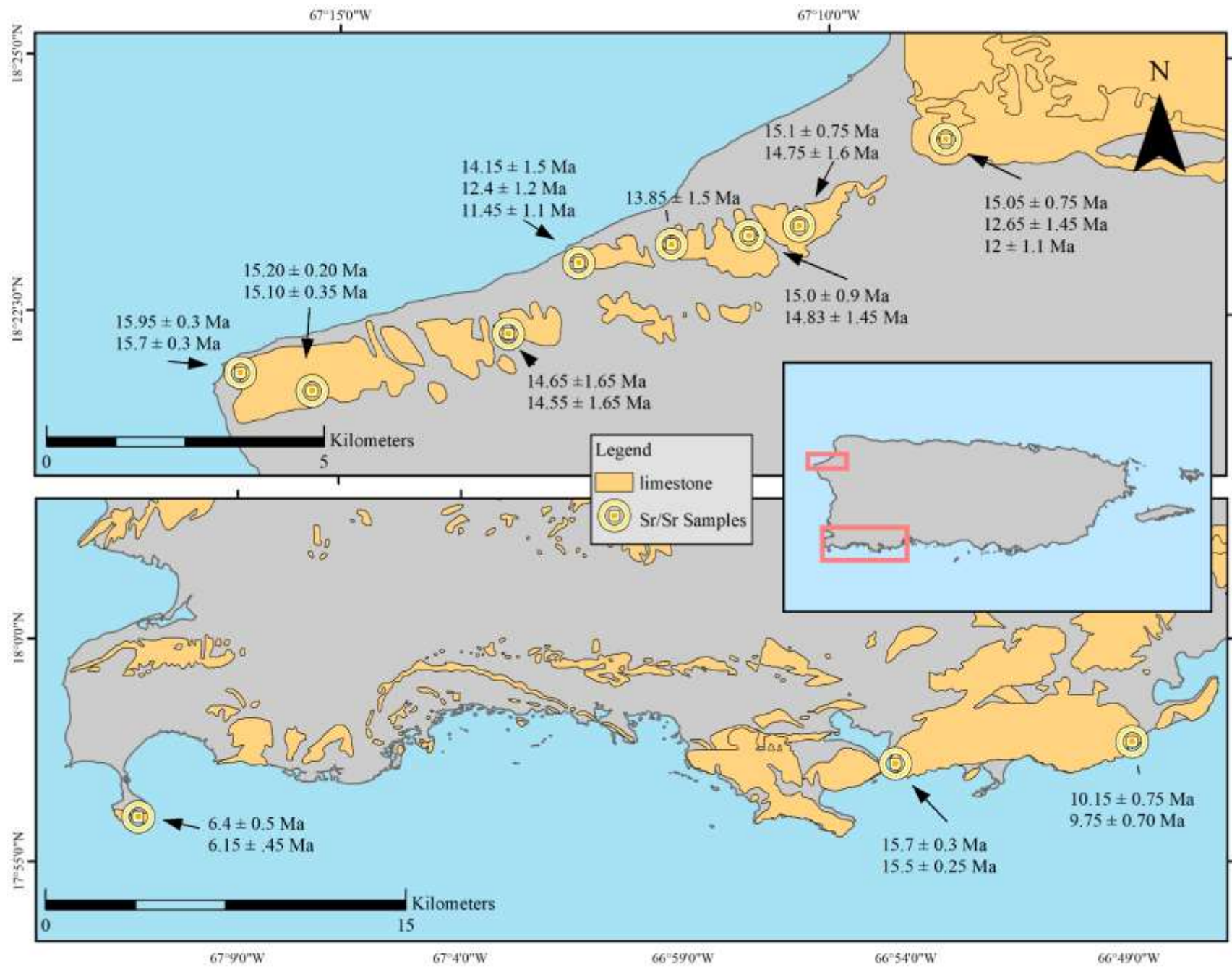


Figure 35 Maps showing sampled limestone in northwestern (*above*), and southwestern (*below*) Puerto Rico with ages from this study and Vicens (2016)

Tables:

Table 1: Quartz OSL Data and Ages for Fluvial Terraces of the Río Culebrinas

Sample	% Water content ^a	K (%) ^b	U (ppm) ^b	Th (ppm) ^b	Total Dose (Gy/ka) ^c	Equivalent Dose (Gy)	n ^d	Scatter ^e	Age (yrs) ^f	Gen
RC-5	11 (35)	1.40 ± 0.04	0.86 ± 0.05	2.59 ± 0.27	1.41 ± 0.07	18.9 ± 2.2	12 (15)	31%	11,390 ± 890	Q ₁
RC-9	30 (46)	1.75 ± 0.07	1.02 ± 0.09	2.77 ± 0.45	1.92 ± 0.12	21.7 ± 1.0	4 (24)	24%	11,300 ± 850	Q ₁
RC-10	27 (64)	1.61 ± 0.10	1.59 ± 0.21	4.06 ± 0.33	1.82 ± 0.13	23.7 ± 1.6	8 (24)	17%	13,020 ± 1,270	Q ₁
RC-6	25 (53)	1.29 ± 0.03	0.91 ± 0.08	2.41 ± 0.31	1.48 ± 0.05	19.6 ± 0.73	10 (15)	7%	13,240 ± 670	Q ₁
RC-8	30 (66)	1.48 ± 0.05	0.67 ± 0.17	1.90 ± 0.34	1.47 ± 0.10	29.3 ± 1.4	10 (15)	0%	19,930 ± 1,680	Q ₂
RC-12	32 (58)	1.10 ± 0.04	1.11 ± 0.15	3.52 ± 0.31	1.38 ± 0.07	32.5 ± 1.1	9 (24)	50%	23,020 ± 1,390	Q ₂
RC-7	27 (58)	1.52 ± 0.05	1.22 ± 0.11	3.08 ± 0.29	1.71 ± 0.08	32.5 ± 0.55	14 (15)	3%	19,010 ± 910	Q ₂
RC-11	18 (38)	1.33 ± 0.08	0.79 ± 0.08	2.56 ± 0.39	1.60 ± 0.10	104 ± 5.1	14 (24)	17%	65,000 ± 5,100	Q ₃

^aField moisture, with figures in parentheses indicating the complete sample saturation %. Dose rates calculated using 50% of the saturated moisture (i.e. 11 (35) = 35* 0.5 = 18).

^bAnalyses obtained using high-resolution gamma spectrometry (high purity Ge detector).

^cIncludes cosmic doses and attenuation with depth calculated using the methods of Prescott and Hutton (1994). Cosmic doses were around 0.19-0.16 Gy/ka.

^dNumber of replicated equivalent dose (D_E) estimates used to calculate the equivalent dose. Figures in parentheses indicate total number of measurements included in calculating the represented D_E and age using the minimum age model (MAM) for T12 and T-9, all others used the central age model (CAM); analyzed via single aliquot regeneration on quartz grains.

^eDefined as "over-dispersion" of the D_E values. Values >30% are considered to be poorly bleached or mixed sediments.

^fFine-grained 250-63-micron sized quartz; age calculated in calendar years. Exponential + linear fit used on equivalent dose, errors to one sigma.

Table 2: Incision Rates for the Río Culebrinas, Northwestern Puerto Rico

Site	Ages			River Point ^a (km)	Elevation ^b (m)	Incision Rates		
	Min	Mean	Max			Modern Channel	Q ₂ - Q ₁ ^c	Q ₃ - Q ₁ ^c
RC-9	10450	11300	12150	47.6	15.6	1.36 mm/yr	2.40 mm/yr	0.22 mm/yr
RC-5	10500	11390	12280	9.2	8.4			
RC-10	11750	13020	14290	46.0	30.0			
RC-6	11970	13240	14510	16.9	11.8			
RC-7	18100	19010	19910	27.0	31.2	1.46 mm/yr	2.40 mm/yr	0.22 mm/yr
RC-8	18250	19930	21610	18.3	24.7			
RC-12	21630	23020	24410	21.2	34.4			
RC-11	59000	65000	71000	36.7	23.8	0.37 mm/yr		

^aDistance from river mouth along the length of the channel

^bElevation above the modern channel

^cRates take into account the Sadler Effect by measuring incision between landforms and not the modern channel.

Table 3:

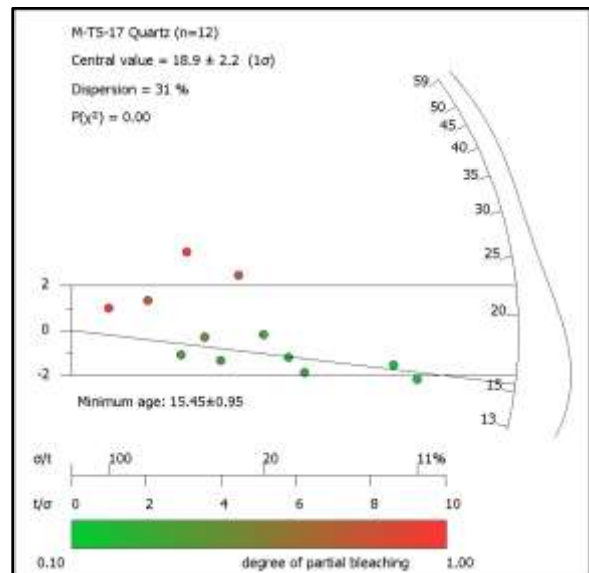
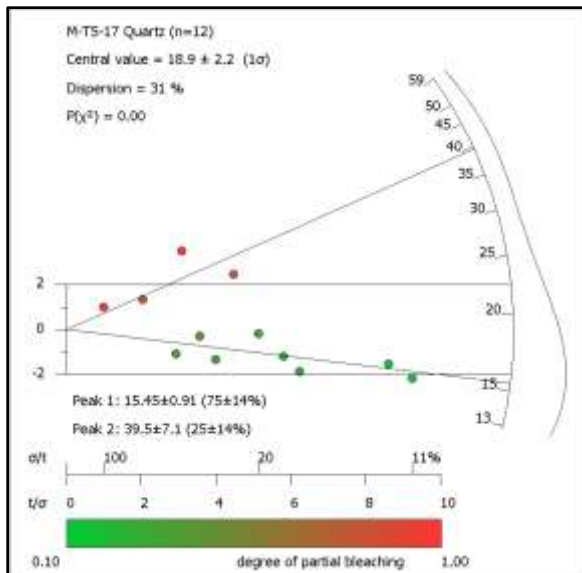
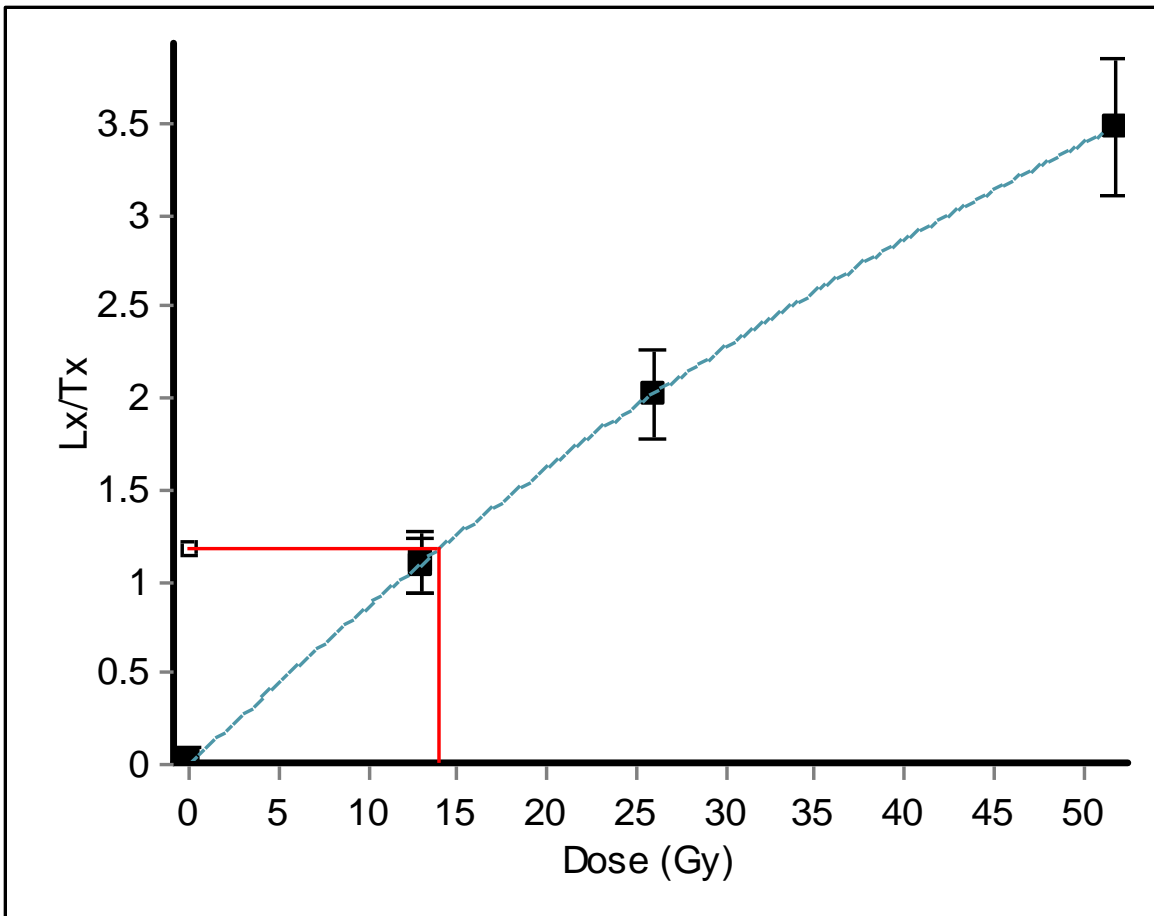
$\delta^{13}\text{C}$ & $\delta^{18}\text{O}$ Stable Isotope Analysis			$^{87}\text{Sr}/^{86}\text{Sr}$ Isotope Analysis							
Sample	$\delta^{13}\text{C}$	$\delta^{18}\text{O}$	Site	-2 σ	$^{87}\text{Sr}/^{86}\text{Sr}$	+2 σ	min	mean	max	Age (Ma) ^a
KF-1a	-5.73	-1.44	KF-1	0.708713	0.708729	0.708745	15.65	15.95	16.20	15.95 ± 0.3
KF-1e	-6.48	-1.51	KF-1	0.708730	0.708746	0.708762	15.40	15.70	16.00	15.70 ± 0.3
KF-2M	-7.04	-3.79	KF-2	0.708790	0.708806	0.708822	12.65	14.15	15.00	14.15 ± 1.5
KF-3e	-9.09	-3.54	KF-3	0.708793	0.708809	0.708825	12.45	13.85	14.90	13.85 ± 1.5
S.ESP-3i	-6.97	-3.50	KF-3	0.708767	0.708783	0.708799	14.45	15.10	15.40	15.10 ± 0.75
KF-4d	-6.37	-3.32	KF-4	0.708780	0.708796	0.708812	13.15	14.75	15.20	14.75 ± 1.6
KF-5OST	-1.69	-3.33	KF-5	0.708777	0.708793	0.708809	13.40	14.85	15.25	14.83 ± 1.45
KF-5OST-2	-5.82	-3.08	KF-5	0.708770	0.708786	0.708802	14.10	15.00	15.40	15.00 ± 0.9
KF-6b	-0.54	-3.23	KF-6	0.708785	0.708801	0.708817	12.90	14.55	15.10	14.55 ± 1.65
KF-6c	-6.94	-3.62	KF-6	0.708783	0.708799	0.708815	13.00	14.65	15.15	14.65 ± 1.65
KF-7a	-5.04	-1.50	KF-7	0.708832	0.708848	0.708864	10.60	11.45	12.55	11.45 ± 1.1
KF-7b	-5.12	-1.61	KF-7	0.708814	0.708830	0.708846	11.35	12.40	13.60	12.40 ± 1.2
KF-8a	-5.95	-1.03	KF-8	0.708821	0.708837	0.708853	11.05	12.00	13.10	12.00 ± 1.1
KF-8b	-1.79	-0.59	KF-8	0.708810	0.708826	0.708842	11.50	12.65	14.10	12.65 ± 1.45
OST-CIB	-8.41	-0.92	KF-8	0.708769	0.708785	0.708801	14.30	15.05	15.40	15.05 ± 0.75
OST-1	-0.32	-1.44	KF-GY	0.708876	0.708892	0.708908	9.05	9.75	10.45	9.75 ± 0.70
OST-2	-1.87	-1.07	KF-GY	0.708864	0.708880	0.708896	9.50	10.15	10.90	10.15 ± 0.75
KF-JB-1	-2.14	-3.66	KF-JB	0.708744	0.708760	0.708776	15.15	15.50	15.75	15.50 ± 0.25
OST-JB	-6.52	-3.48	KF-JB	0.708728	0.708744	0.708760	15.40	15.70	16.00	15.70 ± 0.3
KF-PS-1	-4.59	-1.88	KF-PS	0.708957	0.708973	0.708989	6.00	6.40	6.90	6.40 ± 0.5
KF-PS-2	-6.85	-2.04	KF-PS	0.708967	0.708983	0.708999	5.80	6.15	6.60	6.15 ± .45

^bIn-house standard for $\delta^{13}\text{C}$ & $\delta^{18}\text{O}$ "CM" corrected to PDB (‰)

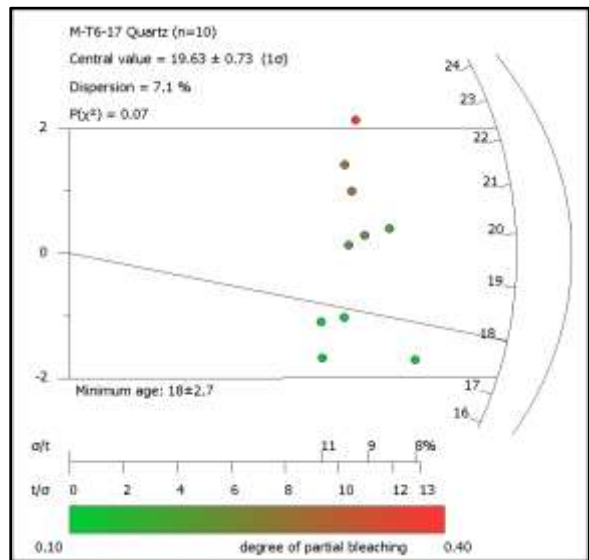
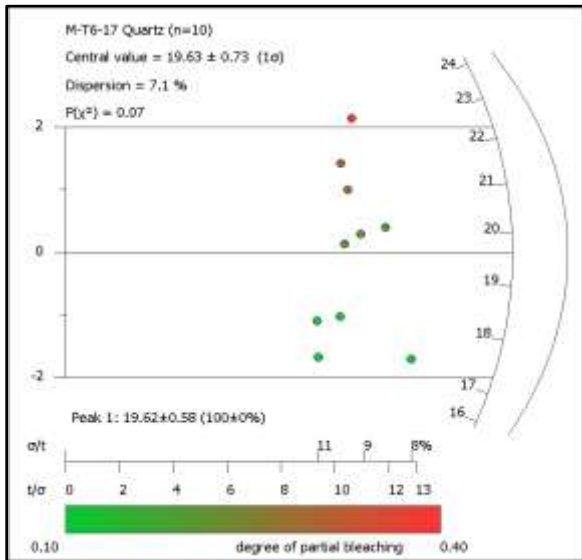
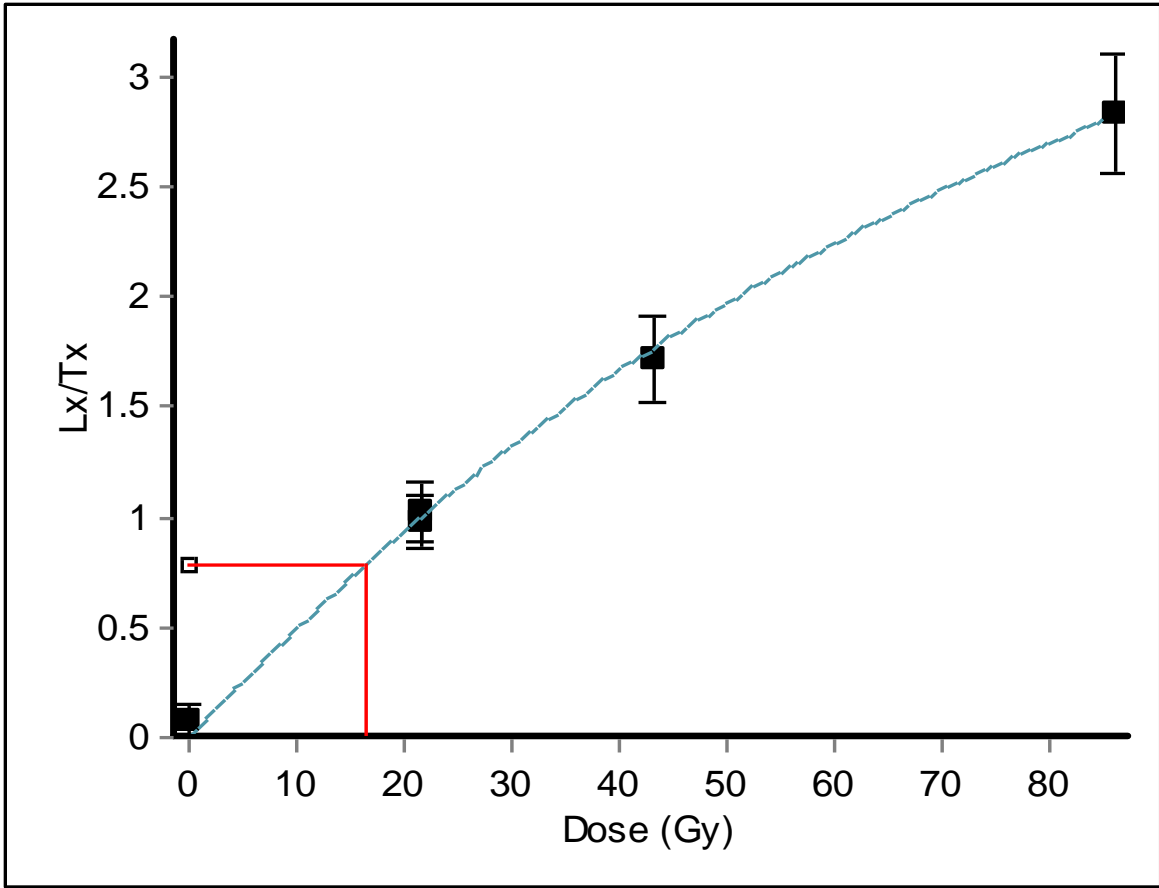
^aFinal reported ages include both analytical errors (2 σ) and the error of the McArthur Sr-Seawater curve (McArthur, 2001)

^cSr data are relative to 0.710250 for NBS 987, 2 σ = 0.000016. Internal precision for each analysis is better than the reproducibility of the standard

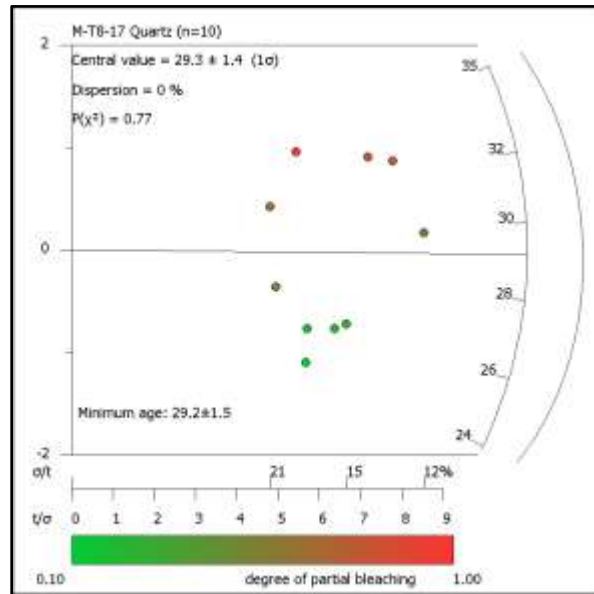
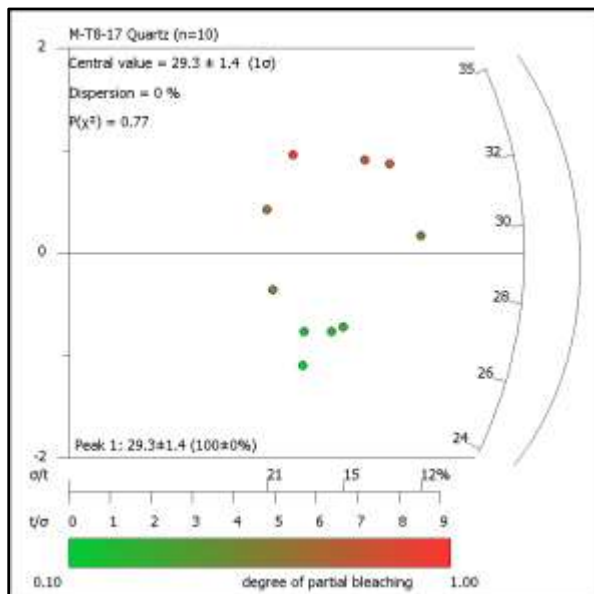
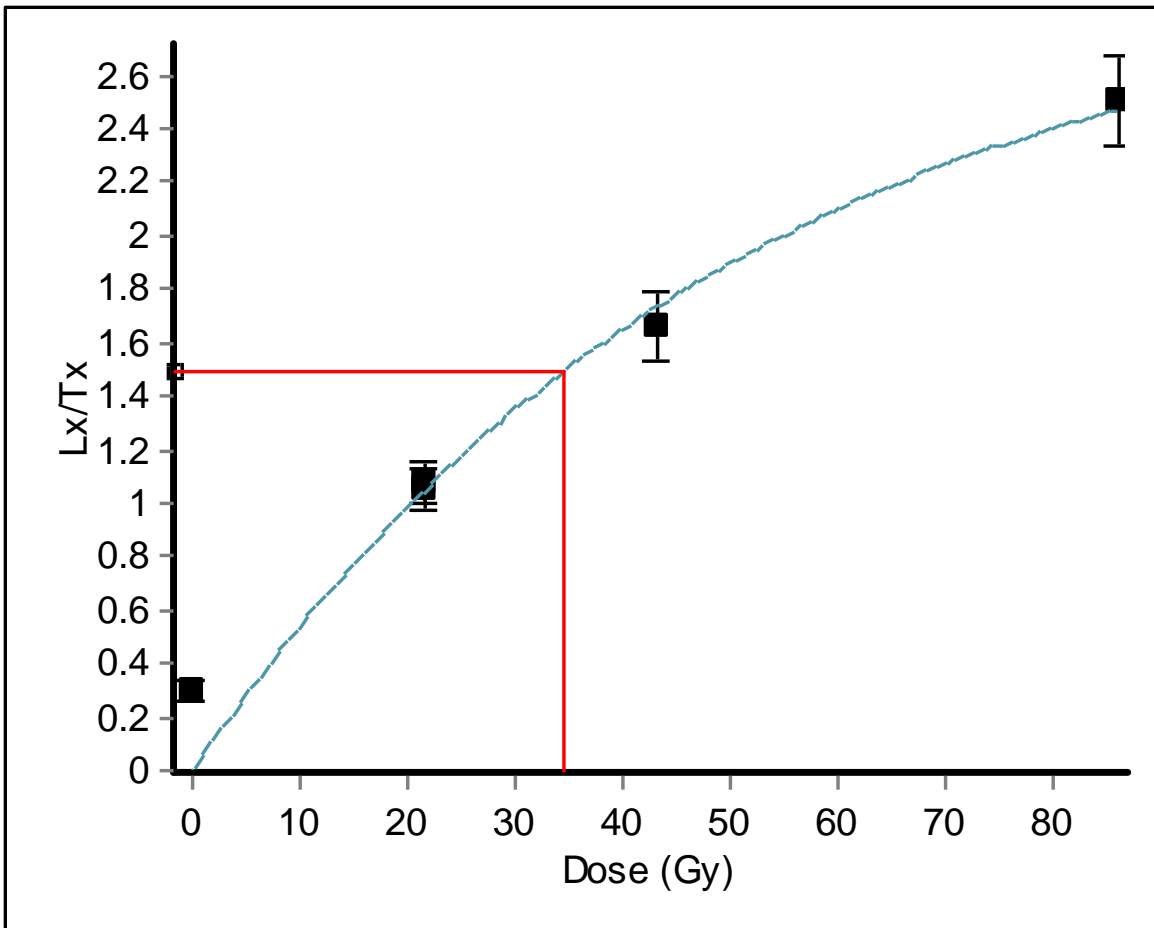
Appendix



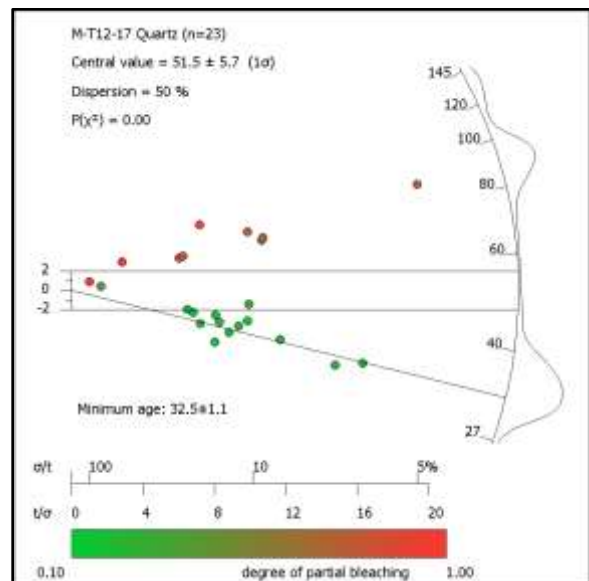
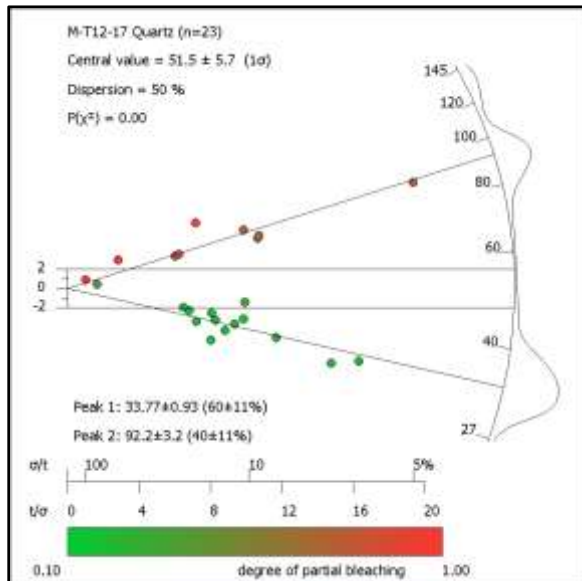
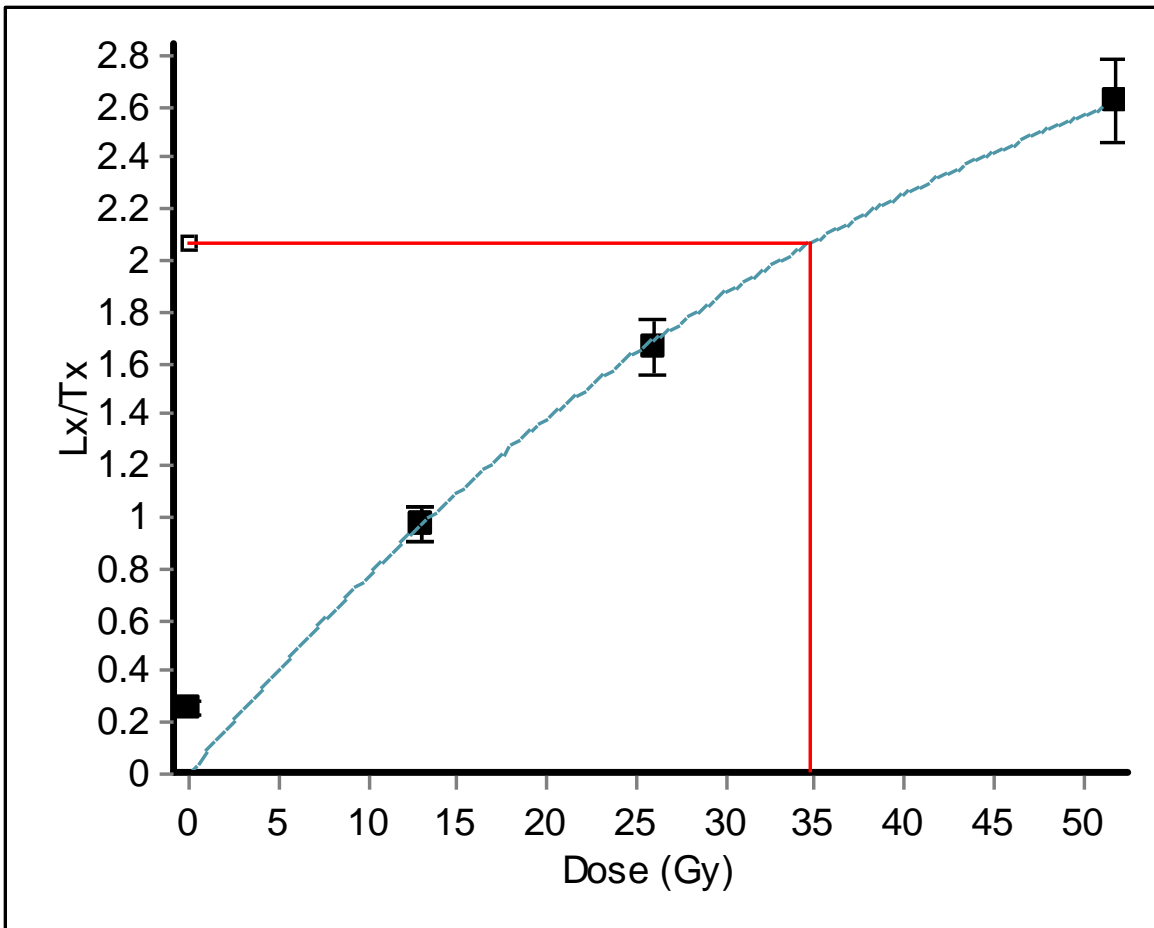
RC-5: Top: OSL Growth Curve. Bottom Radial plots showing CAM and MAM models



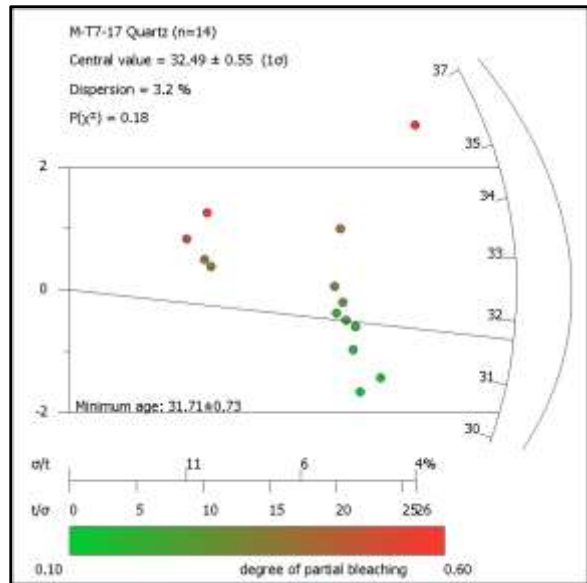
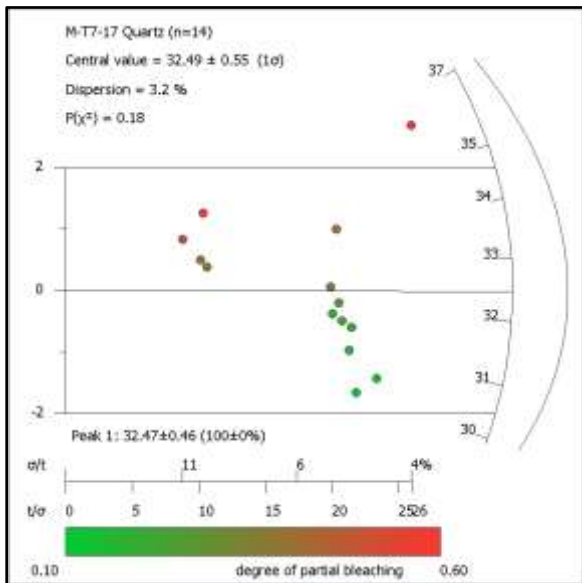
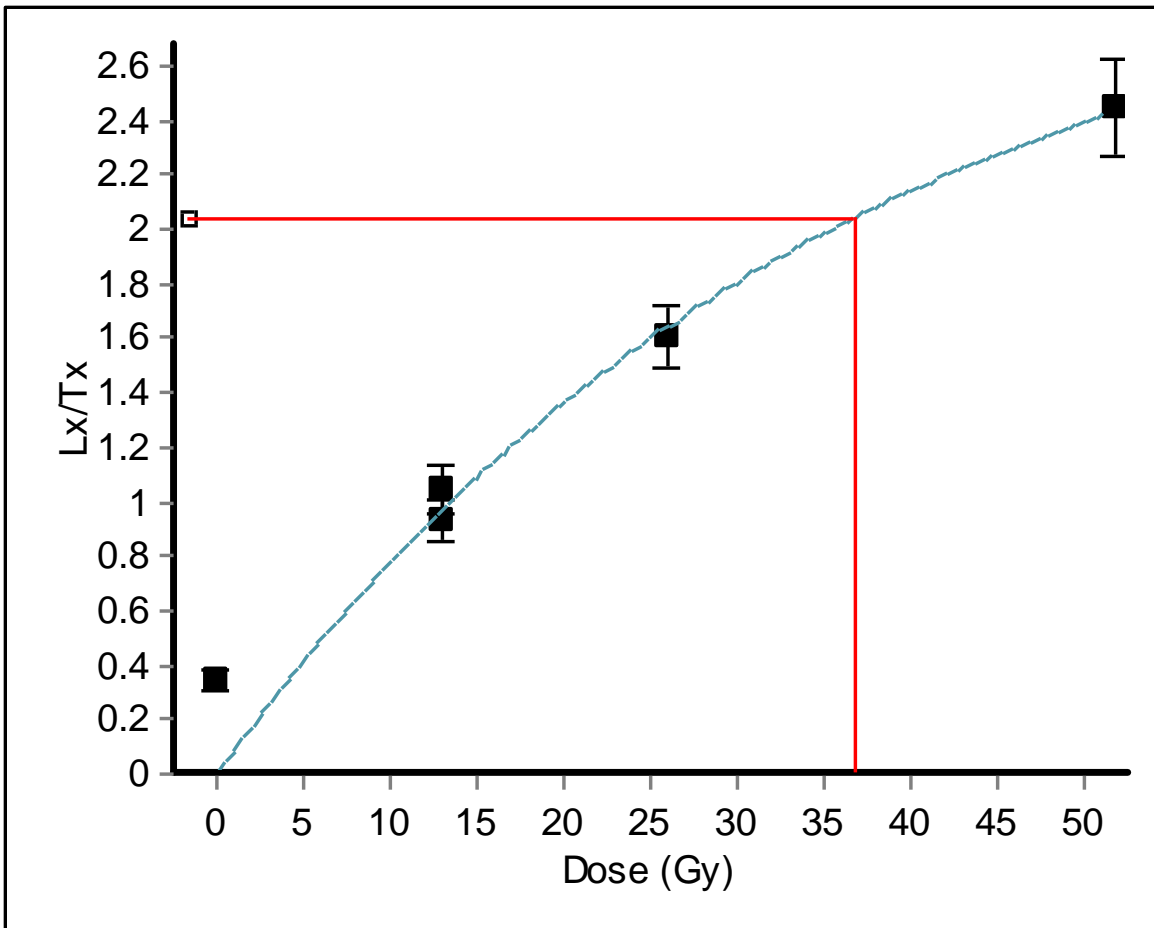
RC-6: Top: OSL Growth Curve. Bottom Radial plots showing CAM and MAM models



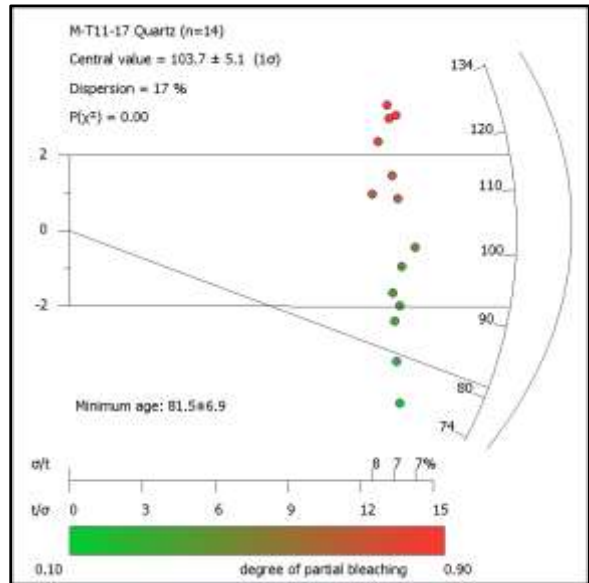
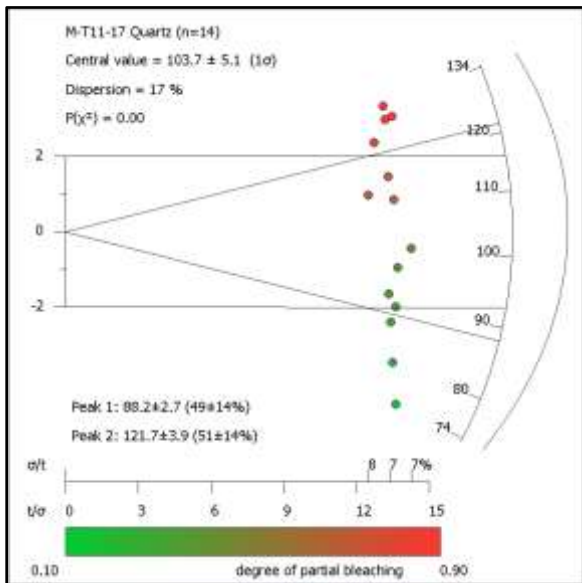
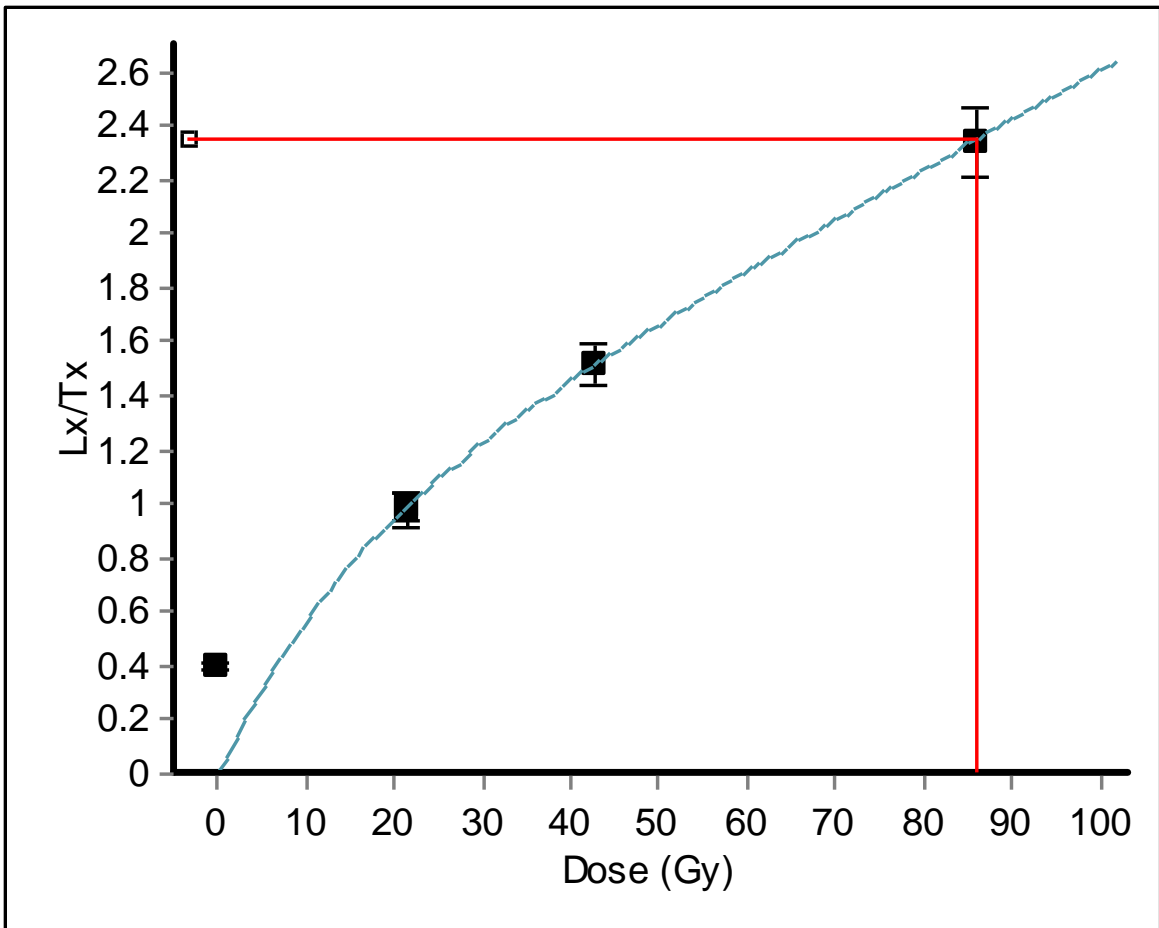
RC-8: Top: OSL Growth Curve. Bottom Radial plots showing CAM and MAM models



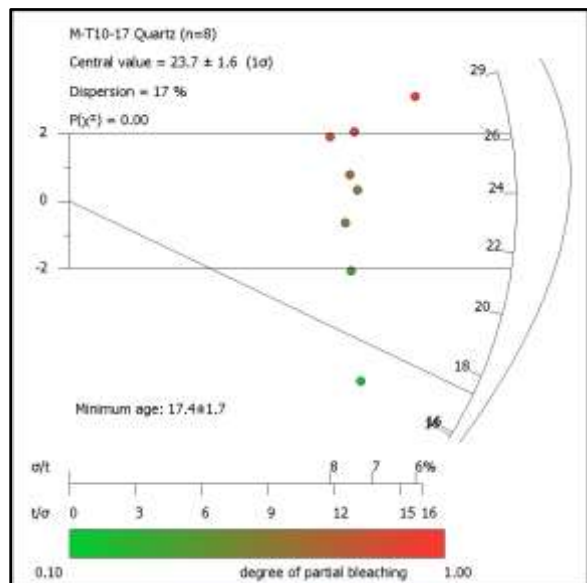
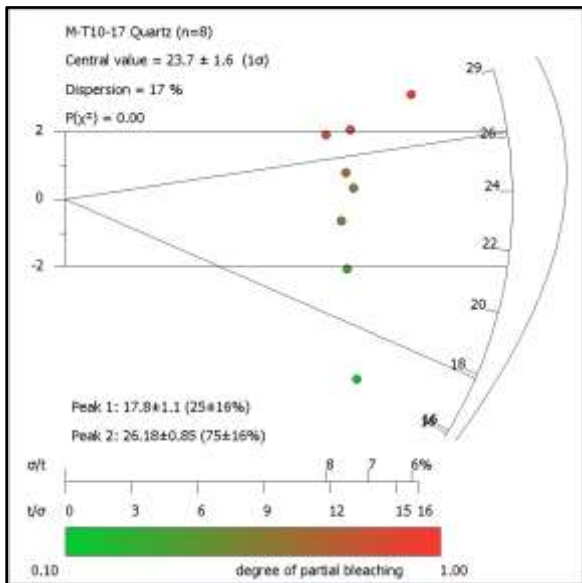
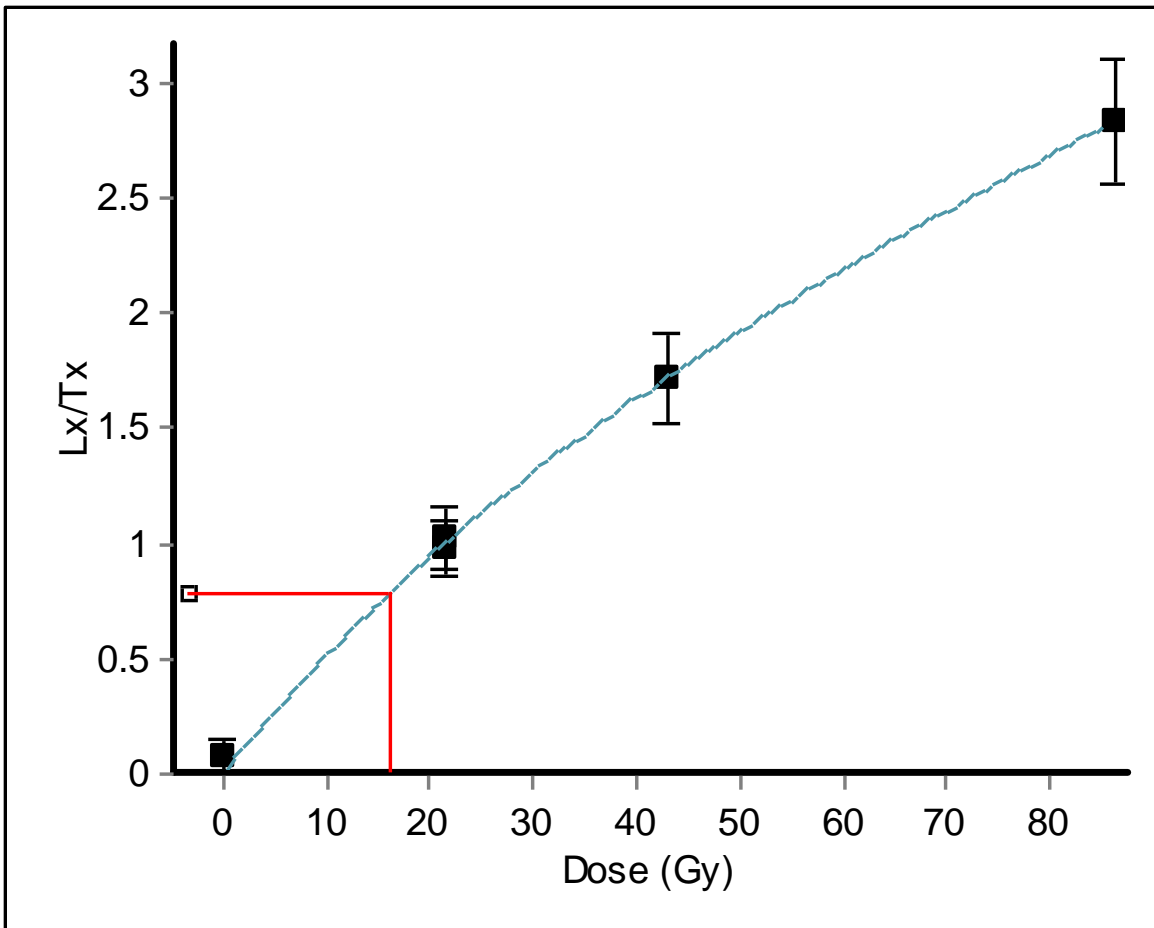
RC-12: Top: OSL Growth Curve. Bottom Radial plots showing CAM and MAM models



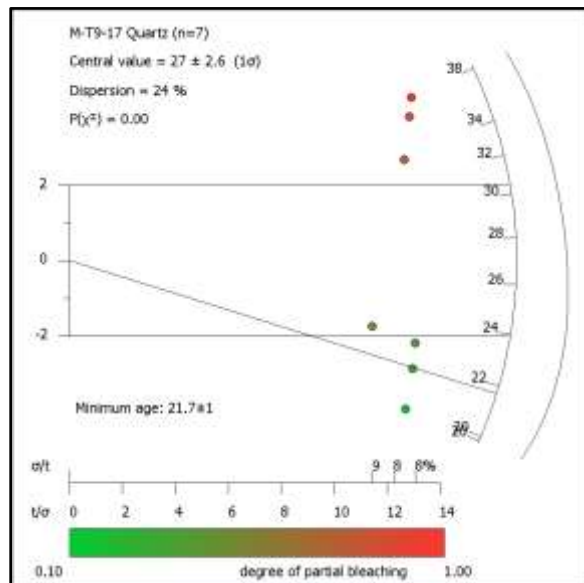
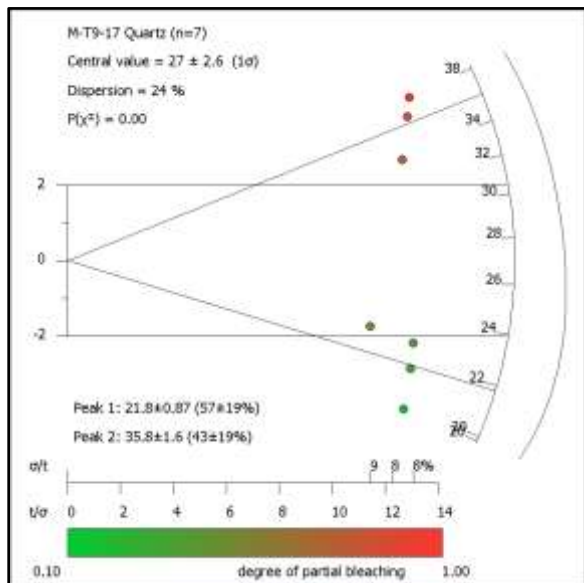
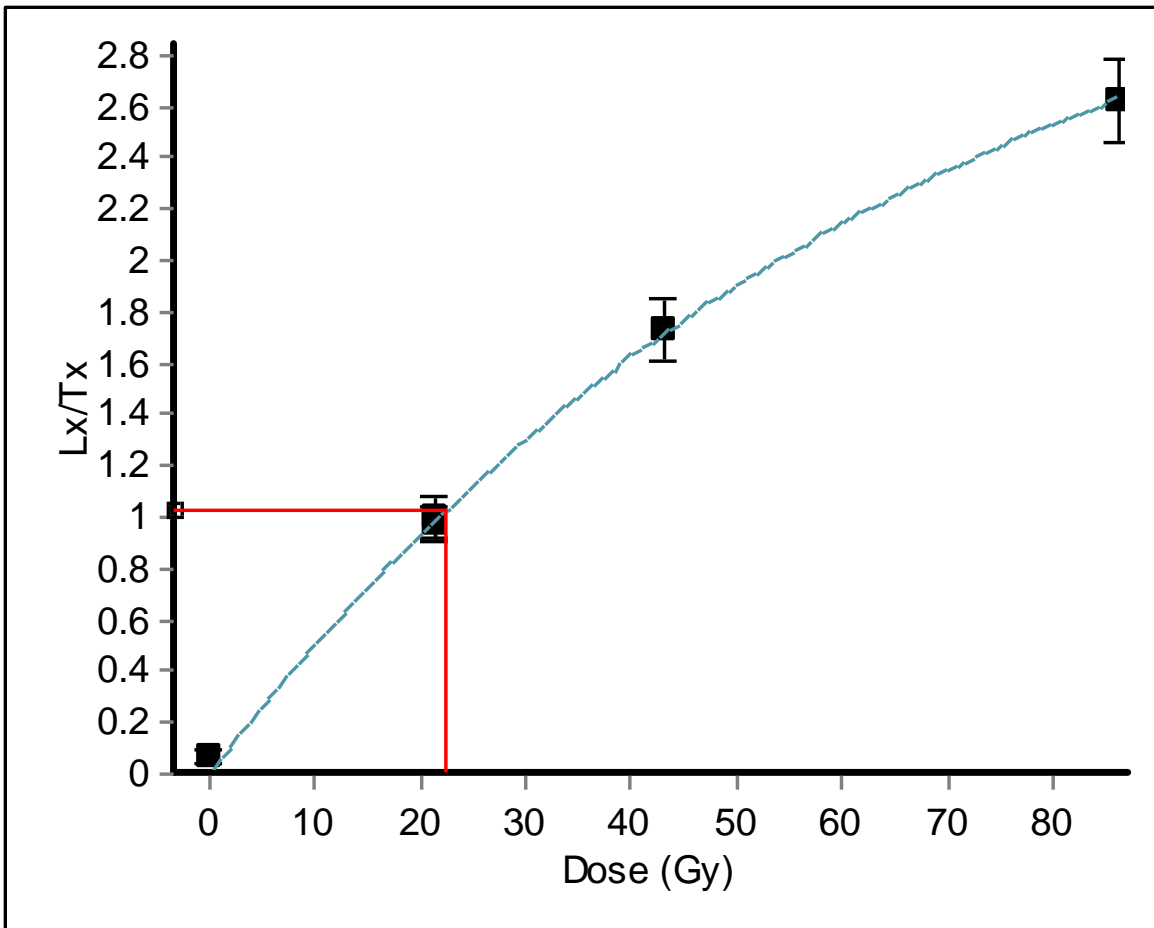
RC-7: Top: OSL Growth Curve. Bottom Radial plots showing CAM and MAM models



RC-11: Top: OSL Growth Curve. Bottom Radial plots showing CAM and MAM models



RC-10: Top: OSL Growth Curve. Bottom Radial plots showing CAM and MAM models



RC-19: Top: OSL Growth Curve. Bottom Radial plots showing CAM and MAM models